Photo-CIDNP studies on reaction centers of rhodobacter sphaeroides

Prakash, Shipra

Photo-CIDNP studies on Reaction Centers of *Rhodobacter sphaeroides*

Shipra Prakash

Photo-CIDNP studies on Reaction Centers of *Rhodobacter sphaeroides*

PROEFSCHRIFT

ter verkrijging van
de graad van Doctor aan de Universiteit Leiden
op gezag van de Rector Magnificus Dr. D. D. Breimer,
hoogleraar in de faculteit der Wiskunde en
Natuurwetenschappen en die der Geneeskunde,
volgens besluit van het College voor Promoties
te verdedigen op woensdag 13 september 2006
klokke 11:15 uur

door

Shipra Prakash
geboren te Bangalore, India
in 1978

Promotiecommissie:

Promotor:
Prof. dr. H. J. M. de Groot

Copromotor:
Dr. J. Matysik

Referent:
Prof. dr. R. Kaptein, Bijvoet Centre for Biomolecular Research, Utrecht

Overige leden:
Dr. M. Huber
Prof. dr. J. Lugtenburg
Prof. dr. S. Völker
Prof. dr. T. Aartsma

CONTENTS

1 Introduction *7*

2 Magnetic field dependence of photo-CIDNP MAS NMR on photosynthetic reaction centers of Rhodobacter sphaeroides WT *15*

3 Field dependent photo-CIDNP in reaction centers of Rhodobacter sphaeroides R26: A sensitive and precise tool for detection of small changes in electronic structure *33*

4 Ground state electronic structure of active cofactors in Rhodobacter sphaeroides reaction centers revealed by ^{13}C photo-CIDNP MAS NMR *43*

5 Photochemically induced dynamic nuclear polarisation in entire bacterial photosynthetic units observed by ^{13}C magic-angle spinning NMR *55*

6 Current view and Outlook *67*

7 Bibliography *73*

List of Abbreviations *81*

Summary *83*

Samenvatting *87*

List of Publications *91*

Curriculum Vitae *93*

Nawoord *95*

1 Introduction

1.1 Photosynthesis

1.1.1 Photosynthesis in bacteria and plants

Photosynthesis is the process by which solar energy is converted to chemical energy (Blankenship, 2002). Plants, algae and cyanobacteria perform oxygenic photosynthesis. In these organisms, light energy is used for reductive fixation of carbon dioxide into carbohydrates while oxidizing water. The produced carbohydrates serve as an energy source for both the photosynthetic organism itself and the non-photosynthetic organisms that directly or indirectly consume photosynthetic organisms. In addition to oxygenic photosynthesis, some organisms perform anoxygenic photosynthesis. These organisms are not capable of oxidizing water and instead they oxidize small inorganic or organic molecules such as hydrogen, hydrogen sulfide or organic acids to gain the reductive power. Anoxygenic photosynthetic bacteria can be classified into four groups of bacteria: the proteobacteria (purple bacteria), the green sulfur bacteria, the green filamentous bacteria and the heliobacteria (Imhoff, 1995; Madigan and Ormerod, 1995; Pierson and Castenholz, 1995; van Gemerden and Mas, 1995).

The primary processes of photosynthetic energy conversion are performed by pigment-protein complexes known as reaction centers (RCs). In general, two types of RCs have been characterized by the nature of their electron acceptors (Blankenship, 1992). The Type I RCs contain iron-sulfur clusters as their acceptors. The Type II RCs have a bacteriopheophytin and quinones as their electron acceptors. Purple bacteria and green filamentous bacteria have Type II RCs while the green sulfur bacteria and the heliobacteria contain Type I RCs. Both types of RCs are present in plants, algae and cyanobacteria. Photosystem I contains an iron-sulfur cluster and Photosystem II is of the pheophytin quinone type.

The purple bacteria may be further divided into two groups: purple sulfur bacteria and purple nonsulfur bacteria. Purple sulfur bacteria can grow in the presence of relatively high concentrations of reduced sulfur compounds like H_2S, while the same levels are toxic for purple nonsulfur bacteria (Brune, 1995). The work described in this thesis relates to the study of the electron-transfer process in RCs of the purple nonsulfur bacterium *Rhodobacter (Rb.) sphaeroides*.

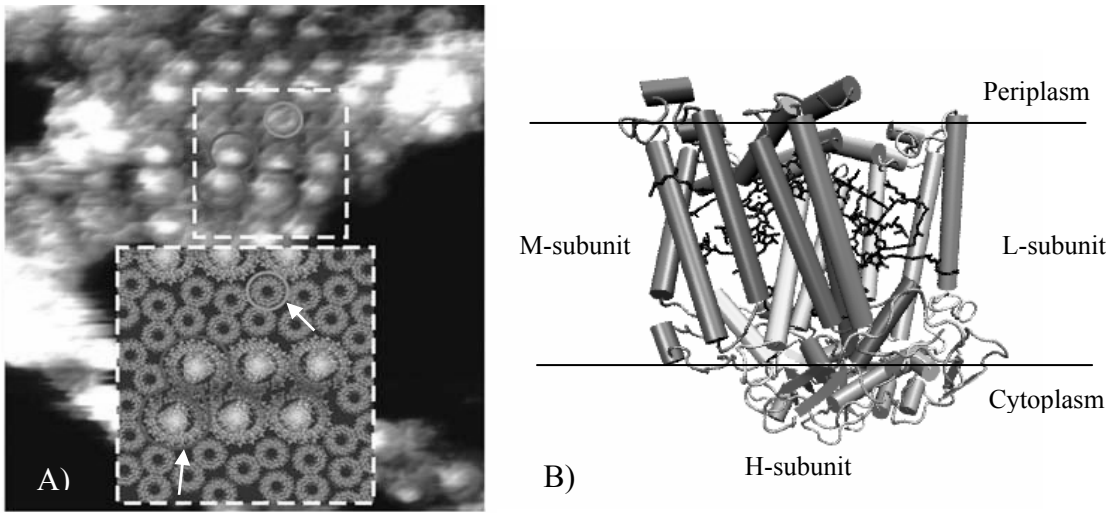

Figure 1.1. A) AFM picture of the PSU from *Rb. sphaeroides* WT consisting of the LH I-RC complex and the LH II surrounding it (shown by white arrows). The RC is present at the center of the LH I (Bahatyrova et al., 2004). B) Schematic representation of the RC in the membrane.

1.1.2 The Reaction Center of Rhodobacter sphaeroides

In the purple bacterium *Rb. sphaeroides*, the photosynthetic apparatus is located in vesicles inside the cytoplasmic membrane. Under anaerobic conditions, the cytoplasmic membrane invaginates and extends inward in vesicles forming the intracytoplasmic membranes. These can extend over the entire cytoplasm. In aerobic conditions of growth, the pigment synthesis and expression of the structural proteins involved in photosynthetic energy conversion is completely suppressed.

The photosynthetic apparatus of *Rb. sphaeroides* is a nanometric assembly in the intracytoplasmic membranes and consists mainly of two types of pigment-protein complexes, the RC and light harvesting (LH) complexes, LH I and LH II (Figure 1.1A). This complex of photosynthetic RC protein and the associated LHs is named the photosynthetic unit (PSU). The function of LHs is to capture sunlight and transfer the excitation energy to the RC. The LH I or B875, with a major absorption peak near 875 nm, surrounds the RC, while LH II, which is not in direct contact to the RC, absorbs maximally at 800 and 850 nm (Sündstrom and van Grondelle, 1995) (for review, see (Hu et al., 2002)).

The RC of *Rb. sphaeroides* is a transmembrane protein complex made of three major polypeptides, H, L and M (for heavy, medium and light) (Yeates et al., 1988; Ermler et al., 1994; Camara-Artigas et al., 2002) (Figure 1.1B). The L and M subunits contain five trans-membrane α-helices, which are packed together in a nearly symmetrical way. Subunit H is more globular in shape and is located mainly in the cytoplasmic side of the membrane. The L and M subunits bind the cofactors. Four molecules of bacteriochlorophyll *a* (BChl *a*), two molecules of bacteriopheophytin a (BPhe *a*), two ubiquinone-10 molecules (Q), a non-haem

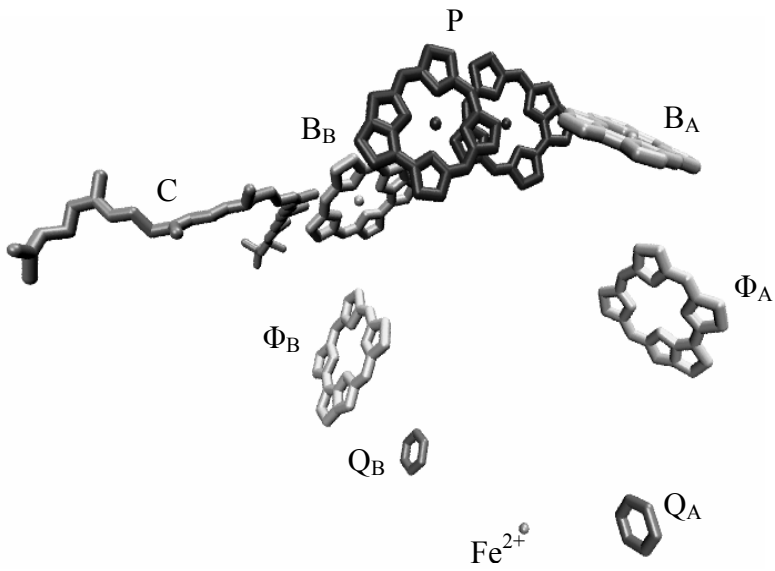

Figure 1.2. Cofactors of the RC of *Rb. sphaeroides WT*. The special pair (P) is a dimer of two BChl molecules. The accessory BChls (B), the bacteriopheophytins (Φ) and the ubiquinones (Q) are arranged in nearly a two fold symmetry. The carotenoid (C) is located in the inactive B-branch. The aliphatic chains from BChl, BPhe and Q are omitted for clarity.

iron (Fe^{2+}) and a caroteniod molecule (C) form the cofactors of the RC protein. The arrangement of the cofactors is shown in Figure 1.2. They are arranged in two nearly symmetric branches, the 'active' A-branch and the 'inactive' B-branch. Two BChls form a tightly interacting dimer called the 'Special Pair' (P). On either side of the special pair an additional BChl molecule is located, known as the accessory BChl (B_A and B_B). The two BPhe (Φ) are positioned 18 Å away from the special pair. Situated under the BPhe are the ubiquinones-10, (Q_A and Q_B). Finally, the non-haem Fe^{2+} ion is located in the center of the two branches near the cytoplasmic side of the membrane. The tenth cofactor, the carotenoid molecule (C), breaks the overall symmetry of the cofactor arrangement and is located near B_B. In the RC of *Rb. sphaeroides* R26, a mutant strain, no carotenoid molecule is present.

Despite symmetry in the structure, the electron-transfer pathway in the RC is asymmetric (for review, see Hoff and Deisenhofer, 1997). The electron transfer proceeds almost exclusively via the A branch. The reason for this functional asymmetry still remains unknown.

After photochemical excitation of P to P*, one electron is emitted which is transferred to the primary electron acceptor Φ_A within 3 ps, forming the radical pair state $P^{+\bullet}\Phi_A^{-\bullet}$(Martin et al., 1986). The $\Phi_A^{-\bullet}$ anion radical decays in about 200 ps and transfers an electron to the ubiquinone Q_A. The electron subsequently moves from Q_A to Q_B in 600 ms reducing Q_B once. Meanwhile, the oxidized primary electron donor P is re-reduced by accepting an electron from cytochrome c at the periplasmic side of the protein. The RC can be excited again and Q_A can give a second electron to Q_B. The doubly reduced and protonated Q_B leaves the RC to the

ubiquinone pool. New ubiquinone from the ubiquinone pool of the membrane replaces the ubiquinol leading to the intial state of the RC.

1.1.3 The Special Pair

The primary electron donor molecule (P) is a dimer formed of two strongly coupled BChl a molecules P_L and P_M corresponding to the polypeptide chains to which they are attached. P_L and P_M overlap in ring I of the BChl ring with an intermolecular distance of approximately 3.5 Å. The Mg atoms of both BChls are coordinated by a histidine ligand (His M202 and His L173).

It has been proposed that the excited state P^* is electronically asymmetric with more electron density on P_M as compared to P_L and this electronic asymmetry is related to the hydrogen-bonding environment of the keto groups (Moore et al., 1999). The electronic structure of the cation radical P^+ has been extensively investigated with EPR, ENDOR and TRIPLE resonance studies (Lendzian et al., 1993; Rautter et al., 1994; Lubitz et al., 2002). The studies have shown that the unpaired electron is unequally distributed over P_L and P_M favoring P_L with a ratio of 2:1. The observed asymmetry was attributed to the difference in energies of the highest filled molecular π-orbitals of the monomeric halves P_L and P_M, caused by differences in structure of the two BChls and/or the environment around the special pair (Lendzian et al., 1993). The knowledge of the electronic structure of P in the ground state is limited. Resonance Raman studies suggest that P_L and P_M are different in the ground state but no details are known (Mattioli et al., 1991; Palaniappan et al., 1993). The application of photochemically induced dynamic nuclear polarization (photo-CIDNP) MAS NMR in combination with site-directed ^{13}C-labeled BChl/BPheo RCs gave a first insight into the ground state electronic structure of the special pair at the atomic scale (Schulten et al., 2002). The studies showed that the ground state electronic structure of P is asymmetric due to the clearly distinct chemical shift patterns. This is interpreted in terms of different electron densities on both cofactors, presumably with higher electron density on P_L.

Current research has focused on applying photo-CIDNP MAS NMR towards building up the complete electronic ground state map of the special pair using site-directed ^{13}C-labeled BChl/BPheo RCs. Although the structure of the bacterial RC is known down to 2-3 Å resolution and the kinetics of the electron transfer has been determined, it is not yet clear how the special pair is tuned in the ground state to facilitate the emission of an electron. An essential parameter in electron transfer is the reorganization energy, which reflects the nuclear configuration associated with the charge transfer process. The involvement of the protein matrix in the emission of an electron from P is not yet clear. The reason for the functional asymmetry in the RC even though it has a very symmetric spatial structure is not known. In addition, the highly asymmetric ground state electronic structure of P with pronounced asymmetry on P_L requires further investigations. Finally, it is not clear whether the protein-

protein interactions inside the bacterial cell affect the local spin densities around the special pair, for example the interactions of LHCs with RCs. Such large systems with atomic resolution are not easily accessible with other spectroscopic methods. Photo-CIDNP MAS NMR even allows the study of RCs in intact cells.

1.2 Solid-State NMR

1.2.1 MAS NMR

NMR spectroscopy is an important tool for chemical analysis, structure determination and the study of dynamics in organic, inorganic and biological systems. Nowadays, it is used for a wide variety of applications from characterization of pharmaceutical products to determining structures of large molecules like polymers and proteins.

Although solution NMR is more routinely performed, solid-state magic-angle spinning (MAS) NMR is rapidly emerging as a powerful method for solid samples and materials. Solution NMR techniques are limited to smaller proteins (<100 kDa) and nucleic acids molecules. Solid-State NMR enables studies of large protein systems like membrane proteins, protein aggregates like prions, amyloids and nucleic acids that cannot be crystallized or are too large for solution NMR. In addition, it is possible with solid-state NMR to examine the functionally important internal dynamics in proteins and nucleic acids in absence of overall motion (Griffin, 1998; Laws et al., 2002). Magic-angle spinning (MAS) overcomes line-broadening by chemical shift anisotropy (CSA) in solids and allows detailed analysis of structure, dynamics and functional mechanisms of membrane-bound protein systems (de Groot, 2000; Zech et al., 2005). The principal limitation of NMR in general is its low sensitivity due to an unfavorable Boltzmann distribution caused by the small Zeeman splitting of nuclear spin levels. Nuclear magnetic moments are small ($\mu \approx 10^{-26}$ J/T), NMR frequencies are low (typically 10-500MHz) and nuclear spin polarizations at thermal equilibrium are small (typically $<10^{-5}$ at 300K). As a result, samples usually require in excess of 10^{17} NMR active nuclei to achieve acceptable signal-to-noise ratio. In general, for this reason NMR samples require isotope enrichment for less abundant nuclei like ^{13}C and ^{15}N. In solid-state NMR, the NMR lines are even broader, particularly in the case of homonuclear dipolar couplings which cannot be averaged completely with MAS.

1.2.2 Photo-CIDNP MAS NMR

Photochemically induced dynamic nuclear polarization (photo-CIDNP) provides a unique opportunity to probe the electronic structure of the special pair in the ground state at the atomic scale. Photo-CIDNP MAS NMR increases NMR intensities by induction of photochemical reactions, which shuffle the nuclear spin system out of its Boltzmann equilibrium. Photo-CIDNP chemical shift information refers to the electronic structure of the

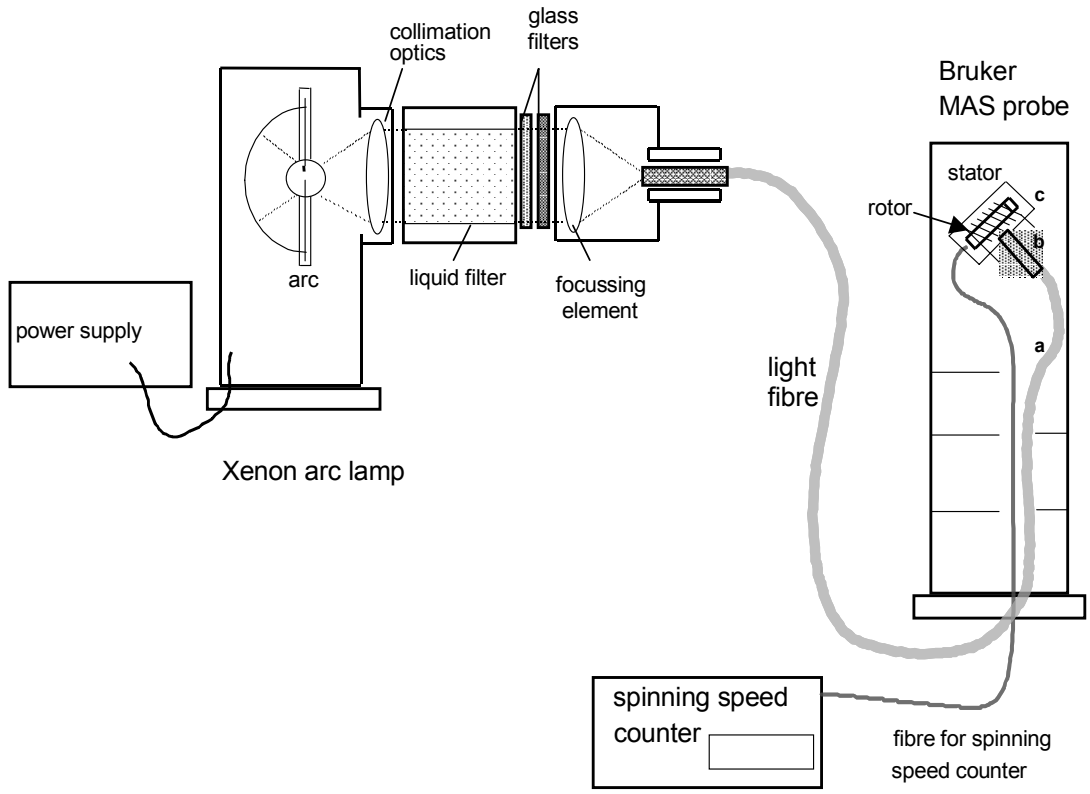

Figure 1.3. Schematic representation of the continuous illumination setup for a photo-CIDNP MAS NMR experiment (a,b,c refer to the points where the modification was made in the probe).

diamagnetic ground state after the photo-reaction and recombination and the intensities relate to the electron spin density distribution in $P^{+\bullet}\Phi_A^{-\bullet}$.

Photo-CIDNP was observed for the first time by solution NMR in 1967 (Bargon et al., 1967; Ward and Lawler, 1967). In the solid-state under continuous illumination, photo-CIDNP was observed for the first time in quinone-blocked frozen bacterial reaction centers (RCs) of *Rb. sphaeroides* R26 and WT (Zysmilich and McDermott, 1994, 1996b, 1996a; Matysik et al., 2000b; Matysik et al., 2001a; Schulten et al., 2002). Later studies on photosystem I of spinach led to a first set of assignments of the aromatic ring carbons to the P2 cofactor of the primary electron donor P700 (Alia et al., 2004b). In the D1D2 complex of the RC of the photosystem II of plants, the observation of a pronounced electron density on rings III and V by photo-CIDNP MAS NMR was taken as an indication for a local electric field, leading to a hypothesis about the origin of the remarkable strength of the redox potential of the primary electron donor P680 (Matysik et al., 2000a; Diller et al., 2005).

The illumination setup that has been used for the photo-CIDNP experiment is designed for a standard Bruker wide bore MAS NMR probe as shown in Figure 1.3. The setup consists of a xenon arc lamp equipped with collimation optics, a liquid filter and glass filters, a focusing

element and a light fibre. The light is transported from the xenon arc lamp to the stator inside the probe with the light fibre (Matysik et al., 2000b).

A standard continuous illumination experiment can be performed with a Hahn echo pulse sequence for the 1D data sets or a modified Radio-Frequency Driven Recoupling sequence (RFDR) or spin diffusion experiments, with the cross polarization (CP) step replaced by a ^{13}C $\pi/2$ pulse, for the 2D dipolar correlation spectra.

1.2.3 Mechanism of photo-CIDNP in solids

Photo-CIDNP in solution NMR is explained by the radical-pair mechanism (RPM). The RPM relies on the different chemical fate of diffusing nuclear-spin selected reaction products (Closs and Closs, 1969; Kaptein and Oosterhoff, 1969; Hore and Broadhurst, 1993; Goez, 1997). However, RPM is not feasible in the solid-state or for cyclic reactions.

Initially, the net nuclear polarization providing photo-CIDNP in solids was assumed to be due to the significant differential relaxation (DR) between the nuclear spins in the special pair triplet ^3P and the nuclear spins in the singlet ground state of P, which would break the symmetry between the two branches (McDermott et al., 1998). However, it has been demonstrated experimentally, that the DR mechanism is not important for RCs from *Rb. sphaeroides* WT (Matysik et al., 2001a; Matysik et al., 2001b; Schulten et al., 2002). Subsequently, two mechanisms have been proposed. First, the electron-electron-nuclear three-spin mixing (TSM) mechanism, in which net nuclear polarization is created in the spin-correlated radical pair due to the presence of both anisotropic hyperfine interaction and coupling between the two electron spins (Jeschke, 1997, 1998). Second, the Differential Decay (DD) mechanism, in which a net photo-CIDNP effect is caused by anisotropic hyperfine coupling without an explicit requirement for electron-electron coupling if spin-correlated radical pairs have different lifetimes in their singlet and triplet states (Polenova and McDermott, 1999). As the two contributions may have different sign, control over both mechanisms may provide a tool to drive intensities in MAS NMR experiments far beyond the Boltzmann state (Jeschke and Matysik, 2003).

The interpretation of the photo-CIDNP intensities and their quantification requires a thorough understanding of the mechanisms that cause the build of this non-equilibrium polarization. Part of the present work aims at resolving the precise mechanisms behind the photo-CIDNP in different biological species. The information may lead to the extension of the solid-state photo-CIDNP approach to other systems.

1.3 Scope of this thesis

This thesis provides a novel experimental method for studying the electronic ground state of the photochemically active cofactors at atomic resolution. Enhancement in NMR intensities achieved with photo-CIDNP raises expectation for a new method that can overcome the

intrinsic insensitivity and non-selectivity of MAS NMR. **Chapter 2** deals with the magnetic-field dependence of photo-CIDNP in *Rb. sphaeroides* WT. The observed field dependence agrees with simulations that assume two competing mechanisms of polarisation transfer from electrons to nuclei, the three-spin mixing (TSM) and the differential decay (DD). The data reveal a ratio of the electron spin density on the special pair cofactors of 3:2 in favour of the P_L in the radical cation state. In **Chapter 3,** the field dependence of photo-CIDNP in *Rb. sphaeroides* R26 is investigated and the observed difference in the photo-CIDNP spectrum between the *Rb. sphaeroides* WT and its mutant R26 is explained. In **Chapter 4,** RCs from *Rb. sphaeroides* WT with site-directed ^{13}C labeled BChl and BPhe are investigated with photo-CIDNP MAS NMR dipolar correlation spectroscopy. The strong enhancement in NMR intensities, at a low field strength of 4.7 T enables, via 2D photo-CIDNP experiments, the assignment of signals of the special pair, the accessory BChl and the BPhe in the RCs. In **Chapter 5,** studies on the photosynthetic units are presented, suggesting for the first time anisotropy effects of photo-CIDNP. In **Chapter 6,** a brief overview of the mechanisms involved in photo-CIDNP is presented. A few ideas for future applications of photo-CIDNP are also introduced.

2 Magnetic field dependence of photo-CIDNP MAS NMR on photosynthetic reaction centers of *Rhodobacter sphaeroides* WT*

2.1 Abstract

Photochemically induced dynamic nuclear polarisation (photo-CIDNP) is observed in frozen and quinone-depleted photosynthetic reaction centers of the purple bacteria *Rhodobacter sphaeroides* wild type (WT) by ^{13}C solid-state NMR at three different magnetic fields. All light-induced signals appear to be emissive at all three fields. At 4.7 Tesla (200 MHz proton frequency), the strongest enhancement of NMR signals is observed, which is more than 10000 above the Boltzmann polarisation. At higher fields, the enhancement factor decreases. At 17.6 Tesla, the enhancement factor is about 60. The field dependence of the enhancement appears to be constant for all nuclei. The observed field dependence is in line with simulations that assume two competing mechanisms of polarisation transfer from electrons to nuclei, three-spin mixing (TSM) and differential decay (DD). These simulations indicate that the ratio of the electron spin density on the special pair cofactors of 3:2 in favour of the L-BChl during the radical cation state. The good agreement of simulations with the experiments raises expectations that artificial reaction centers can be tuned to show photo-CIDNP in the near future.

2.2 Introduction

Solid-state NMR is a rapidly developing technique for the study of samples, such as membrane proteins, that are difficult to tackle by solution NMR or diffraction methods. Magic-angle spinning (MAS) overcomes line-broadening by chemical shift anisotropy (CSA) in solids and allows detailed analysis of structure, dynamics and functional mechanisms of membrane-bound protein systems (de Groot, 2000; Laws et al., 2002). The central drawback of NMR methods is their low sensitivity due to an unfavorable Boltzmann distribution caused by the small Zeeman splitting of nuclear spin levels. The general problem of sensitivity in NMR is even more evident in the case of solids, due to the lower resolution in terms of achievable linewidths relative to the chemical shift range. In order to improve the sensitivity of solid-state NMR several strategies have been developed. Usage of ultra-high fields increases Zeeman splitting and chemical shift dispersion and allows, especially in conjunction with pattern labelling and multidimensional data analysis, full backbone and side-chain

*This Chapter has been published as:
S. Prakash, Alia, P. Gast, H. J. M. de Groot, G. Jeschke, J. Matysik. (2005) *J. Am. Chem. Soc.* 127, 14290-14298.

assignment of proteins (McDermott et al., 2000; Pauli et al., 2001; Castellani et al., 2002). Cross-polarisation (CP) allows transfer of magnetisation from highly polarised nuclei to those having lower polarisation (Hartmann and Hahn, 1962; Pines et al., 1973). The theoretical enhancement factor is given by the ratio of the gyromagnetic constants. In a typical case, $^{1}H \rightarrow ^{13}C$ CP, using the proton bath to enhance ^{13}C signals, the enhancement is by a factor of four. Recently, there has been excellent progress in the use of dynamic nuclear polarization (DNP) for MAS NMR (Hall et al., 1997; Hu et al., 2004). In these experiments, stable radicals are incorporated into the sample and the thermal equilibrium polarization of the electron spins is transferred to nuclei under microwave irradiation by a thermal mixing mechanism. Because of the much larger magnetic moment of electron spins compared to nuclear spins, theoretical enhancements are as large as 660 and 2600 for ^{1}H and ^{13}C, respectively. Another strategy to enhance NMR intensities in solids relies on optical pumping by *polarised* electromagnetic radiation (Suter and Mlynek, 1991; Tycko and Reimer, 1996). In inorganic semiconductors, near-infrared laser excitation of unpolarised valence-band electrons produces spin-polarised electron-hole pairs which polarise nuclear spins to which they are coupled. In atomic systems, such as alkali atoms containing unpaired electrons, pumping optical transitions with circularly polarised radiation results in selective excitation within the Zeeman-perturbed energy levels via the selection rules for electric dipole transitions. In "transferred optically-pumped NMR" (TOPNMR), this magnetisation is transferred to noble gases such as ^{129}Xe or to biological relevant nuclei such as ^{31}P (Raftery and Chmelka, 1994; Tycko, 1998; Cherubini and Bifone, 2003).

Photochemically induced dynamic nuclear polarization (photo-CIDNP) is a method to increase NMR intensities by induction of photochemical reactions, which shuffle the nuclear spin system out of its Boltzmann equilibrium. Photo-CIDNP in solution NMR is explained by the radical-pair mechanism which relies on the different chemical fate of diffusing nuclear-spin selected reaction products (Closs and Closs, 1969; Kaptein and Oosterhoff, 1969) (for review, see: (Hore and Broadhurst, 1993; Goez, 1997). This mechanism is not feasible in the solid-state or for cyclic reactions.

In the solid-state, photo-CIDNP has been observed for the first time in quinone-blocked frozen bacterial reaction centers (RCs) of *Rhodobacter (Rb.) sphaeroides* R26 and WT in continuous illumination with white light at 9.4 Tesla, allowing an enhancement factor of about 200 to 1000 (Zysmilich and McDermott, 1994, 1996b, 1996a; Matysik et al., 2000b; Matysik et al., 2001a; Schulten et al., 2002). Plant RCs have been studied under the same conditions, and similar enhancement factors were observed. Studies on photosystem I of spinach lead to an almost complete set of assignments of the aromatic ring carbons to the P2 cofactor of the primary electron donor P700 (Alia et al., 2004b). In the D1D2 complex of the RC of the photosystem II of plants, the observation of a pronounced electron density on rings III and V by photo-CIDNP MAS NMR was taken as an indication for a local electric field,

leading to a hypothesis about the origin of the remarkable strength of the redox potential of the primary electron donor P680 (Matysik et al., 2000a; Diller et al., 2005). Combining photo-CIDNP at 9.4 Tesla with selective ^{13}C-isotope labeling, two-dimensional photo-CIDNP MAS NMR spectra were obtained, which demonstrates that the electron density in the two BChl molecules of the special pair (P) of a bacterial RC is already asymmetric in its electronic ground state (Schulten et al., 2002). In addition, NMR signals were detected in entire membrane-bound bacterial photosynthetic units (>1.5 MDa) with the same label patern (Prakash et al., 2003).

The possibility to observe photo-CIDNP in photosynthetic RCs has been predicted already two decades ago, since both magnetic field effect and photochemically induced dynamic *electron* polarisation (photo-CIDEP) were interpreted in terms of electron-nuclear interactions (Blankenship et al., 1975; Blankenship et al., 1977; Hoff et al., 1977a; Hoff et al., 1977b; Goldstein and Boxer, 1987) (for historical review, see Hoff, 1981). Upon photochemical excitation of the primary electron donor P, which is in bacterial RCs from *Rb. sphaeroides* a dimer assembled from the two BChl cofactors L and M, an electron is emitted to the primary acceptor, a BPhe molecule Φ, forming an electron-polarised singlet radical pair (Figure 2.1). In quinone-reduced or depleted RCs, further electron transfer is blocked. Therefore, the singlet radical pair can either relax to the electronic ground state or, depending on the strength of the applied magnetic field, being transferred to a triplet radical pair. The triplet radical pair recombines to a special pair triplet ^{3}P and an acceptor singlet. Finally the special pair triplet also relaxes to the singlet ground state, so that the whole process is cyclic and no net effect on the nuclei due to the branching of the reaction pathway would be expected.

Initially, the net nuclear polarization providing photo-CIDNP in solids was assumed to be due to the significant differential relaxation (DR) between the nuclear spins in the special pair triplet ^{3}P and the nuclear spins in the singlet ground state of P, which would break the symmetry between the two branches (McDermott et al., 1998). Meanwhile, it has been demonstrated experimentally that the DR mechanism does not have much significance for RCs of *Rb. sphaeroides* WT (Matysik et al., 2001a; Matysik et al., 2001b; Schulten et al., 2002). Currently, two further mechanisms are under discussion (Jeschke and Matysik, 2003). In the electron-electron-nuclear three-spin mixing (TSM) mechanism, net nuclear polarization is created in the spin-correlated radical pair due to the presence of both anisotropic hyperfine interaction and coupling between the two electron spins (Jeschke, 1998). In the Differential Decay (DD) mechanism, a net photo-CIDNP effect is caused by anisotropic hyperfine coupling without an explicit requirement for electron-electron coupling if spin-correlated radical pairs have different lifetimes in their singlet and triplet states (Polenova and McDermott, 1999). A better understanding of the interplay between TSM and DD mechanisms, however, require further studies.

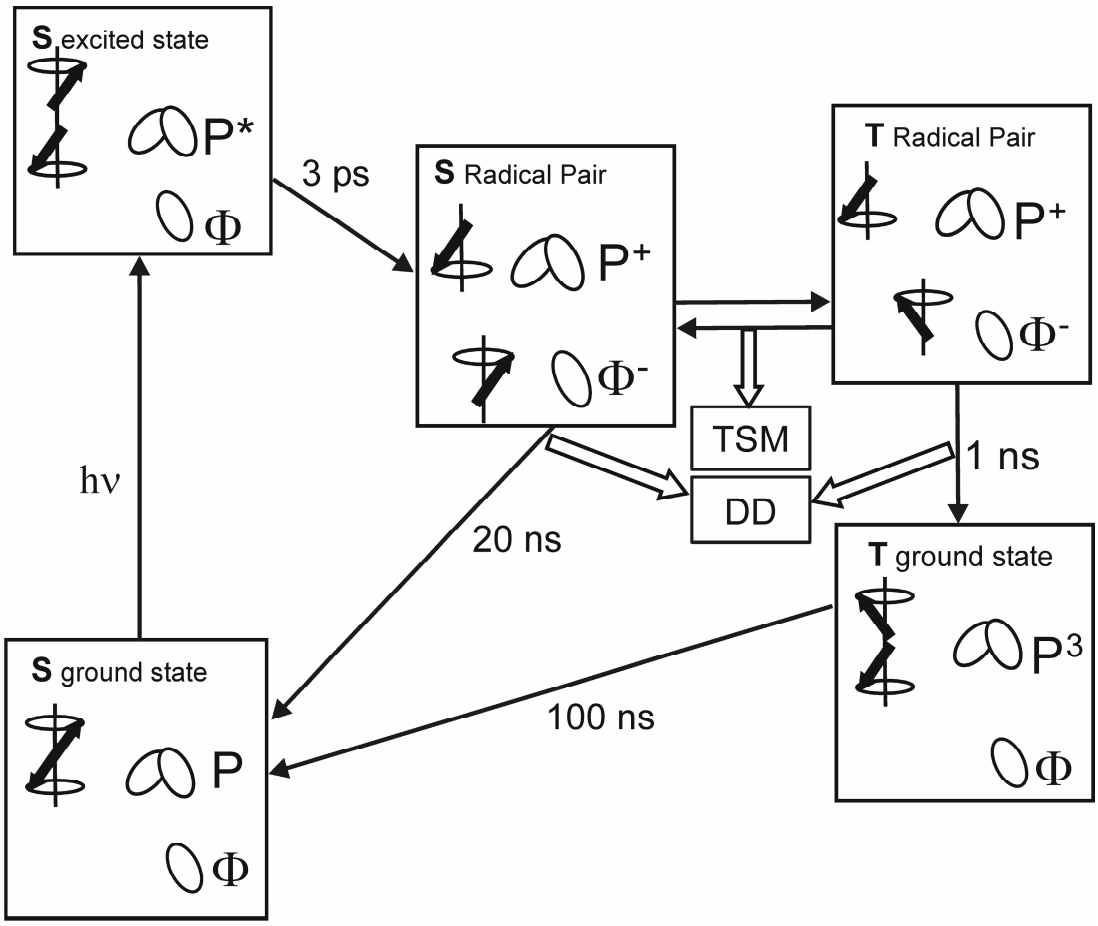

Figure 2.1. Reaction cycle in quinone-blocked bacterial RCs. After light-induced electron transfer from the primary donor (P) to the bacteriopheophytin (ϕ), an electron-polarized singlet radical pair is formed. The electron polarization is transferred to nuclei via three-spin mixing (TSM) within the radical pair and via differential decay (DD), the difference in lifetime of the two radical pair states.

As the two contributions may have different sign, control over both mechanisms may provide a tool to drive intensities in MAS NMR experiments far beyond the Boltzmann state (Jeschke and Matysik, 2003). The field dependence of photo-CIDNP is of particular relevance for such studies. For studying the field dependence of photo-CIDNP, we have chosen the RC of *Rb. sphaeroides* WT, since its kinetics is well-known and, due to the short triplet lifetime of 100 ns, comparatively simple (for review, see (Hoff and Deisenhofer, 1997). The good agreement between the experimental data, obtained at 4.7 Tesla (200 MHz proton frequency), 9.4 Tesla (400 MHz) and 17.6 Tesla (750 MHz), and the theoretical simulations, reported in this paper, suggests that a new method to overcome the intrinsic insensitivity and non-selectivity of MAS NMR can become reality.

2.3 Materials and Methods

2.3.1 Sample Preparation

The RCs from *Rb. sphaeroides* WT were isolated as described by (Shochat et al., 1994). Removal of Q_A was achieved by incubating the RCs at a concentration of 0.6 μM in 4% LDAO, 10 mM o-phenanthroline, 10 mM Tris buffer, pH 8.0, for 6 h at 26 °C, followed by washing with 0.5 M NaCl in 10 mM Tris buffer, pH 8.0, containing 0.025% LDAO and 1 mM EDTA (Okamura et al., 1975). Approximately 15 mg of the RC protein complex embedded in LDAO micelles were used for NMR measurements.

2.3.2 MAS-NMR Measurements

The NMR experiments at different fields were performed with AV-750, DMX-400 and DMX-200 NMR spectrometers equipped with magic angle spinning (MAS) probes. The sample was loaded into a clear 4-mm sapphire rotor and inserted into the MAS probe. It was then frozen slowly at a low spinning frequency of $\nu_r = 400$ Hz to ensure a homogenous sample distribution against the rotor wall (Fischer et al., 1992). The light and dark spectra were collected with a Hahn echo pulse sequence and TPPM proton decoupling (Bennett et al., 1995). ^{13}C MAS NMR spectra were obtained at a temperature of 223 K under continuous illumination with white light (Matysik et al., 2000b).

The rotational frequency for MAS was 8 kHz. For the three fields of 4.7, 9.4 and 17.6 Tesla, a line broadening of 20 Hz, 50 Hz and 120 Hz, respectively, was applied prior to Fourier transformation. At all fields, a cycle delay of 4 s was used. All the ^{13}C-MAS NMR spectra were referenced to the ^{13}COOH response of solid tyrosine·HCl at 172.1 ppm.

The tyrosine spectrum was phased by using zeroth order phase correction until all signals were absorptive (positive). A small first order phase correction was applied to correct slight line shape asymmetry of the signals far from the center. The same set of phase correction parameters has been applied to the dark and photo-CIDNP spectra of the RC.

2.3.3 Simulations

Numerical simulations of the photo-CIDNP effect were based on the theory described in (Jeschke and Matysik, 2003) as implemented in a home-written Matlab program for density matrix computation using the EasySpin library (Stoll, 2003). The program starts from a pure singlet state of the pair and computes time evolution under a Hamiltonian including electron Zeeman, nuclear Zeeman, and hyperfine interaction as well as dipole-dipole and exchange coupling between the two electron spins. The part of the density matrix that decays to the ground state from either singlet or triplet radical pairs is projected out (diamagnetic part) and is further evolved under a Hamiltonian including only the nuclear Zeeman interaction. Evolution is continued until radical pairs have completely decayed (100 ns) and after that nuclear polarization of the diamagnetic part of the density matrix is determined. As an

extension to the approach described in (Jeschke and Matysik, 2003), this procedure is performed for a full powder average, describing all interactions by tensors, except for the nuclear Zeeman interaction whose anisotropy is negligible on a time scale of 100 ns. A spherical grid (EasySpin function *sphgrid*) with 16 knots and C_i symmetry (481 orientations) was found to be sufficient for powder averaging. Nuclear polarization was normalized to the thermal polarization at the measurement temperature of 223 K.

As far as possible, parameters were taken from experimental work. Missing parameters were obtained by density functional theory (DFT) computations (see below). A lifetime of triplet radical pairs of 1 ns, a lifetime of singlet radical pairs of 20 ns, an exchange coupling J = 7 G, and a dipole-dipole coupling d = 5 G were assumed (Till et al., 1997; Hulsebosch et al., 1999, 2001). The principal values of the g tensor of the donor cation radical were taken as 2.00329, 2.00239, and 2.00203 (Klette et al., 1993). For the g tensor of the acceptor anion radical, we resorted to the values 2.00437, 2.00340, and 2.00239 for the BPhe anion radical in *R. viridis*, which we assume to be much closer to actual values for *Rb. sphaeroides* than values computed by DFT. Principal values of ^{13}C hyperfine tensors as well as all tensor principal axis systems were obtained by DFT (Dorlet et al., 2000).

DFT computations were performed with the program ADF 2004.1 using the BLYP functional (Velde et al., 2001). The starting geometry was taken from the crystal structure of the photosynthetic reaction center of *Rb. sphaeroides* R26 in the charge-neutral state (PDB file, identifier 1AIJ). The two chlorophyll molecules of the special pair as well as the two directly coordinated histidine residues (His L 173 and His M 202) were extracted for a donor model, and BPhe was extracted for an acceptor model (Stowell et al., 1997). Hydrogen atoms were added with the program Titan (Wavefunction, Inc., Irvine, CA, USA). In this procedure some sp^3 carbons were wrongly assigned as sp^2 carbons- these were edited by hand to sp^3 in the same program. The phytyl chains in both the BChl and BPhe molecules were replaced by methyl groups and the histidine residues were edited to methylimidazol ligands. A spin-restricted computation with the TZP basis set and frozen first shells for carbon and oxygen was used for geometry optimization of the acceptor anion radical and a spin-restricted computation with the DZ basis set and frozen first shells for carbon and oxygen for the special pair donor cation radical. Hyperfine couplings were computed in spin-unrestricted computations with a TZ2P all-electron basis set for the acceptor anion radical and a TZP all-electron basis set for the donor cation radical. Spin-restricted spin-orbit relativistic computations within the ZORA formalism were used for g tensor computations, employing a TZ2P all-electron basis set for the acceptor anion radical and a DZP basis set for the donor cation radical (van Lenthe et al., 1997). Control computations of EPR parameters in the starting geometries revealed only slight changes in the parameters that are smaller than the expected accuracy of the DFT computations (±20% for hyperfine couplings, ±5° for principal axes directions). For the donor cation radical, the computed principal axis directions could be

compared to the experimental directions (Huber, 1997). All three axes deviate by approximately 4° from the corresponding experimental axes, with the experimental errors being ±1-2°.

Chemical shift values for simulating photo-CIDNP spectra were taken from assignments made in this work (Table 2, values at 4.7 T) where possible. Missing values were taken from (Schulten et al., 2002) if available there and from (Facelli, 1998) otherwise (Table 1). Signals were represented by Gaussian peaks with a width of 0.5 ppm.

2.3.4 Enhancement Factor

The enhancement factor for the photo-CIDNP spectrum has been empirically determined. The enhancement factor has been computed as a ratio of the signal due to a single carbon at 160.1 ppm (in light) to one at 31 ppm (in dark). It has been estimated that the signal in dark is caused by about 3300 methyl groups in the bacterial RC. Hence, the signal from a single carbon in dark has been calculated. An enhancement factor of 60 (17.6 Tesla), 1000 (9.4 Tesla) and about 10000 (4.7 Tesla) has thus been calculated.

2.4 Results

2.4.1 Field effects in the dark spectra

Figure 2.2 shows the spectra of the bacterial RC sample in the dark at three different magnetic fields, A: 17.6 T (750 MHz proton frequency), B: 9.4 T (400 MHz) and C: 4.7 T (200 MHz). All spectra have been recorded at a MAS rotational frequency of 8 kHz. The spectral quality obtained at 17.6 Tesla is slightly above that obtained at 9.6 Tesla. Both spectra 2.2A and 2.2B are clearly better resolved than spectrum 2.2C, obtained at 4.7 Tesla. The observed field dependence of the signal-to-noise ratio and the spectral dispersion is in line with the expectations for NMR spectroscopy under Boltzmann conditions. Independent of those field effects, all dark spectra show similar features. All signals appear between 80 and 10 ppm. The amino acid backbone and aromatic carbons of aromatic amino acids and cofactors are difficult to detect. The data are characteristic for ^{13}C MAS NMR spectra of large proteins. No spinning sidebands are observed in the three spectra. This is due to the small chemical shift anisotropy (CSA) of aliphatic carbons and the small signal intensity of the carbonylic and aromatic signals.

2.4.2 Field effects in the light spectra

Upon illumination, strong signals emerge in the aromatic region at all fields (Figure 2.3). All light-induced signals appear to be emissive (negative). Re-evaluation of previous photo-CIDNP data from WT confirms this finding (Matysik et al., 2001a; Schulten et al., 2002). This pattern is similar to that of photosystem I and in contrast to RCs of *Rb. sphaeroides* R26 and of photosystem II showing enhanced absorptive photo-CIDNP signals, except for the

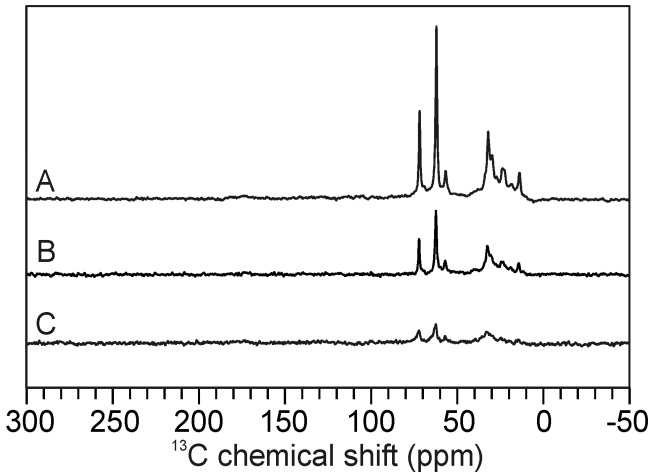

Figure 2.2 ^{13}C MAS NMR spectra of quinone-depleted RCs of *Rb. sphaeroides* WT obtained at 223 K in the dark at different magnetic fields at 17.6 T (A), 9.4 T (B) and 4.7 T (C).

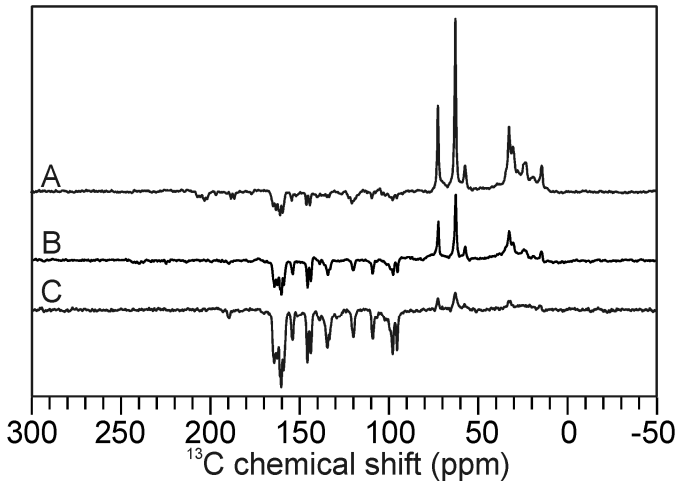

Figure 2.3. ^{13}C MAS NMR spectra of quinone-depleted RCs of *Rb. sphaeroides* WT obtained at 223 K under illumination with continuous white light at different magnetic fields at 17.6 T (A), 9.4 T (B) and 4.7 T (C).

chemical shift range between 140 and 80 ppm where most signals appear emissive (Zysmilich and McDermott, 1996a; Matysik et al., 2000a; Matysik et al., 2000b; Matysik et al., 2001a; Alia et al., 2004b; Diller et al., 2005).

The enhancement pattern in Figure 2.3 appears to be independent of the magnetic field strength, although the absolute enhancement factor is different at various fields. Spectrum 2.3A, obtained at 17.6 T, shows the weakest enhancement, while in spectrum 2.3C, measured at 4.7 Tesla, the strongest enhancement is observed. These patterns can be easily observed in spectrum 2.4A (marked by asterisk), whereas no spinning sidebands are visible in spectrum 2.4C. Finally, higher fields generally require longer cycle delays. Therefore, photo-CIDNP MAS NMR experiments at the lower field provide (i) stronger signal intensity enhancement, (ii) smaller signal widths, (iii) less spinning sidebands and (iv) faster scanning.

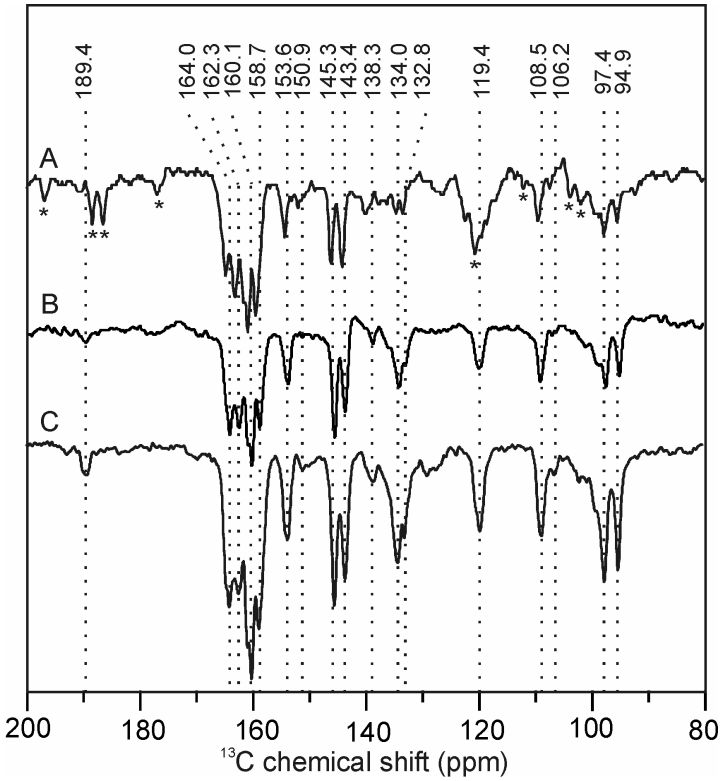

Figure 2.4. ^{13}C MAS NMR spectra of quinone-depleted RCs of *Rb. sphaeroides* WT obtained at 223 K under illumination with continuous white light at different magnetic fields at 17.6 T (A), 9.4 T (B) and 4.7 T (C). Discussed centerbands are visualised by dashed lines. Spinning sidebands are labeled by an asterisk.

2.4.3 Signal assignments

At all three fields, the light-induced signals appear in the region of carbonyl and aromatic carbons, between 190 and 90 ppm. No light-induced signal is observed from aliphatic carbons. In Figure 2.4, the region of the light-induced signals is presented in detail. Some characteristic signals are marked by dashed lines. Table 2.1 compiles the ^{13}C chemical shift data of BChl *a* and BPhe *a* cofactors, on which our assignments are based. Figure 2.5 shows the numbering of the carbon atoms of a BChl *a* molecule. The signal at 189.4 ppm, which is observed in spectra B and C, can clearly be assigned to a carbonyl. Our simulations suggest an assignment to the carbonyl carbons C-Φ13^1 und C-Φ3^1 of the BPhe acceptor Φ. It is the first time that a carbonyl resonance has been detected in a bacterial RC. In spectrum A, the signal is hidden below spinning sidebands. Interestingly, in the photo-CIDNP spectrum of photosystem I showing a completely emissive set of light-induced signals, also an emissive signal of a C-13^1 carbonyl has been detected (Alia et al., 2004b). The strongest signal in WT appears at 160.1 ppm, as also observed in R26 (see figure 2.8). It belongs to the most prominent group, appearing between 165 and 155 ppm and composed of at least five signals. These five signals can be conveniently assigned to the three carbons C-9, C-14 and C-19 of a donor BChl. The two additional signals may arise from the second BChl of the special pair, demonstrating the difference in the electronic ground state of these two BChl cofactors

(Schulten et al., 2002). Between 155 and 140 ppm, four signals are clearly identified, which can be assigned tentatively to the carbons C-16 (150.9 ppm), C-1 (153.6 ppm), C-11 (145.3 ppm) and C-2 (143.4 ppm). In contrast to R26, the signal at 148.5 ppm, assigned to a C-4, cannot be observed in WT (figure 2.8)(Matysik et al., 2001a). In the spectral range from 140 to 130 ppm, three signals are resolved. For the weak signal at 138.3 ppm, the most straightforward assignment would be either a C-3 of a BChl donor or a C-Φ1 of a BPhe *a* acceptor. Our simulations suggest an assignment to the latter. The emissive strong signal at 134.0 ppm has also been observed in R26 and tentatively assigned to the C-ε of an axial histidine (Matysik et al., 2001b). Alternatively, an assignment to a C- Φ2 of BPhe is also possible. The weaker emissive signal at 132.8 ppm could either be assigned to a second axial histidine, to C- Φ2 of BPhe *a* or to a C-13 of BChl *a* or BPhe *a*. Similarly, the next significant signal appears at 119.4 ppm and may arise from a C-δ of an axial histidine or of a C-12 of BChl *a* or BPhe *a*. Comparison of all the safely assigned peaks in WT and R-26 spectra suggests that signals of BChl *a* change from emissive to absorptive when going from WT to R26. The fact that both signals, at 134.0 and 119.4 ppm appear emissive in R26 thus discourages an assignment to a BChl carbon. They would match very well to the shifts of C-δ and C-ε of a Mg-bound histidine having similar distance to the BChl macrocycle (Alia et al., 2001; Alia et al., 2004a). Histidines have indeed been observed by ^{15}N photo-CIDNP MAS NMR in R26, however, it was shown that the intensity has been obtained via spin-diffusion (Zysmilich and McDermott, 1996b). In addition, there is no hint from other spectroscopic methods for electron spin density on an axial histidine. Indeed, our simulations suggest an assignment of the signals at 134.0 and 119.4 ppm to the C- Φ2 and C- Φ12 carbons of BPhe *a*.

A conclusive assignment to either axial histidines or the BPhe acceptor could be obtained from experiments with selective isotope labeling or with oriented samples. Between 110 and 90 ppm, three strong emissive signals are resolved at 108.5, 97.4 and 94.9 ppm. In addition, several weak features appear, for example at 106.2 and 101.0 ppm, where emissive signals have been observed in R26. Signals in this region can be assigned conveniently to methine carbons of BChl and BPhe cofactors. Assignment to histidines is unlikely since these resonances are not expected below 110 ppm.

The enhancement pattern in WT is rather different to that observed in R26, allowing identification of at least seven methine carbon resonances. Signals at 108.5 (prominent in WT) and 106.2 ppm (R26) can be assigned to C-15 carbons. The C-10 carbons may resonate at 101.0 (weakly observable in WT) and 101.0 ppm (R26). Signals at 99.2, 97.4 and 94.9 ppm can be assigned to C-5 and C-20 carbons. Simulations suggest that all three signals strongly

	BChl *a*				BPhe *a*	
carbon no.	σ_{liq} [a]	σ_{ss} [b]	σ_{ss} [c]	σ_{calc} [d]	σ_{ss} [c]	σ_{calc} [d]
3[1]	199.3	194.5		203.4		190.2
13[1]	189.0	188.2		197.1		188.1
17[3]	173.4	174.0		187.2		191.9
13[3]	171.6	171.4		183.7		162.8
6	168.9	170.2	166.8, 164.6	174.2	171.1	172.3
19	167.3	168.9	162.5, 159.7	174.4	169.9	168.4
14	160.8	160.7		164.7		147.4
9	158.5	158.0		162.8		167.2
16	152.2	150.1		160.1		162.6
1	151.2	153.5	148.2, 143.4	151.3	138.3	136.3
4	150.2	152.2		155.7		134.5
11	149.5	147.2	150.3, 154.2	160.6	138.9	140.3
2	142.1	140.7		150.8		132.1
3	137.7	136.1	130.2, 127.6	137.0	134.7	126.3
13	130.5	124.1	131.0, 131.3	134.4	126.4	125.6
12	123.9	119.9		132.9		120.4
15	109.7	105.8		119.0		110.6
10	102.4	100.0		109.5		99.6
5	99.6	98.8		106.4		101.7
20	96.3	93.7		105.9		97.2

[a]The liquid NMR chemical shift data σ_{liq} have been obtained in acetone-d_6.
[b](Matysik et al., 2001a), [c](Schulten et al., 2002), [d](Facelli, 1998).

Table 2.1. Chemical shifts of BChl *a* and BPhe *a*.

appearing in WT arise from the BPhe acceptor. A full list of light-induced signals with their tentative assignments is given in Table 2.2.

2.4.4 Simulated CIDNP spectra

To test for agreement between experiment and current theory of solid-state photo-CIDNP, we have simulated spectra for the polarization arising from a single photocycle (Figure 2.6 and 2.7) (Jeschke and Matysik, 2003). As a substitute for the dark signal, peaks at 30 ppm with 250 times the thermal polarization of a single ^{13}C nucleus at the respective field were added (asterisks). The field dependence of the photo-CIDNP amplitude is reproduced satisfactorily by these simulations (compare Fig. 2.3). Also in agreement with the experiment, the intensity pattern depends only weakly on the field (see normalized detail plots in Figure 2.7). The number of significantly enhanced signals agrees quite well between experiment and simulation. A more detailed comparison of the simulated and experimental patterns relies on the proper assignment of chemical shifts to the simulated peaks. The isotropic chemical shifts were originally taken from the reassigned solution data in (Facelli, 1998).

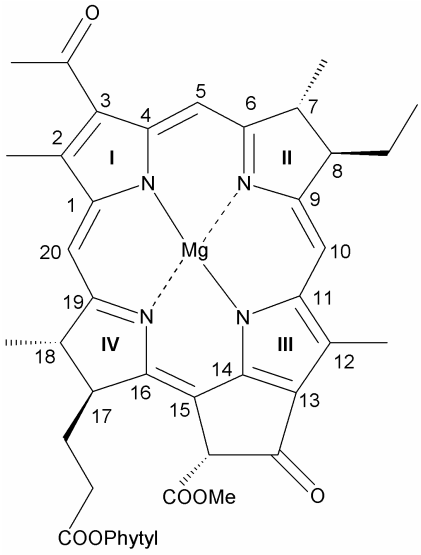

Figure 2.5. Structure of a BChl *a* molecule with numbering of carbon atoms.

For carbons that were safely assigned by 2D NMR techniques in (Schulten et al., 2002), these solution shifts were replaced by the solid-state isotropic shifts. For the remaining carbons the solution shifts were corrected to solid-state shifts whenever a clear assignment had been made in the present work (see above). The assignment of all signals in the simulated spectrum is given in Figure 2.7C. As the most obvious difference between experimental and simulated spectra, we note that the strongest enhancements in the simulated spectra are for carbon nuclei from the acceptor BPheo *a*, while in the experimental spectra, the strongest enhancements are observed for donor nuclei. Relative intensities of the acceptor Φ signals from carbons C-Φ1, C-Φ2, C-Φ3, C-Φ10, C-Φ12, C-Φ13, C-Φ15, and C-Φ20 in the simulation are in satisfying agreement with experiment, while the intensity of carbon C-Φ5 is clearly much smaller in the experiment than in the simulation. Interestingly, in the mutant strain R26 this signal does have the intensity expected from the simulation (see Figure 2.8).

The relative intensity of the carbonyl signal at 189.1 ppm is in quite good agreement with the intensities simulated for the acceptor carbonyls C-Φ3[1] and C-Φ13[1], although it has to be said that in the simulations two carbonyl signals are seen at all fields, while in the experimental spectra only one such signal is observed at 4.7 and 9.4 T.

For the signals assigned to the donor, agreement of relative intensities between experiment and simulation is clearly worse than for the acceptor signals. In particular, the signal of carbons C-M12 and C-L12 at 124.3 ppm is not observed experimentally at any field, except possibly at 17.6 T. Similarly, the signal of C-M4 and C-L4 at 149.9 ppm is hardly significant in the experimental spectra. In contrast, the group of signals between 153 and 165 ppm has

Cofactor and carbon no.	photo-CIDNP		
	$\sigma_{4.7T}$	$\sigma_{9.4T}$	$\sigma_{17.6T}$
Φ13[1]	189.4	-	-
M6	-	-	-
L19, M19	164.0	163.9	-
?	162.3	162.3	
?	160.8	160.7	161.0
M14	160.1	160.1	159.3
L9, M9	158.7	158.6	158.0
L16, M16	150.9	-	-
M1	153.6	153.6	153.0
M4	-	-	-
M11	145.3	145.5	144.7
M2	143.4	143.6	142.9
Φ1, Φ3	138.3	138.7	-
Φ2	134.0	133.9	-
?	132.8	132.8	-
Φ12	119.4	119.8	119.3
Φ15	108.5	109.1	108.4
Φ10, Φ5	101.8	-	-
	97.4	97.3	96.5
Φ20	94.9	95.0	94.2

Φ = BPhe acceptor, L, M = BChl cofactors L and M of the special pair.

Table 2.2. Tentative assignments of observed photo-CIDNP signals.

lower intensity in the simulation than in the experiment. However, most of the expected signals are indeed observed with relative intensities that do not differ too strongly from the simulations. All experimentally observed signals can be assigned to carbon nuclei that do exhibit strong signal enhancements in the simulations.

2.4.5 Comparison to R26

In WT all signals are emissive, whereas in R26 all low-frequency signals are absorptive and the signals at 132.8, 119.4 as well as all methine carbon resonances are emissive (Figure 2.8). In both WT and R26, the strongest photo-CIDNP signal appears at 160.8 ppm, however with opposite sign. The overall envelopes in the low-frequency region of the emissive photo-CIDNP spectrum of WT and the enhanced absorptive photo-CIDNP spectrum of R26 appear to be similar.

Our tentative assignments (Table 2.2, Figure 2.6C) suggest that, compared to the WT spectrum, donor signals in R26 have opposite sign while acceptor signals are hardly changed (see Chapter 3). Interestingly in R26, peaks appear at shifts where the signals of carbons C-

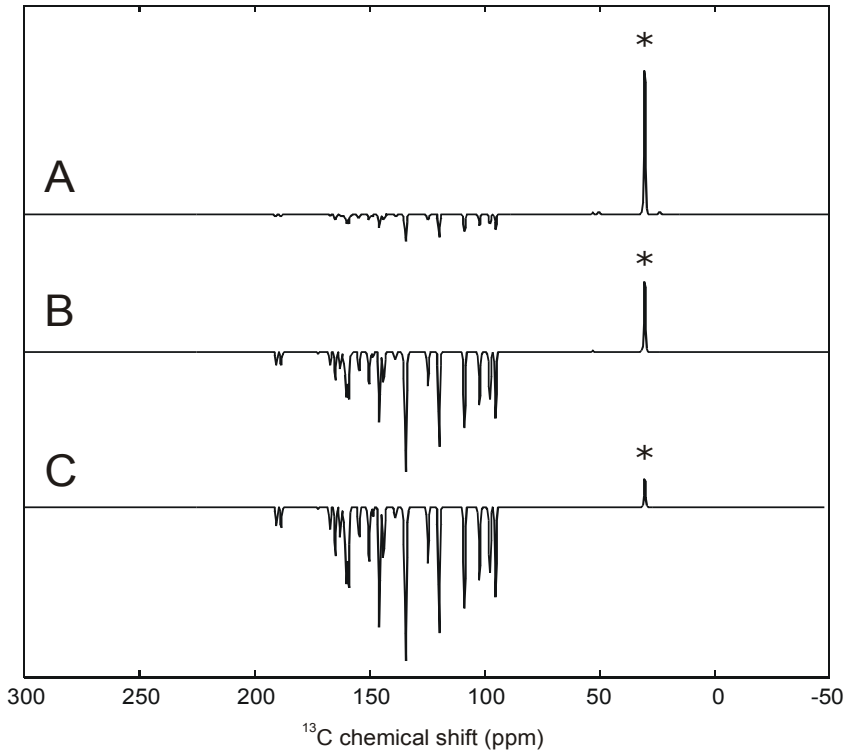

Figure 2.6. Simulated ^{13}C MAS NMR photo-CIDNP spectra corresponding to polarization generated in a single photocycle at 17.6 T (A), 9.4 T (B) and 4.7 T (C). The signals at 30 ppm (asterisks) were added for reference and correspond to 250 times the thermal polarization of a single ^{13}C nucleus at the respective field.

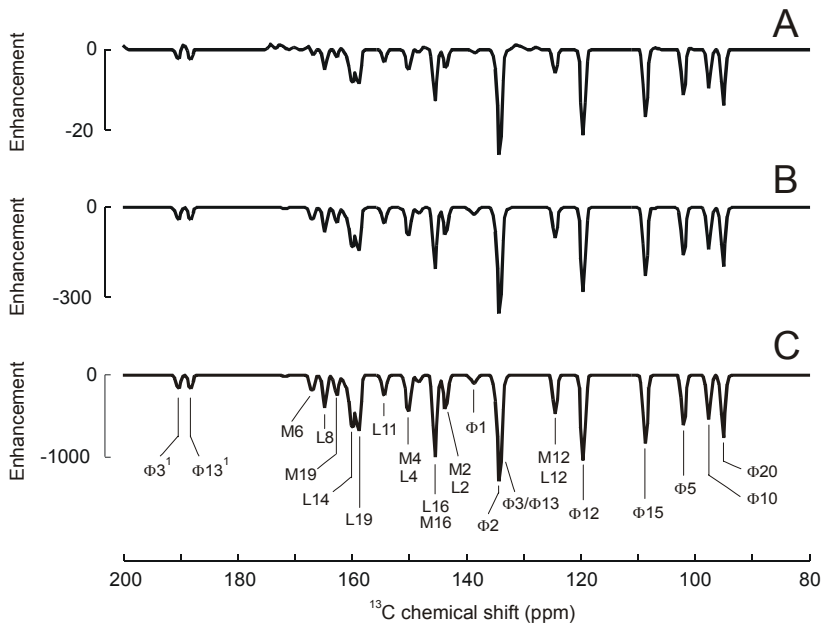

Figure 2.7. Details from the simulated ^{13}C MAS NMR photo-CIDNP spectra corresponding to polarisation generated in a single photocycle at 17.6 T (A), 9.4 T (B) and 4.7 T (C). All spectra were normalized to the intensity of the largest peak at 132 ppm. Abbreviations: Φ = BPhe acceptor, L, M = BChl cofactors L and M of the special pair.

Φ5 (101.0 ppm), C-M12/L12 (124 ppm), and C-M4/L4 (150.9 ppm) are expected from the simulations but not observed in WT. Experimental photo-CIDNP enhancements are a factor of ten higher than enhancements simulated for a single photocycle. This implies that the rate of photon absorption by a given RC is at least a factor of ten faster than the rate of longitudinal nuclear relaxation. As true photon absorption rates are difficult to estimate, we refrain here from a quantitative discussion of the absolute enhancement factors under steady state conditions.

2.5 Discussion

2.5.1 The electronic structure of the radical pair

The photo-CIDNP data presented here are obtained from unlabelled RCs. Therefore, the obtained photo-CIDNP intensities cannot be equalized by spin-diffusion processes but refer to the electron spin densities localised at the particular carbon atoms. Until now, signal assignments were difficult to check due to a lack of simulation methods. Here we obtain broad agreement of the number of signals and many relative intensities, between experiment and simulation. Hence, we can demonstrate for the first time that photo-CIDNP MAS NMR allows to study the radical pair state of a RC at atomic resolution, whereas other methods are usually limited to molecular resolution. Based on ^{1}H ENDOR data, an electron spin density distribution of the two donor BChl cofactors of 2:1 in favour of cofactor L in the active branch has been modeled for R26 (Lendzian et al., 1993). Our DFT computations suggest an electron spin density distribution of 3:2 in favour of cofactor L. Theoretical considerations show that for a polarization transfer based on the pseudosecular hyperfine coupling, the leading term of nuclear polarisation is proportional to the square of the anisotropy of the hyperfine coupling (Jeschke, 1998). One may thus expect that signals from cofactor L are by a factor of 1.5^2=2.25 stronger than those of cofactor M. In good agreement with this expectation we find intensity ratios in the range from 2 to 2.5 for equivalent carbon atoms in the L and M cofactor, respectively. Experimental resolution does not yet permit the extraction of reliable relative intensities of signals from equivalent carbons in the L and M cofactors from the experimental spectra. An experimental determination of this ratio should be feasible using a ^{13}C-labelled sample with the labelling pattern of (Schulten et al., 2002). Signals C-M19 and C-L19 should then be resolved.

Interestingly, the electron density distribution is significantly asymmetric in our DFT computation that neglects all matrix effects except for histidine coordination. Closer examination of the structures shows that the two cofactors differ in deviations of the macrocycle from planarity and in sidegroup conformations. These differences are very likely imposed by the matrix. They appear to correspond to sufficiently deep local minima on the energy hypersurface to be stable in a geometry optimization by DFT. The sidegroups in

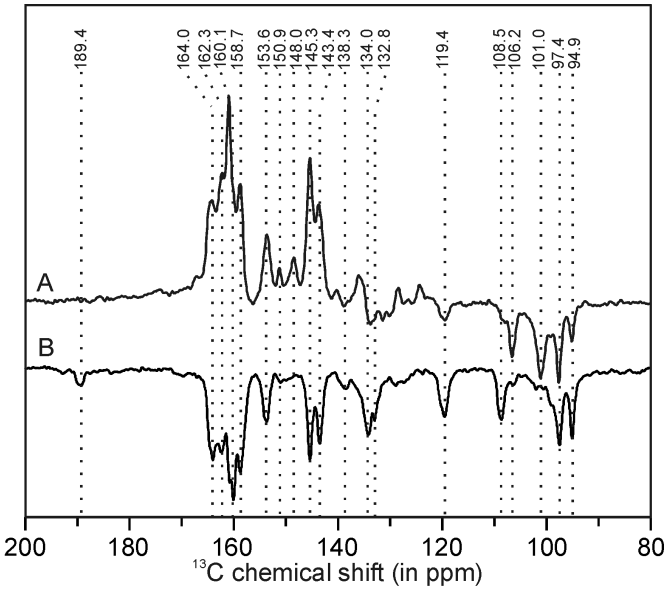

Figure 2.8. Comparison of ^{13}C MAS NMR photo-CIDNP spectra of bacterial photosynthetic reaction centers: (A) Carotinoidless mutant strain R26. (B) Wild type.

chlorophylls and pheophytins might thus be levers used by nature for fine tuning of the electronic structure of these pigments or their assemblies. It is somewhat surprising that enhanced aromatic signals of the BPhe *a* macrocycle are almost exclusively situated at lower shifts than those of the BChl *a* macrocycles. Possibly this is related to a correlation between electronic ground state and radical electron densities. The strongly enhanced nuclei in BPhe *a* correspond to high spin density in an anion radical, whose singly occupied molecular orbital (SOMO) is related to the lowest unoccupied molecular orbital (LUMO) of the ground state. Conversely, enhanced signals in BChl *a* correspond to high spin density in a cation radical, whose SOMO is related to the highest occupied molecular orbital (HOMO) of the ground state.

2.5.2 Strongest effect

For carbons C-Φ3[1], C-Φ10, C-L8, and C- L19 we have computed the photo-CIDNP effect as a function of the magnetic field B_0 in steps of 1 T (Figure 2.9). The maximum absolute nuclear polarisation is obtained at fields between 3 and 5 T. Field dependence of detection sensitivity for constant polarisation follows a scaling law with an exponent between 1 and 7/4 (Minard and Wind, 2001). Even with $B_0^{7/4}$ scaling, the maxima of photo-CIDNP sensitivity virtually coincide with the maxima of absolute nuclear polarisation. Therefore, photo-CIDNP ^{13}C MAS NMR experiments at fields between 3 and 5 T are expected to provide best sensitivity. The photo-CIDNP enhancement with respect to thermal polarisation increases monotonously with decreasing field. Photo-CIDNP signals that overlap with dark signals may thus be easier to recognize at even lower fields. We have also checked by simulations for selected nuclei how much of the polarisation is contributed by the individual mechanisms. For

instance, the total polarisation of -1238 times thermal equilibrium polarisation (TEP) for carbon C-Φ2 is composed of a larger negative contribution from the TSM mechanism (-1449 TEP) and a smaller positive contribution from the DD mechanism (211 TEP). For carbon C-L16, the total polarisation of -727 TEP is made up of a TSM contribution of -603 TEP and a DD contribution of -124 TEP. For donor nuclei, the DD and TSM contributions have the same sign, while they counteract each other for acceptor nuclei. This is because the sign of the DD contribution depends on the sign of the *g* value difference, which is opposite for acceptor and donor nuclei (Jeschke and Matysik, 2003).

2.5.3 Completeness of theory

Several relevant parameters, such as exchange and dipole-dipole coupling between the two electron spins and lifetimes of singlet and triplet pairs are known with only limited precision. Furthermore, principal axes directions of interaction tensors computed by DFT may deviate from true directions by a few degree and hyperfine couplings computed by DFT may well deviate by 20-30% from true values for the computed molecule and geometry. The neglect of the protein matrix, except for the directly coordinated histidines, may introduce further errors of the hyperfine couplings, and possibly even into the detailed spin density distribution over the molecule. Considering all these uncertainties, the agreement of the simulated and experimental photo-CIDNP spectra for WT reaction centers is as good as it can be expected. The same is not true for spectra of R26 reaction centers (see Chapter 3). Even when varying the *J* coupling, dipole-dipole coupling, and the radical pair lifetimes within reasonable ranges, we cannot reproduce the pattern of mainly absorptive donor polarization and mainly emissive acceptor polarization that we observe experimentally. In fact, we do not find any parameter set that produces both strong emissive and strong absorptive polarization for any assignment of the nuclei. This finding and the fact that even in WT the agreement is worse for donor than for acceptor nuclei suggest that the nuclear polarisation changes during the lifetime of the donor triplet.

In WT, where this lifetime is only 100 ns, the changes are relatively minor. Apparently, the emissive polarization of donor nuclei is somewhat enhanced, as it is larger than expected relative to the acceptor polarisation. In R26, where the triplet lifetime is 100 µs, the donor polarization changes sign, although relative intensities change only slightly. A detailed study of possible mechanisms for polarisation build-up during the triplet lifetime is shown in Chapter 3. It may be remarked that, in contrast to the situation in the radical pair, in the triplet state transfer of electron spin polarisation to nuclear polarisation by coherent spin evolution is negligible. This is because in the triplet state there is no near degeneracy of levels with different electron spin quantum numbers that could be mixed by the hyperfine interaction. Hence it is more likely that the additional polarisation is generated from chemically induced nuclear coherence (CIDNC) (Jeschke, 1997). In the radical pair state, build-up of CIDNC is

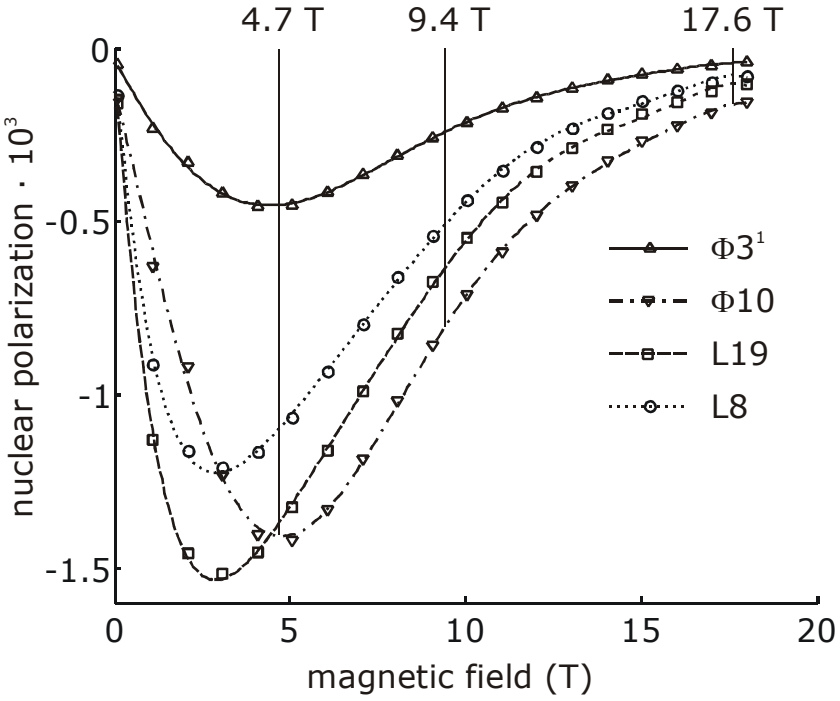

Figure 2.9. Simulated field dependence of ^{13}C NMR photo-CIDNP effects for nuclei C-Φ3^1 and C-Φ10 of the BPheo *a* (acceptor) and C-L8 and C-L19 of BChl *a* (cofactor L of the special pair donor). Computed values are plotted as marker symbols, lines are guides to the eyes.

expected to be stronger than build-up of CIDNP (Jeschke and Matysik, 2003). As the hyperfine field at the nuclei is negligible in the T_0 manifold of the donor triplet but has significant pseudo-secular components in the T_{-1} and T_{+1} manifolds, CIDNC is transferred to CIDNP to a significant extent if and only if recombination of the triplet radical pair also populates T_{-1} or T_{+1} sublevels. This consideration is supported by preliminary simulations. Depending on the relative populations of T_{-1} or T_{+1} sublevels, such a mechanism could explain the sign change. It could also explain that relative intensities change only slightly. Further theoretical and experimental work is needed to prove or refute this mechanism.

3 Field dependent photo-CIDNP in reaction centers of *Rhodobacter sphaeroides* R26: A sensitive and precise tool for detection of small changes in electronic structure

3.1 Abstract

Photochemically induced dynamic nuclear polarisation (photo-CIDNP) is observed in frozen photosynthetic reaction centers of the carotenoid-less strain R26 of the purple bacteria *Rhodobacter sphaeroides* by ^{13}C solid-state NMR at three different magnetic fields (4.7 T, 9.4 T and 17.6 T). The overall shape of the spectra remains independent of the magnetic field and can be semi-quantitatively explained by simulating spin dynamics in the radical pair state and nuclear relaxation in the donor triplet state. The strongest enhancement is observed at 4.7 Tesla, allowing observation of photo-CIDNP enhanced NMR signals from reaction center cofactors in entire bacterial cells. The correlation of chemical shift in the electronic ground state with the hyperfine interaction in the radical pair and triplet states inherent in this experiment and its high sensitivity allow for the detection of subtle changes in the electronic structure.

3.2 Introduction

Photochemically induced dynamic nuclear polarization (photo-CIDNP) is a method to increase NMR intensities by induction of photochemical reactions, which shuffle the nuclear spin system out of its Boltzmann equilibrium. In contrast to optical pumping, photo-CIDNP does not require polarized radiation. Photo-CIDNP in solution NMR is explained by the radical-pair mechanism where nuclei in singlet and triplet radical pairs gain opposite polarization (Hore and Broadhurst, 1993; Goez, 1997). They can later be observed separately as the radicals diffuse apart and, depending on their spin state, meet a different chemical fate (Closs and Closs, 1969; Kaptein and Oosterhoff, 1969). This mechanism is not feasible in the solid-state for lack of diffusion and not observable for cyclic reactions where the opposite polarization cancels. In solids, photo-CIDNP can be observed by magic-angle spinning (MAS) NMR, a method which overcomes line-broadening due to chemical shift anisotropy (CSA) in solids and allows for detailed analysis of structure, dynamics and functional mechanisms of membrane-bound protein systems (de Groot, 2000; Laws et al., 2002).

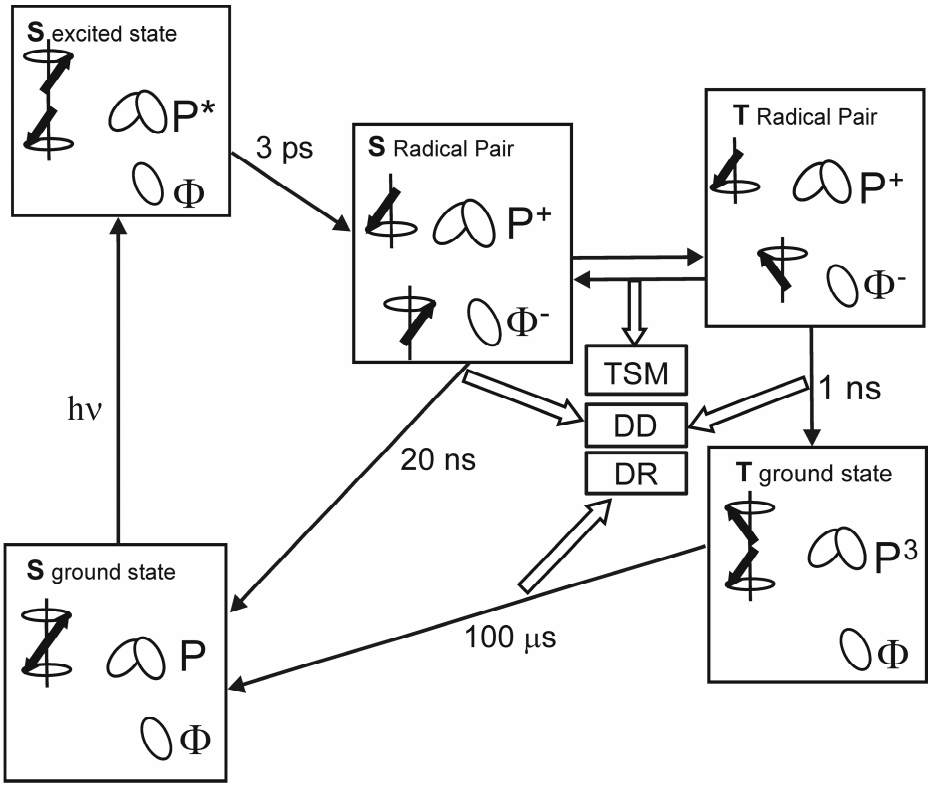

Figure 3.1. Reaction cycle in quinone blocked bacterial RCs. After light-induced electron transfer from the primary donor (P) to the bacteriopheophytin (ϕ), an electron polarized singlet radical pair is formed. The electron polarization is transferred to nuclei via three-spin mixing (TSM) within the radical pair and, via differential decay (DD) due to the difference in lifetime of the two radical pair states. Cancellation of incomplete nuclear spin polarization during long-lived donor triplet is by differential relaxation (DR).

In the solid-state, photo-CIDNP has been observed for the first time in quinone blocked frozen reaction centers (RCs) of *Rhodobacter (Rb.) sphaeroides* R26 and WT under continuous illumination with white light (Zysmilich and McDermott, 1994, 1996b, 1996a; Matysik et al., 2000b; Matysik et al., 2001a; Schulten et al., 2002) (Chapter 2). Photo-CIDNP has not only been observed in bacterial RCs, but in plant photosystems I and II as well (Matysik et al., 2000a; Alia et al., 2004b; Diller et al., 2005).

Upon photochemical excitation of the primary electron donor P, which in RCs of purple bacteria is a BChl dimer composed of P_L and P_M, an electron is emitted to the primary acceptor, a bacteriopheophytin (BPhe) molecule Φ, forming an electron-polarised singlet radical pair (Figure 3.1). In quinone-reduced or depleted RCs, further electron transfer is blocked. Therefore, the singlet radical pair can either relax to the electronic ground state or, depending on the strength of the applied magnetic field, is transferred to a triplet radical pair. The triplet radical pair recombines to a special pair triplet ^3P and an acceptor singlet. Finally, the donor triplet also relaxes to the singlet ground state, so that the entire process is cyclic and opposite polarization originating from singlet and triplet spin-correlated radical pairs cancels.

If the nuclear spin relaxation is significant during the lifetime of the triplet state, this cancellation is not complete (Hore and Kaptein, 1982). Such differential relaxation (DR) was predicted for photosynthetic RCs and later invoked as explanation for the first experimental solid-state photo-CIDNP results (Goldstein and Boxer, 1989; McDermott et al., 1998). However, the DR mechanism could not explain the observed signals from the bacteriopheophytin acceptor, which does not undergo intersystem crossing, and from wild type RCs with a triplet lifetime that is three orders of magnitude shorter. Photo-CIDNP in solids has thus been explained by the simultaneous action of two other mechanisms (Jeschke and Matysik, 2003). In the electron-electron-nuclear three-spin mixing (TSM) mechanism, net nuclear polarization is created in the spin-correlated radical pair due to the presence of both anisotropic hyperfine interaction and coupling between the two electron spins (Jeschke, 1998). In the Differential Decay (DD) mechanism, a net photo-CIDNP effect is caused by anisotropic hyperfine coupling without an explicit requirement for electron-electron coupling if spin-correlated radical pairs have different lifetimes in their singlet and triplet states (Polenova and McDermott, 1999). Based on this approach of two parallel mechanisms, we have been able to explain the ^{13}C photo-CIDNP spectrum of WT RCs, which shows entirely emissive photo-CIDNP signals (Chapter 2). However, in RCs of the carotenoidless R26 strain, having a long lifetime of the donor triplet, the donor signals appear enhanced absorptive. This raises the question whether the DR mechanism is operative in the carotenoidless strain in addition to the two other mechanisms. This Chapter examines this question and, based on the understanding of the origin of the polarization patterns, discusses subtle differences in the electronic structure of the radical pair between RCs of the WT and R26 strains as well as between isolated RCs and whole cells of the R26 strain.

3.3 Materials and Methods

3.3.1 Sample Preparation

The reaction centers (RCs) from *Rb. sphaeroides* R26 were isolated by the procedure of Feher and Okamura (Feher and Okamura, 1978). The removal of Q_A has been done by incubating the RCs at a concentration of 0.6 μM in 4% LDAO, 10 mM o-phenanthroline, 10 mM Tris buffer, pH 8.0, for 6 h at 26 °C, followed by washing with 0.5 M NaCl in 10 mM Tris buffer, pH 8.0, containing 0.025% LDAO and 1 mM EDTA (Okamura et al., 1975). Approximately 5 mg of the RC protein complex embedded in LDAO micelles was used for NMR measurements.

The cells were harvested and suspended in Tris buffer. 70 μL of this cell suspension was used for the experiment. The RCs in the cells were reduced with 0.05 M sodium dithionite in Tris buffer prior to experiments.

3.3.2 MAS-NMR Measurements

The NMR experiments at different fields were performed with DSX-750, DMX-400 and DMX-200 NMR spectrometers equipped with magic angle spinning (MAS) probes. The sample was loaded into a clear 4-mm sapphire rotor and inserted into the MAS probe. The sample was frozen slowly at a low spinning frequency of $\nu_r = 400$ Hz to ensure a homogenous sample distribution against the rotor wall (Fischer et al., 1992). The light and dark spectra were collected with a Hahn echo pulse sequence and TPPM proton decoupling (Bennett et al., 1995). ^{13}C MAS NMR spectra were obtained at a temperature of 223 K under continuous illumination with white light (Matysik et al., 2000b). The rotational frequency for MAS was 8 kHz. For the three fields of 4.7, 9.6 and 17.6 Tesla, a line broadening of 20 Hz, 50 Hz and 120 Hz, respectively, was applied prior to Fourier transformation. In all cases, a cycle delay of 4 s was used. All the ^{13}C-MAS NMR spectra were referenced to the ^{13}COOH response of solid tyrosine•HCl at 172.1 ppm.

3.3.3 Concentration of special pair BChl molecules

Optical density of the sample at 865 nm has been determined to be 1.28. Using an absorbtion coefficient of 75 $mM^{-1}cm^{-1}$ and a ratio of special pair BChls to all BChl *a* cofactors of 2:300 a sample concentration of ~100 nM has been calculated (Hu et al., 2002).

3.3.4 Simulations

Simulations of the coherent spin evolution in the radical pair state and Density Functional Theory (DFT) computations of hyperfine couplings for the triplet state of the special pair donor were performed as described in Chapter 2. The hyperfine anisotropy ΔA of individual carbon nuclei was calculated from the DFT-computed eigenvalues A_{xx}, A_{yy}, and A_{zz} of the hyperfine tensor as $\Delta A = A_{zz}-(A_{xx}+A_{yy})/2$, where A_{zz} is the eigenvalue whose absolute value is maximum. Polarization originating from singlet and triplet pairs was stored separately. Nuclear spin relaxation in the triplet state was taken into account on the basis of Solomon theory by multiplying triplet polarization with a decay factor $\exp(-C\,\Delta A^2\,T_T)$, where T_T is the lifetime of the special pair triplet (Solomon, 1955). The fit parameter C takes the same value for all ^{13}C nuclei within the same spectrum but may vary with magnetic field.

3.4 Results and discussion

3.4.1 Polarization pattern for the R26 strain

The photo-CIDNP spectrum of R26 RCs (Figure 3.2A) exhibits peaks at very similar chemical shifts as the one from WT RCs (Figure 3.2B). However, signals at chemical shifts larger than 135 ppm are absorptive for R26 in agreement with previous work, whereas the whole spectrum is emissive for WT (Zysmilich and McDermott, 1994, 1996b, 1996a; Matysik et al., 2000b). The magnetic field dependence has been measured in dark (Figure 3.3) and in

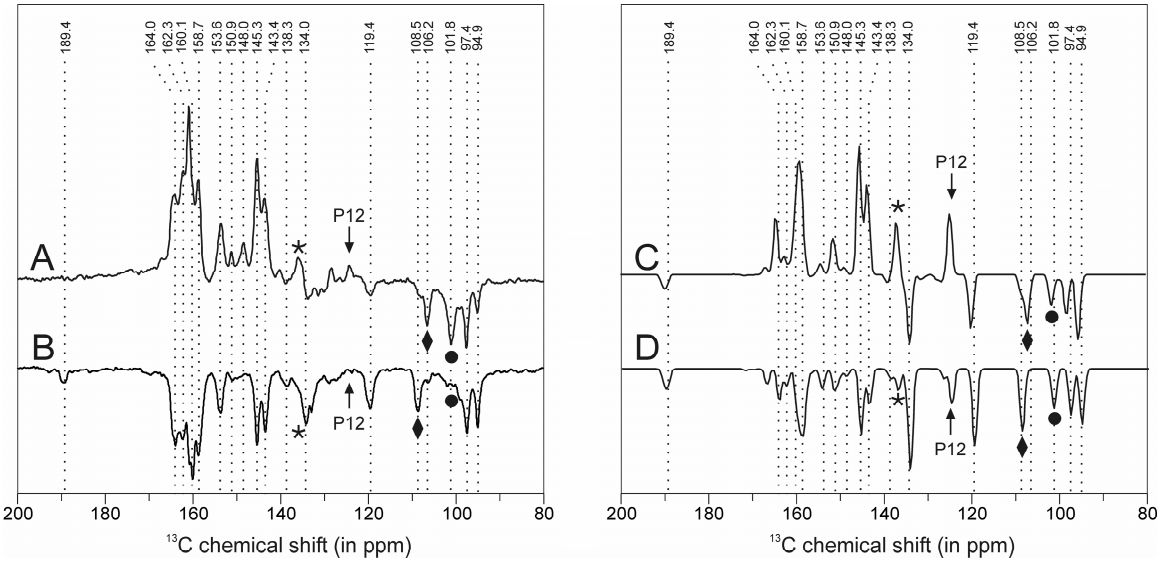

Figure 3.2. ^{13}C photo-CIDNP MAS NMR spectra of RCs of *Rb. sphaeroides* at 223 K and a field strength of 4.7 T. Arrows, asterisks, diamonds, and full circles denote signals that appear to be sensitive to the environment of the RCs and are discussed in the text. Experimental spectrum of (A) R26 RCs and (B) WT RCs. Simulated spectrum of (C) R26 RCs, assuming a lifetime of 100 µs for the triplet state of the special pair. (D) WT RCs assuming a lifetime of 100 ns for the triplet state of the pair.

light (Figure 3.4) for R26 at A: 17.6 T (750 MHz), B: 9.4 T (400 MHz) and C: 4.7 T (200 MHz). For WT, the field dependence has been reported in Chapter 2. This general photo-CIDNP pattern persists at all magnetic fields where the spectra were studied. Our previous assignment (Chapter 2) suggests that the sign change is restricted to signals from ^{13}C nuclei of the special pair. Indeed a simulation including the DR mechanism reproduces the sign change in this range of chemical shifts (Figure 3.2C, D) assuming $C = 4 \cdot 10^{-11}$ s and triplet lifetimes of 100 µs for R26 RCs. We have tested the plausibility of the only fit parameter C by computing the longitudinal relaxation time T_1 for a hypothetic ^{13}C nucleus that is 5 Å away from a paramagnetic center with the same C value (ΔA = 159 kHz). We find T_1 = 0.99 s, which appears reasonable. The fast decay of polarization of some nuclei in the triplet state of the special pair is due to anisotropic hyperfine couplings of the order of 10 MHz. These large couplings are in turn caused by substantial spin density of up to 11.4% in p orbitals on these carbon atoms. The simulations also reproduce the field dependence of the polarization (Figure 3.5), with C values corresponding to T_1 = 0.66 s at 9.4 T and 0.40 s at 17.6 T for a hypothetical ^{13}C nucleus 5 Å away from the paramagnetic center.

In both, WT and R26 centers, the relative peak intensities are only roughly reproduced by the simulations (compare Figure 3.2A, B with C, D). This is not unexpected, as experimental values like the exchange coupling between the two electron spins in the pair as well as life times of singlet and triplet radical pairs and DFT-computed values, such as the ^{13}C hyperfine couplings can well deviate by 20-30% from right values. The only deviation that appears

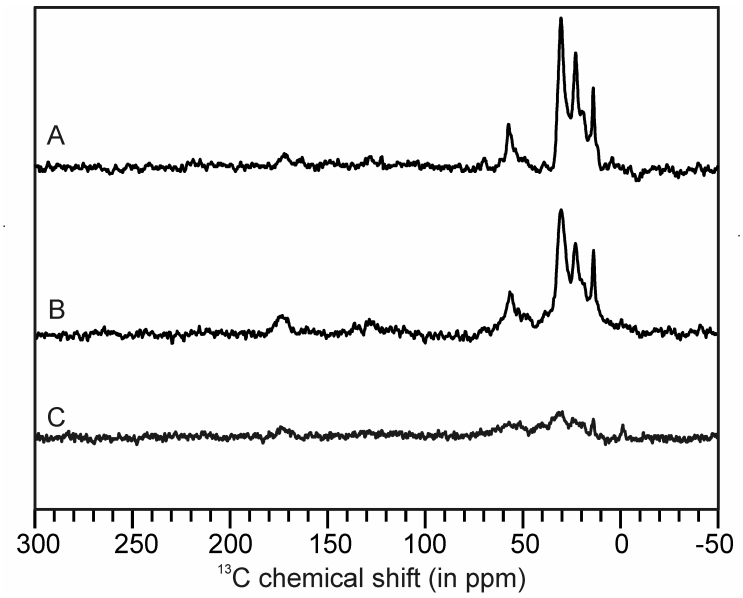

Figure 3.3. ^{13}C MAS NMR spectra of quinone-depleted RCs of *Rb. sphaeroides* obtained at 223 K in the dark at different magnetic fields of 17.6 T (A), 9.4 T (B) and 4.7 T (C).

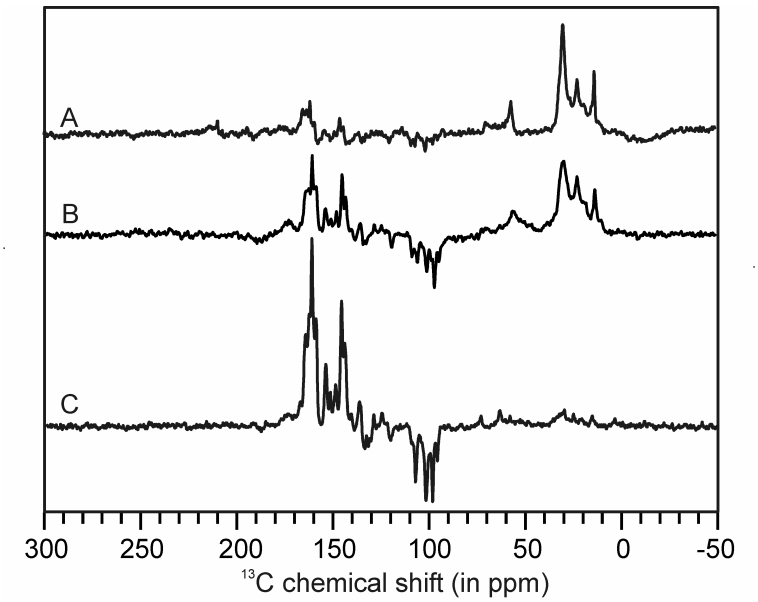

Figure 3.4. ^{13}C MAS NMR spectra of quinone-depleted RCs of Rb. sphaeroides obtained at 223 K under illumination with continuous white light at different magnetic fields of 17.6 T (A), 9.4 T (B) and 4.7 T (C).

really significant is the substantial polarization of the ^{13}C nucleus C-L12/ C-M12 that is predicted by the simulations for both WT and R26 centers, whereas only a weak emissive signal in R26 RCs is observed experimentally at 124.6 ppm (arrows in Figure 3.2). Interestingly, earlier ENDOR and special TRIPLE measurements have detected a sizeable isotropic proton hyperfine coupling for the methyl group attached to this carbon atom (Lendzian et al., 1993; Lubitz et al., 2002). This coupling changes strongly when His M202,

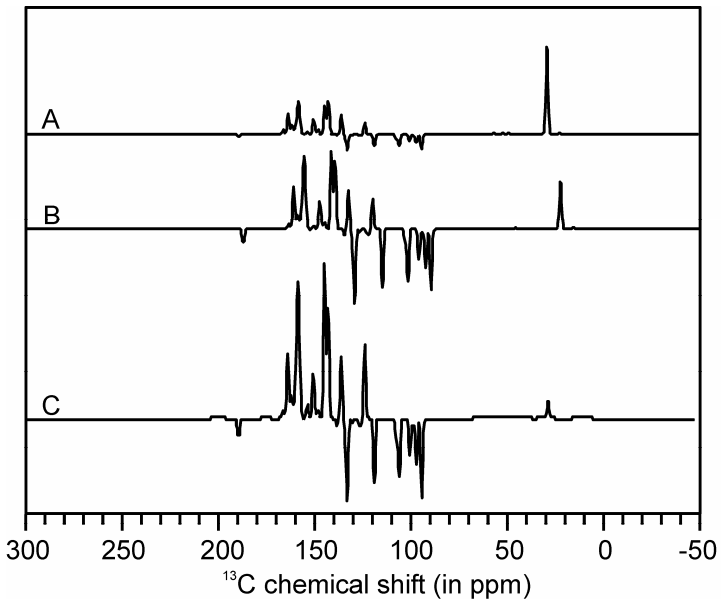

Figure 3.5. Simulated ^{13}C MAS NMR spectra of RCs of *Rb. sphaeroides* strain R26 at different magnetic fields assuming a lifetime of 100 µs for the triplet state of the special pair. The magnetic fields are 17.6 T (A), 9.4 T (B) and 4.7 T (C).

which is directly coordinated to the special pair, is mutated to Leu or Glu. The unexpectedly low photo-CIDNP intensity at position C-L12/ C-M12 may thus indicate an influence of the protein environment on the spin density distribution that is not accounted for in the simplified model of the RC used in our DFT computations.

3.4.2 Implications for the interpretation of solid-state photo-CIDNP spectra

The broad agreement of the photo-CIDNP patterns and their field dependence between experiment and *ab initio* simulations for both WT and R26 RCs lends confidence to the notion that a combination of the DR, TSM, and DD mechanisms is responsible for the non-equilibrium nuclear polarization. In addition, it supports our previous chemical shift assignments (Table 3.1) that were based on results from 2D NMR and DFT computations of chemical shifts by others and ourselves (Facelli, 1998), (Schulten et al., 2002) (Chapter 2 and 4). We may thus interpret the polarization pattern of WT RCs in terms of the spin density distribution in the radical pair state and the polarization change between the WT and R26 spectra in terms of the spin density distribution in the triplet state of the donor. To do so, we note that for all three mechanisms the polarization of a given ^{13}C nucleus is roughly proportional to the square of the anisotropic hyperfine coupling of that nucleus. The technique is thus particularly sensitive to spin density in p orbitals. For instance, the ^{13}C with a shift of 136.8 ppm (asterisks in Figure 3.2), assigned to C-L4 in the special pair, has a higher spin density in its p orbital in the triplet state than in the radical pair state, according to both experiment (Figure 3.2A, B) and simulation (Figure 3.2C, D).

Cofactor carbon no	photo-CIDNP WT[a]	photo-CIDNP R26[b]
Φ13[1]	189.4	-
L6	164.0	164.4 A
M19	162.3	162.5 A
M14	160.1	161.0 A
L9, M9	158.7	158.8 A
M16	150.9	151.3 A
L11	153.6	153.7 A
M1	-	148.6 A
L16	145.3	145.6 A
M2	143.4	143.8 A
Φ1, Φ3	138.3	138.8 E
L4	-	136.8 A
Φ2	134.0	133.7 E
L12, M12	-	124.6 A
Φ12	119.4	119.7 E
Φ15	108.5	106.8 E
Φ10	-	101.3 E
Φ5	97.4	97.8 E
Φ20	94.9	95.2 E

A = absorptive, E = emissive.
[a] (Schulten et al., 2002), Chapters 2 and 4
[b] This work

Table 3.1. Tentative assignments of the ^{13}C photo-CIDNP NMR signals.

The high sensitivity of chemical shifts to changes in the electronic structure of the ground state allows for a detailed comparison of WT and R26 RCs. Two remarkable changes are apparent in Figure 3.2A, B. First, a strong peak is detected at 108.5 ppm in WT (♦) and a weak peak at 106.2 ppm, while in R26 the ratio is inverted. This peak is assigned to the acceptor nucleus C-Φ15. Possibly, the difference may be due to different states of the protein pocket from which the quinone has been removed (see below). Second, the peak at 101.8 ppm that is predicted for both WT and R26 centers is actually observed only in R26 (●). This peak is assigned to the acceptor nucleus C-Φ10, for which a strong signal has been calculated (Figure 2D). Therefore, the absence of this signal in Figure 3.2B indicates a disturbed environment, which may be due to the empty quinone pocket, while this pocket may be refilled with a substituting molecule maintaining the structure in Figure 3.2A.

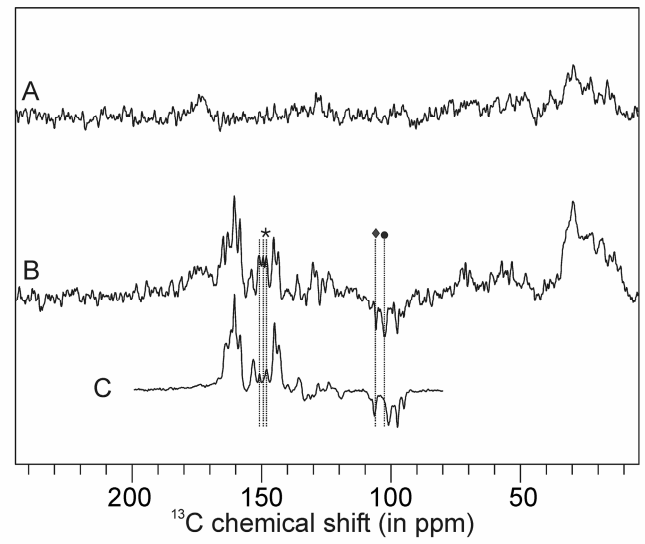

Figure 3.5. ^{13}C solid-state MAS NMR spectra of intact *Rb. sphaeroides* R26 cells at a field strength of 4.7 T and spinning frequency of 8 kHz in (A) dark, (B) light and RCs in (C) light.

3.4.3 Nanomolar concentrations probed in intact cells

The strong photo-CIDNP enhancement at a field strength of 4.7 T enables the study of cofactor molecules in their native cellular environment at a concentration of ~100 nM without isotope enrichment. The dark spectrum of the intact cells of *Rb. sphaeroides* R26 (Figure 3.5A) shows broad peaks at 173 and 35 ppm. Under illumination (Figure 3.5B) the photo-CIDNP signals from the donor and acceptor appear. The light-induced signals appear in the region from 90 to 170 ppm. The overall photo-CIDNP intensity pattern is similar, but in some respects distinct from the spectrum of isolated reaction centers at 4.7 T (Figure 3.5C). The similarity between the photo-CIDNP spectrum from the isolated RCs and intact cells suggests that the ground state electronic structure of the special pair is not strongly influenced by the surrounding protein complexes in the natural environment of an intact cell. The signals of acceptor nucleus C-Φ15 and C-Φ10 in R26 cells (♦, ●) (quinone-reduced) are observed at 106.1 ppm and 102.3 ppm, in agreement with the isolated R26 RCs (quinone-depleted), suggesting that in isolation the quinone binding site is not disturbed. In the shift range between 148 and 152 ppm, signals that are assigned to C-M1 and C-M16 exhibit significantly stronger absorptive polarization in cells compared to isolated reaction centers. Considering the behavior of the same peaks in isolated RCs of WT and R26 as well as in cells, we can identify position C-M1 and C-M16 as a hot spot, where electron spin density appears to depend strongly on small changes in the environment of the special pair.

In conclusion, photo-CIDNP MAS NMR allows for the selective study of moderately sized molecules in an intact cell at natural abundance (1% ^{13}C). Combination with ^{13}C-isotope labeling is expected to further increase the signal by a factor of 100 to a total enhancement factor of a million. Such a strong polarization source might be used in the near future as a

"spin torch" for illuminating the vicinity of RCs, or their artificial equivalents, by secondary polarization transfer.

4 Ground state electronic structure of active cofactors in *Rhodobacter sphaeroides* reaction centers revealed by ^{13}C photo-CIDNP MAS NMR

4.1 Abstract

Photo-CIDNP MAS NMR studies have been performed on reaction centers (RC) of *Rhodobacter sphaeroides* wild type (WT) that have been selectively isotope labelled using (5-^{13}C)-δ-aminolevulinic acid•HCl in all the BChl and BPhe cofactors at positions C-4,5,9,10,14,15,16 and 20. ^{13}C solid-state CP/MAS NMR and ^{13}C-^{13}C dipolar correlation photo-CIDNP MAS NMR provides insight into the ground state electronic structure of the cofactors involved in the electron transfer process in the RC at the atomic scale. The ^{13}C-^{13}C dipolar correlation spectra reveal three strong components assigned to two BChls, P1 and P2, and one BPhe, Φ_A. There is in addition a weak component observed assigned to another BChl, denoted as P3. In the BChls the electron spin density appears to be strongly delocalised over P1 and P2. An almost complete assignment of all the carbon atoms in the aromatic systems of BChl and BPhe has been achieved in combination with previous photo-CIDNP studies on site-directed BChl/BPhe labelled RC (Schulten et al., 2002). The entire ground state electronic structure of all the photochemically active cofactors has been effectively mapped for the first time. One BChl, P2 has well distinguished chemical shifts among the photochemically active BChls suggesting a 'special' BChl. The other two BChls P1 and P3 have similar chemical shifts as BChl *a* in solution and are quite normal. The reason for the anomaly of P2 is discussed.

4.2 Introduction

Photosynthesis in purple bacteria is driven by light-induced electron transfer in the reaction center protein (RC) located in the intracytoplasmic membrane RC of *Rhodobacter (Rb.) sphaeroides* wild type (WT). The RC is a transmembrane protein complex consisting of three polypeptide chains H, M and L and nine cofactors (Yeates et al., 1988; Ermler et al., 1994; Camara-Artigas et al., 2002) (for review, see (Hoff and Deisenhofer, 1997)). Four BChl molecules, two BPhe molecules, two ubiquinones (Q) and a non-heme ferrous iron (Fe^{2+}) are arranged in two nearly symmetric branches (Figure 4.1). The initial process of electron transfer takes place via the "active" A-branch while the B-branch is "inactive". It is generally believed that the primary donor is the 'special pair' (P), a dimer formed of two strongly

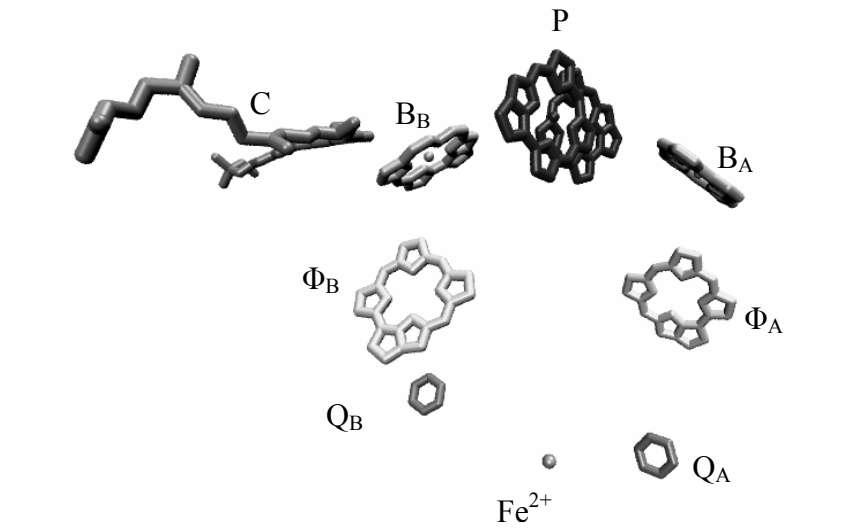

Figure 4.1. Detailed view of the cofactor arrangement in the RC of *Rb. sphaeroides* WT. The aliphatic chains from BChl, BPhe and Q are omitted for clarity.

coupled BChl cofactors P_L and P_M. The primary acceptor is a BPhe molecule, Φ_A. The remaining two accessory BChls, B_A and B_B, are monomers. The tenth cofactor in *Rb. sphaeroides* WT is a carotenoid molecule (C) that breaks the overall symmetry of the cofactor arrangement. It is located near B_B.

After photochemical excitation of P to P*, an electron is transferred to the primary electron acceptor Φ_A within 3 ps, forming the radical pair state $P^{+\bullet}\Phi_A^{-\bullet}$. In the next step, an electron is transferred to the primary quinone acceptor Q_A in about 200 ps. Subsequently, an electron is transferred from Q_A to the final acceptor Q_B. In quinone-depleted reaction centers, the forward transfer from BPhe to Q_A is blocked.

It has been proposed that the excited state P* is electronically asymmetric with more electron density centered on P_M. This electronic asymmetry may be related to the hydrogen-bonding environment of the keto groups (Moore et al., 1999). The electronic structure of the cation radical P^+ has been extensively investigated with EPR, ENDOR and TRIPLE resonance studies (Lendzian et al., 1993; Rautter et al., 1994; Lubitz et al., 2002). The studies have shown that the unpaired electron is unequally distributed over P_L and P_M favoring P_L with a ratio of 2:1. This agrees well with photo-CIDNP MAS NMR investigations on RCs from *Rb. sphaeroides* (WT) reporting a ratio of electron spin density 3:2 in favour of P_L (Chapter 2). The knowledge of P in the electronic-ground state is limited. Resonance Raman studies suggest differences with P_L and P_M in the special pair (Mattioli et al., 1991; Palaniappan et al., 1993) but no details are known.

The involvement of accessory BChl B_A molecule as a real intermediate in the electron transfer to Φ_A has been a matter of debate (for review, see: (Hoff and Deisenhofer, 1997) Absorbance difference spectroscopy with femtosecond time resolution did not see any

involvement of B_A (Martin et al., 1986). On the other hand, transient femtosecond measurements found a biphasic kinetics which could only be interpreted as a two-step model of electron transfer suggesting the involvement of B_A. (Holzapfel et al., 1989, 1990; Holzwarth and Muller, 1996) Subpicosecond transient measurements however have suggested that both, the two-step hopping and the one-step superexchange model of ET may co-exist (Chan et al., 1991). Recently, both these mechanisms have found relevance in the development of molecular wires (Weiss et al., 2004). There has also been a suggestion for a pathway of electron transfer that does not involve the excited state of the special pair dimer (P*), but instead is driven by the excited state of the monomeric BChl (B_A*) (van Brederode et al., 1999). An alternative interpretation based on spin couplings suggest electron transfer from P* to $P^{+\bullet}\Phi_A^{-\bullet}$ with the involvement of a trip-trip-singlet $B^TB_A{}^T$ as a real intermediate between the excited charge separated P* state and the primary charge separated, $P^{+\bullet}\Phi_A^{-\bullet}$(Fischer et al., 1992).

Magic-Angle Spinning (MAS) solid-state NMR is a powerful tool for studying structure and dynamics of membrane proteins (de Groot, 2000). Photochemically induced dynamic nuclear polarization (photo-CIDNP) MAS NMR in combination with site-directed ^{13}C-labeled BChl/BPheo RCs provides an opportunity to study the ground state electronic structure of the cofactors involved in the electron transfer process with atomic selectivity. Photo-CIDNP was observed for the first time in a field of 9.4 T for quinone-blocked frozen bacterial reaction centers (RCs) of *Rhodobacter sphaeroides* R26 using continuous illumination with white light, allowing an enhancement factor of about 200 till 1000 and WT (Zysmilich and McDermott, 1994, 1996b, 1996a; Matysik et al., 2000b; Matysik et al., 2001a; Schulten et al., 2002). Studies on photosystem I of spinach lead to an almost complete set of assignments of the aromatic ring carbons to the P2 cofactor of the primary electron donor P700 (Alia et al., 2004b). In the D1D2 complex of the RC of the photosystem II of plants, observation of the pronounced electron density on rings III and V by photo-CIDNP MAS NMR was taken as an indication for a local electric field, leading to a hypothesis about the origin of the remarkable strength of the redox potential of the primary electron donor P680 (Matysik et al., 2000a; Diller et al., 2005). In addition, NMR signals have been also detected in entire membrane-bound bacterial photosynthetic units (>1.5 MDa) (Chapter 5). Recently, it has been shown that photo-CIDNP can overcome the intrinsic insensitivity and nonselectivity of MAS NMR spectroscopy by enhancing the NMR intensities by a factor of 10000 at a field strength of 4.7 T (Chapter 2).

For the RCs from WT, photo-CIDNP has been described by a combination of two mechanisms (Jeschke and Matysik, 2003) (Chapter 2). In the electron-electron-nuclear three-spin mixing (TSM) mechanism, net nuclear polarization is created in the spin-correlated radical pair due to the presence of both anisotropic hyperfine interaction and coupling between the two electron spins (Jeschke, 1998). In the Differential Decay (DD) mechanism, a

net photo-CIDNP effect is caused by anisotropic hyperfine coupling without an explicit requirement for electron-electron coupling if spin-correlated radical pairs have different lifetimes in their singlet and triplet states (Polenova and McDermott, 1999).

Photo-CIDNP MAS NMR in combination with site-directed ^{13}C-labeled BChl/BPheo RCs, labelled at positions C-1,3,6,8,11,13,17,19 in the porphyrin ring, gave the first insight into the ground state electronic structure of the special pair at the atomic scale (Schulten et al., 2002). The studies have shown that two BChls, P1 and P2, have different chemical shift values. This has been interpreted in terms of different electron densities on both cofactors, presumably with higher electron density on P2. In addition, a small fraction of π-spin density was observed on a third BChl, designated as P3 (Schulten et al., 2002).

Photo-CIDNP MAS NMR studies performed on selectively labelled BChl/BPhe RCs, labelled at positions C-4,5,9,10,14,15,16,20, are reported here. These RCs have been prepared using (5-^{13}C)-δ-aminolevulinic acid•HCl as a precursor for BChl/BPhe biosynthesis. 1D CP/MAS and photo-CIDNP MAS NMR experiments confirm the remarkable similarity between the ground state electronic structures before and after illumination. To probe the ground state electronic structure of the cofactors involved in the electron transfer process, ^{13}C-^{13}C dipolar correlation photo-CIDNP MAS NMR experiments on the ^{13}C-labelled BChl/BPhe RCs have been performed. The ^{13}C chemical shifts from these photo-CIDNP studies in combination with previous studies have lead to for the first time, to a comprehensive map of the molecular electronic ground state of the photochemically active cofactors with the atomic selectively.

4.3 Materials and Methods

4.3.1 Sample preparation

Cultures of *Rb. sphaeroides* WT (480 mL) were grown anaerobically in the presence of 1.0 mM (5-^{13}C)-δ-aminolevulinic acid•HCl ($COOHCH_2CH_2{}^{13}COCH_2NH_2$•HCl, 99% ^{13}C-enriched), which was purchased from Cambridge Isotope Laboratories (Andover, USA). Incorporation of (5-^{13}C)-ALA, as reported in this paper, produces BChl and BPhe macrocycles, labeled at the C-4, C-5, C-9, C-10, C-14, C-15, C-16 and C-20 (Figure 4.2). The cultures were grown for 7 days in light. Prior to harvesting the cells for the preparation of RCs, a 4 mL aliquot was taken from the culture and the extent of ^{13}C incorporation of (4-^{13}C)-ALA into BChl has been determined as described in detail earlier (Schulten et al., 2002). The total ^{13}C-label incorporation in BChl/BPhe ($^{13}C_{0\text{-}8}$) was ~ 60±5%. The culture was centrifuged for 10 min at 5500 × g, and the combined pellet was resuspended in 0.1 M phosphate buffer (pH = 7.5). The RCs were isolated as described by (Shochat et al., 1994).

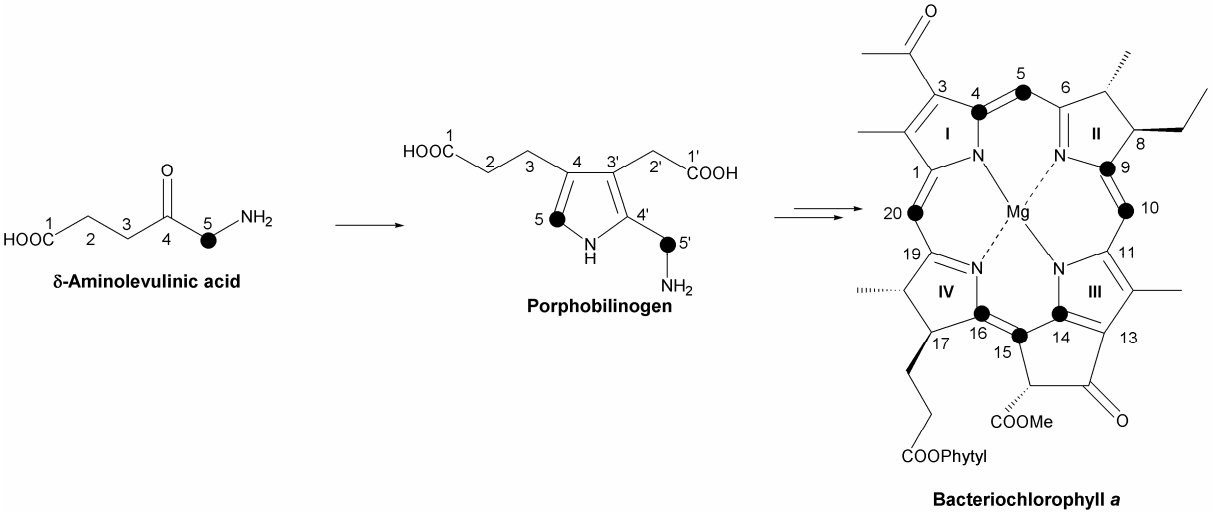

Figure 4.2. Schematic representation of the biosynthesis of BChl *a* and BPhe *a* starting from δ–aminolevulinic acid (ALA). The positions of ^{13}C labels are indicated by filled circles *(●)*. The numbering of BChl *a* is according to the IUPAC nomenclature.

Approximately 15 mg of the labeled RC was reduced with 0.05 M sodium dithionite and used for the NMR experiments.

4.3.2 MAS-NMR Measurements

Photo-CIDNP MAS NMR experiments were performed with a DMX-200 NMR spectrometer equipped with a double-resonance MAS probe operating at 200 MHz for ^{1}H and 50 MHz for ^{13}C. The RC sample was loaded into a clear sapphire 4 mm rotor, and ^{13}C MAS NMR spectra were recorded at a temperature of 223 K and a spinning frequency of 8 kHz. The sample was continuously illuminated during the course of the experiment. The illumination setup has been described in detail in Chapter 1. 1D photo-CIDNP MAS NMR spectra were collected with a Hahn echo-pulse sequence and two pulse-phase modulation (TPPM) proton decoupling. A recycle delay of 4 s was used.^{13}C CP MAS NMR data were obtained with a AV-750 NMR spectrometer. A total of 4k scans were recorded at a temperature of 223 K with a spinning frequency of 12 kHz. For the 2D homonuclear (^{13}C -^{13}C) dipolar correlation spectra, an adapted RFDR pulse sequence was applied with the initial cross polarization step replaced by a $\pi/2$ pulse. The RFDR experiments were recorded with mixing times of 4 and 8 ms. In the t_2 dimension, 2k data points with a sweep width of 50 kHz were recorded. Zero-filling to 4k and an exponential line broadening of 25 Hz were applied prior to Fourier transformation. In the t_1 dimension, 256 scans using 1k data points were recorded. A sine squared apodisation shifted by $\pi/2$ was applied prior to Fourier transformation. All spectra were externally referenced to the $^{13}COOH$ response of solid tyrosine·HCl at 172.1 ppm.

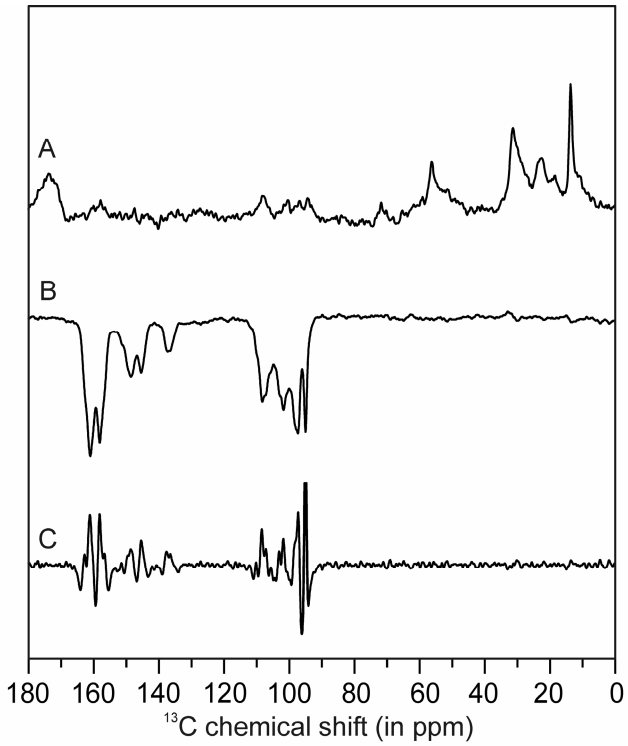

Figure 4.3. 1D solid-state MAS NMR spectra of BChl/Bphe labelled RC of *Rb. sphaeroides* WT. The dark ^{13}C CP/MAS NMR spectrum (A) was recorded at a field strength of 17.6 T at 223 K with a spinning frequency of 12 kHz. The photo-CIDNP spectrum (B) was recorded with continuous illumination in white light at a field strength of 4.7 T and at a temperature of 223 K with a spinning frequency of 8 kHz. Spectrum in (C) is the second derivative of the 1D photo-CIDNP spectrum (B).

4.4 Results and Discussion

4.4.1 Comparison of light with dark spectra

The ^{13}C CP MAS NMR spectrum from labelled RCs obtained in the dark is shown in Figure 4.3A. Several broad natural abundance ^{13}C responses are observed between 10 and 70 ppm from the saturated carbons in the apoprotein and another signal at 173 ppm is observed due to the carbonyl groups in the protein. Weak signals are observed in the region from 90 to 110 ppm corresponding to the response from ^{13}C-enriched BChl and BPhe in the RC. Continuous illumination with white light generates the photo-CIDNP MAS NMR spectrum as shown in Figure 4.3B. Strong emissive peaks appear in the region between 90 ppm to 110 ppm due to the photo-CIDNP from the methine carbons, ^{13}C-5, ^{13}C-10, ^{13}C-15 and ^{13}C-20. In the aromatic region of the spectrum from 135 ppm to 165 ppm the responses from the ^{13}C-4, ^{13}C-9, ^{13}C-14 and ^{13}C-16 are detected. To resolve the responses from the various labelled carbons, the second derivative of the 1D photo-CIDNP spectrum (Figure 4.3B) of the labelled RCs was calculated as shown in Figure 4.3C.

There are photo-CIDNP signals from more than eight carbons indicating that more than a single BChl is polarised. The broad peaks at 108.4, 97.2 and 95.2 ppm in the ^{13}C CP MAS spectrum (Figure 4.3A) are narrower and strongly emissive in the photo-CIDNP spectrum

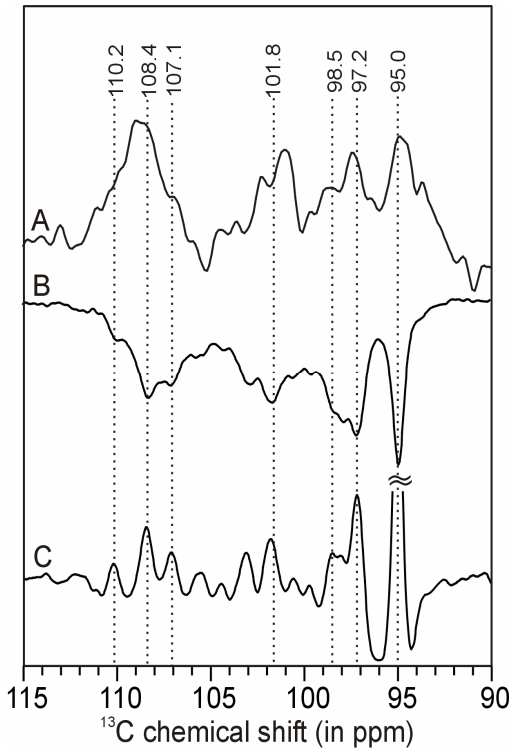

Figure 4.4. Detailed view of the methine region in the spectra in Figure 4.3. In both light and dark spectra the labelled carbons resonate with comparable chemical shifts, visualized by dashed lines.

(Figure 4.3B). These peaks are better resolved by taking the second derivative of the 1D photo-CIDNP spectrum (Figure 4.3C). The chemical shifts of the responses that were recorded in the dark are comparable to the shifts recorded with illumination. A detailed view of the spectra from 90 to 115 ppm is shown in Figure 4.4.

4.4.2 Assignment of the ^{13}C-^{13}C dipolar correlation spectra

To gain information on the ground state electronic structure of the donor molecule, P and the acceptor molecule Φ, 2D RFDR data sets were collected from polarized samples.

The RFDR spectrum (Figure 4.5) was recorded with a mixing time of 4 ms. In the BChl and BPhe rings separated by a single bond, strong correlations appear within each pair of enriched carbons, i.e. C-4/C-5, C-9/C-10, C-14/C-15, and C-15/C-16. In addition cross peaks are observed between C-14/C-16 over a distance of ~2.3 Å. Four sets of correlation networks are visible. Three networks which give strong correlations are assigned to two BChl molecules denoted as P1, P2 and one to BPhe, Φ_A. The fourth network is weak and is assigned to a BChl, denoted as P3.

The NMR shifts for monomeric BChl *a* and BPhe *a* in solution are shown in Table 4.1. The methine carbons in BChl *a* and BPhe *a* in acetone-d_6 resonate between 95 ppm and 110 ppm and the methine shift differences between the BChl and BPhe are 2 ppm or less. Hence, the diagonal peaks in this region can be attributed to the C-5, 10, 15 and 20 and can be used as starting points in the assignment procedure.

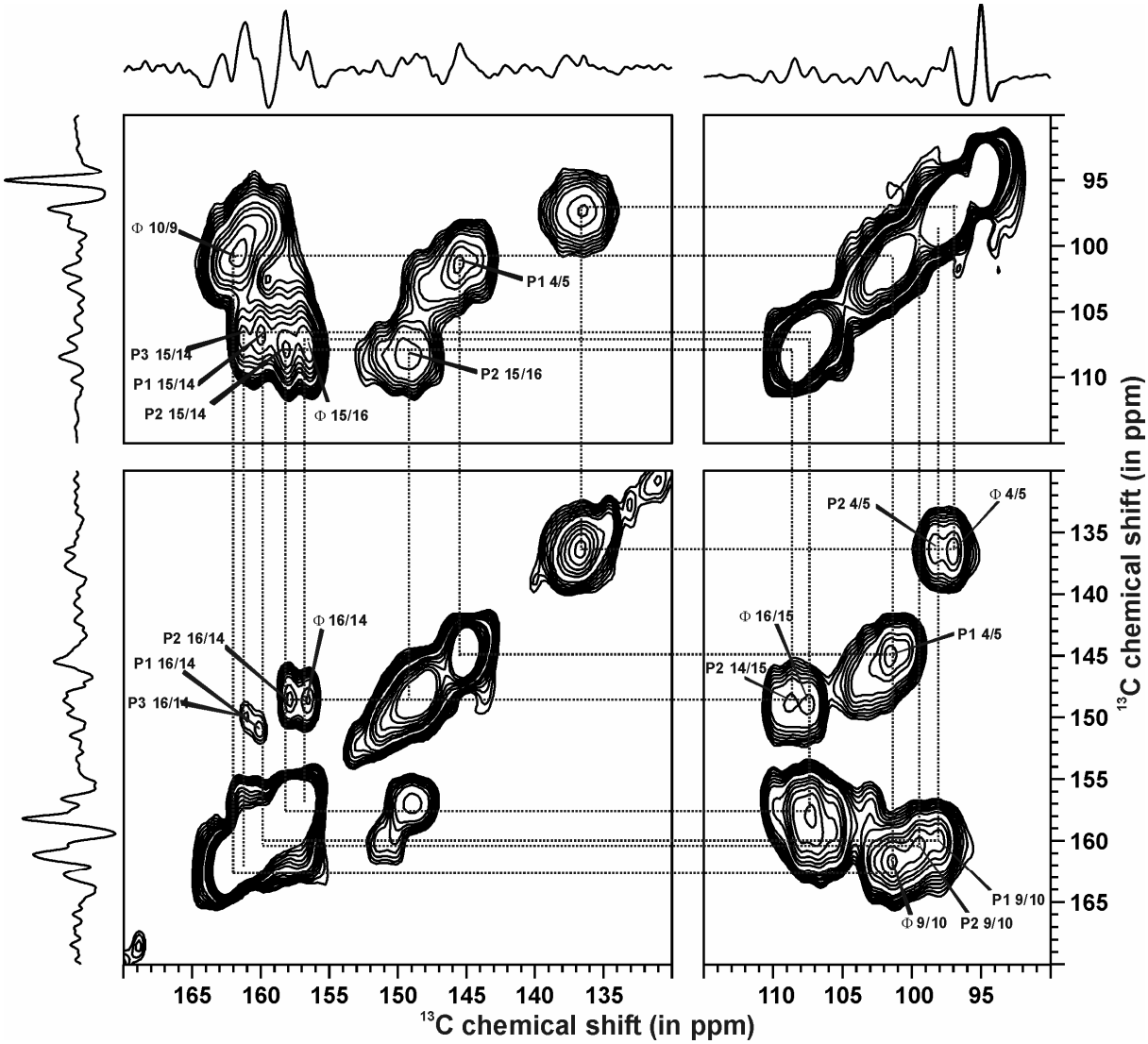

Figure 4.5. Contour plot sections of a ^{13}C- ^{13}C dipolar correlation photo-CIDNP MAS NMR spectrum of ($^{13}C_{0\text{-}8}$ BChl/BPhe)-RCs of *Rb. sphaeroides* WT recorded at a field strength of 4.7 T and 223 K, using a spinning frequency of 8 kHz and a mixing time of 4 ms. The labels refer to the cross peaks for the three BChl correlation networks P1, P2 and P3 and the BPhe component Φ. The upper trace shows parts of the second derivative of 1D photo-CIDNP MAS NMR spectrum.

A major difference in chemical shift of 12.1 ppm between BChl and BPhe is detected for C-4 and 14. The ^{13}C responses of C-14 and C-16 of Φ in acetone d_6 at 148.7 and 158.7 ppm, respectively, overlap with the C-16 and C-14 of BChl at 152.2 and 160.8 ppm, respectively. Three correlations are observed for C-14/C-15 at 160.0/106.8 (P1), 158.0/108.2 (P2) and 161.2/107.1 ppm (P3). A correlation is also observed for C-16/C-15 of Φ at 149.1/107.5 ppm. In addition, correlations are observed for C-16/C-15 of P2 at 148.8/108.2 and C-14/C-15 of Φ at 149.1/107.5 ppm. These assignments are confirmed by cross peaks detected between C-14 of ring III and C-16 of ring II. Two strong correlations are observed for C-14/C-16 at 158.0/148.8 ppm (P2) and for C-16/C-14 at 149.1/156.6 ppm (Φ). In addition, two weak correlations are observed for C-14/C-16 at 160.0/151.4 ppm (P1) and at

carbon no.	BChl *a*				BPhe *a*	
	σ_{liq} [a]	P1[b]	P2[b]	P3[b]	σ_{liq} [a]	Φ[b]
1	150.8	148.2	143.4	148.5	139.7	138.3
3	137.4	130.2	127.6	133.2	134.8	134.7
4	150.2	145.4	136.8		138.1	136.8
5	99.6	101.6	98.4		98.4	97.2
6	168.4	166.8	164.6	167.0	170.9	171.1
8	55.6	53.0	55.4	50.6	55.4	54.6
9	158.5	160.2	161.0		164.3	162.2
10	102.4	98.1	99.6		100.4	101.5
11	149.4	150.3	154.2	149.4	139.3	138.9
13	130.3	131.0	131.3	130.2	129.3	126.4
14	160.8	160.0	158.0	161.2	148.7	149.1
15	109.7	106.8	108.2	107.1	109.9	107.5
16	152.2	151.4	148.8	150.3	158.7	156.6
17	50.4	47.3	49.7	48.7	51.5	52.5
19	167.1	162.5	159.7	162.7	169.8	169.9
20	96.3				97.6	

[a] The liquid NMR chemical shift data σ_{liq} have been obtained in acetone-d_6.
[b] Assignment for carbons 1,3,6,8,11,13,17 and 19 from (Schulten et al., 2002).

Table 4.1. Chemical shifts of monomeric BChl a and BPhe a cofactors.

161.2/150.3 ppm (P3). The ^{13}C response of C-4 of Φ in acetone-d_6 at 138.1 ppm is very different from the ^{13}C response of C-4 of BChl at 150.2 ppm. A correlation is detected at 136.8/97.2 ppm which is assigned to C-4/C-5 of Φ.

There is another C-4/C-5 correlation observed at 136.8/98.4 ppm which cannot be assigned to a Φ, since only one Φ is present in the active branch. This can only be assigned to a C-4/C-5 correlation of BChl revealing an upfield shifted C-4 by 13.4 ppm. Previously 2D photo-CIDNP MAS NMR studies on BChl/BPhe ($^{13}C_{0\text{-}8}$)-RCs, with a different labeling pattern, have shown that the ^{13}C responses from ring I carbons of P2 are upfield shifted by 10.2 and 7.4 ppm respectively (Schulten et al., 2002). ^{13}C responses from ring I carbons of P1 are also upfield shifted but to a smaller extent. Thus the C-4/C-5 correlation at 136.8/98.4 ppm is assigned to P2. Another correlation observed at 145.4/101.6 ppm, is assigned to C-4/C-5 of P1.

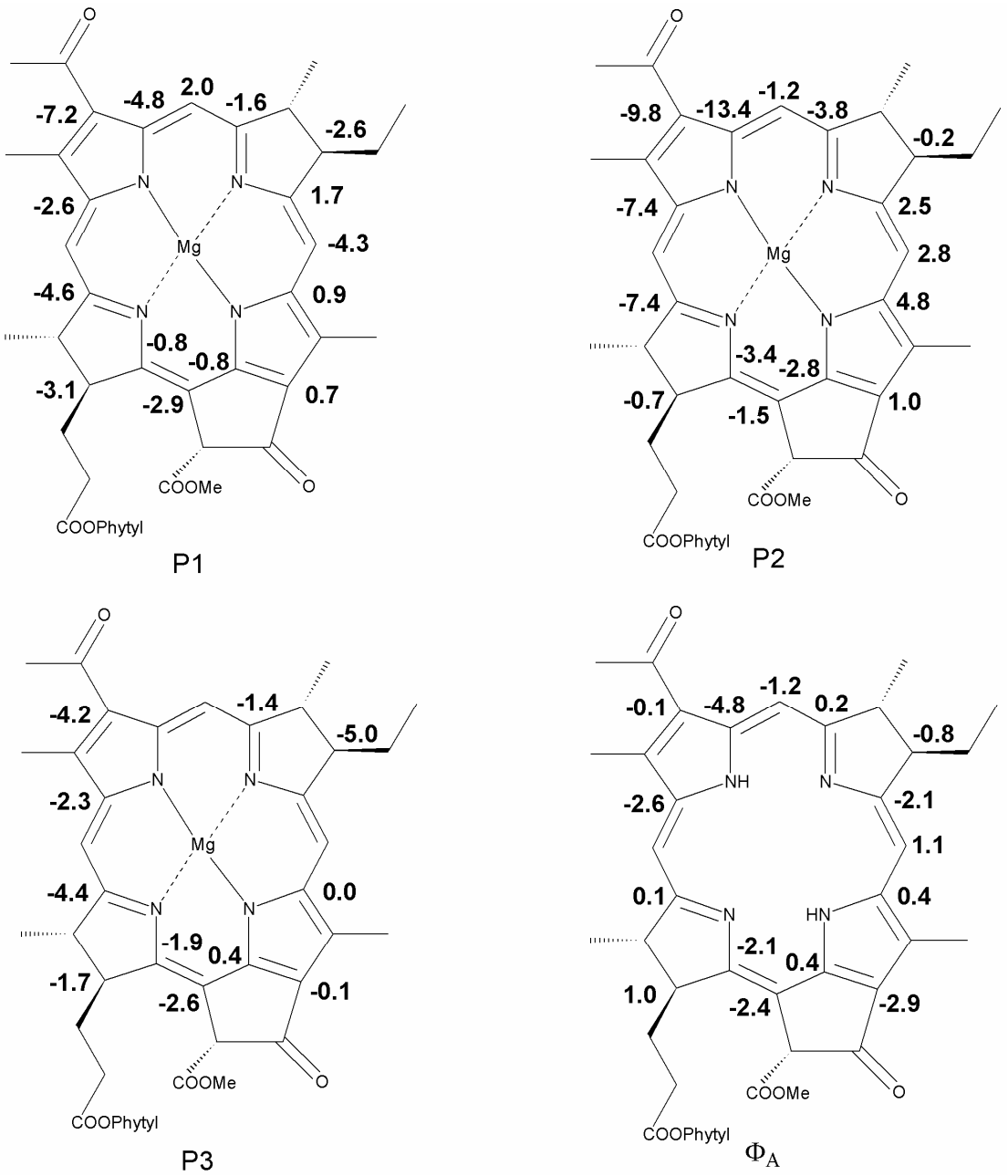

Figure 4.6. Detected chemical shift differences $\Delta\sigma = \sigma_{ss}$-$\sigma_{liq}$ for the three BChls P1, P2, P3 and the BPhe Φ_A.The positive values denote an upfield and the negative values a downfield shift.

Finally, a correlation is observed for C-9/C-10 of Φ at 162.2/101.5 ppm. The ^{13}C response from C-9 of BChl overlaps with ^{13}C response of C-14 of BChl. Cross peaks observed between C-9/C-10 of P2 at 161.0/99.6 and at 160.2/98.1 for P1 make it possible to assign C-9. The complete list of the ^{13}C assignments for all the photochemically active cofactors is presented in Table 4.1. ^{13}C assignments from previous photo-CIDNP MAS NMR studies are also shown in Table 4.1 to build a comprehensive map of the electronic ground state structure of the photochemically active cofactors (Schulten et al., 2002). Since no correlations are observed for C-9/C-10, C-4/C-5 for P3, it was not possible to make these assignments. The same is also

true for C-20 for which no cross peaks were seen. Comparing the chemical shifts of P1, P2 and P3, it can be concluded that P2 is 'special' among them.

Protein-pigment upfield shifts are observed for several carbons of P1, P2 and P3 (Table 4.1). The chemical shift differences $\Delta\sigma = \sigma_{ss} - \sigma_{liq}$ for the three BChls P1, P2, P3 and one BPhe Φ_A are shown in Figure 4.6. The BPhe Φ_A, exhibits both upfield and downfield shifts of < 3 ppm except for carbon C-4 which shows an upfield shift of 4.8 ppm. In the BChls P1, P2 and P3, the carbons around rings I and IV are upfield shifted as compared to other carbons. Pronounced upfield shifts are observed for P2 in the pyrrole ring I as compared to P1 and P3. This effect is clearly visible in the carbons C-1, C-3 and C-4 of P2, upfield shifted by 7.4, 9.8 and 13.4 ppm respectively. On the other hand, for P1 and P3, carbons around rings I and IV are upfield shifted by 2-7 ppm. The two BChls P_L and P_M of P overlap over ring I. Ring current shifts could therefore explain the strong upfield shifts around ring I for P2. However, ring current shifts are less than ~ 3 ppm and therefore cannot explain upfield shifts in the range of 7-13 ppm.

4.4.3 Identity of the cofactors

The pronounced upfield shifts in ring I of P2 suggest strong interactions in the vicinity of the photochemically active cofactors, that is P (P_L and P_M) and B_A.There are many polar amino acid residues surrounding the cofactors. The large upfield shifts could be explained by a strong interaction like a hydrogen bond to one of the amino acid residues. The X-ray structure of the RC reveals that a histidine residue (His L168) is located near the 3-acetyl group of P_L (Figure 4.7). Resonance Raman studies have already given evidence that a hydrogen bond exists at 3-acetyl group of P_L (Mattioli et al., 1991). In addition, site-directed mutants at positions His L168 and Phe M197 also have shown that an addition of a hydrogen bond can be correlated with an increase of the dimer midpoint potential (Lin et al., 1994). The appearance of the upfield shifts in ring I of P2 could then be tentatively assigned to the local hydrogen bonding between the acetyl carbonyl and the NH of the imidazole side chain of His L168. This leads to the assignment of P2 to BChl P_L located at the active A-branch. The other strong BChl component P1 is assigned to P_M and the weak component P3 is assigned to the accessory BChl B_A. The different chemical shifts of P_L in comparison to P_M and B_A indicate a 'special' local electronic environment in the ground state around P_L. The upfield shift of 13.4 ppm on C-4 of P_L indicates a stabilization of ~ -0.08 electronic equivalent negative charge on this atom relative to the monomer in solution. Strong upfield shifts around ring I of P_L, to a lesser extent around ring IV, suggest a localisation of the electronic charge over these rings primarily. The role of His L168 may be is to stabilise the charge on P_L. The comprehensive map of the electronic ground state of the special pair confirms previous results that P is asymmetric already in the ground state with excess negative charge on P_L. The functional asymmetry in the RC is thus introduced in the ground state.

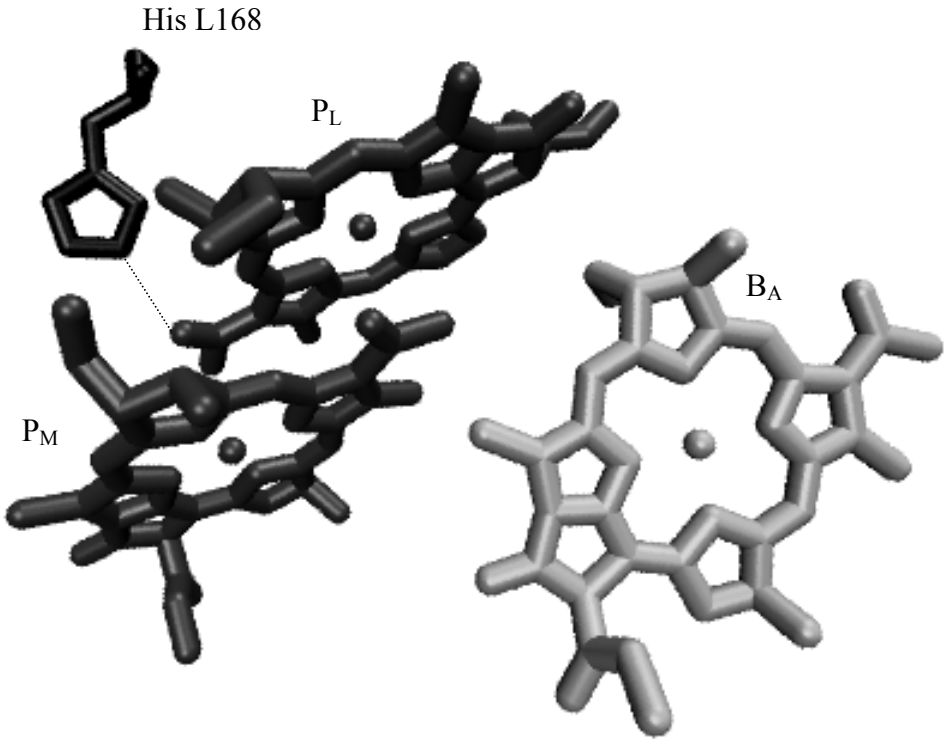

Figure 4.7. View from the top of the special pair, P_L and P_M and the accessory BChl B_A. His L168 in the back interacts with the 3-acetyl group of P_L.

5 Photochemically induced dynamic nuclear polarisation in entire bacterial photosynthetic units observed by ^{13}C magic-angle spinning NMR*

5.1 Abstract

Photochemically induced dynamic nuclear polarisation has been observed from entire photosynthetic units (PSU) bound to chromatophore membrane (membrane-bound PSU) of the purple bacteria *Rhodobacter sphaeroides*, which have been selectively ^{13}C-isotope enriched at all BChl and BPheo cofactors. These 1.5 MDa membrane-bound protein complexes comprise reaction centers as well as the antenna systems called light harvesting complexes I and II. Due to light-induced enhancement of nuclear polarisation, the ^{13}C magic-angle spinning (MAS) NMR spectrum shows absorptive lines originating from the cofactors involved into the photochemical machinery and allowing the determination of the electronic ground state structure at atomic resolution. Addition of detergent released intact PSU from the chromatophore membrane (so called detergent-solubilized PSU) and caused significant changes in the sign and intensity pattern of the light-induced MAS NMR spectrum. In contrast, detergent-solubilised PSU and detergent-solubilised bacterial reaction centers with the same isotope label pattern exhibit essentially the same chemical shifts with only minor differences in the intensity pattern. The pronounced differences between intact membrane-bound and detergent-solubilised photosynthetic units are tentatively explained by the loss of self-orientation of the membrane-bound samples by solubilisation. This interpretation suggests that the theoretically predicted anisotropy of the light-induced nuclear polarisation has been observed for the first time.

5.2 Introduction

Due to the unsurpassed electron pumping efficiency of photosynthetic reaction centers (RCs), photon flux is limiting for photosynthesis (for a review on the photophysics of RCs of purple bacteria, see (Hoff and Deisenhofer, 1997). Therefore, increasing the number of RCs would not increase the photosynthetic activity. Instead, the RCs are embedded in arrays of antenna pigments. In purple bacteria, the entire photosynthetic apparatus containing RCs and light-harvesting (LH) antenna complexes is called the photosynthetic unit (PSU) (Papiz et al., 1996; Hu et al., 2002). In the PSU, an RC is directly surrounded by the core LH I (B875). Around such RC-LH I complexes, other antenna systems called LH II (B800-850) are located.

*This chapter has been published as:
S. Prakash, Alia, P. Gast, G. Jeschke, H. J. M. de Groot, J. Matysik. (2003) *J. Mol. Struc.* 661, 625-633.

Kinetics and optical properties of RCs in PSUs are slightly different from isolated and detergent-solubilised RCs. In *Rhodobacter (Rb.) sphaeroides,* isolation from membranes by detergents causes a small blue shift of the monomeric BChls (from 802 to 801 nm) and a small red shift of the BPheos from 754 to 755 nm (Beekman et al., 1995). Absorbance-detected magnetic resonance (ADMR) experiments suggest interaction between exciton states of antenna and RCs (Owen et al., 1997). It has also been shown that the charge separation is slower in PSU (τ = 4.5 ps compared to 3.3 ps), due to an increase of the slower of the two exponential components (Schmidt et al., 1993). It has been speculated that a slight increase of the redox midpoint potential E_m for the P/P^+ couple may be the reason, since similar phenomena were observed in mutants of *Rb. capsulatus* (Jia et al., 1993). In *Rhodopseudomonas (Rps.) viridis*, the lifetime of the primary radical pair (P^+H^-) with pre-reduced secondary acceptor Q_A has been found to be 2.4 to 3 ns in intact membranes and about 5 ns in isolated RCs (Gibasiewicz et al., 1999). The differences in the recombination kinetics may be either due to efficient exciton back-transfer opening an additional decay path, or caused by an influence of the LH I antenna complex on the energetics of the primary charge separation (Visschers et al., 1999; Bernhardt and Trissl, 2000). Another difference between PSU membranes and detergent-solubilised RCs arises from the fluid mechanics of membranes: PSU samples have the tendency to orient under appropriate conditions, as under centrifugal forces or in thin layers (Alegria and Dutton, 1991; Hara et al., 1993).

In a first attempt to probe the differences between RCs embedded in intact PSUs and in solution conditions, we applied magic-angle spinning (MAS) solid-state NMR, which is a powerful method for studying structure and dynamics of membrane proteins (de Groot, 2000). In principle, NMR chemical shift information can allow for the exploration of spatial, protonic and electronic structure at atomic resolution in the electronic ground state, and NMR analysis can provide detailed insight into functional mechanisms of proteins. In case of several photosynthetic RCs of bacteria and plants, it has been shown that photochemically induced dynamic nuclear polarisation (photo-CIDNP) can overcome the intrinsic insensitivity of NMR spectroscopy by photochemical induction of non-Boltzmann nuclear spin states. Photo-CIDNP has been observed initially in quinone-blocked bacterial RCs from *Rb. sphaeroides* R26 (Chapter 3) (Zysmilich and McDermott, 1994, 1996b, 1996a; Matysik et al., 2000b). As a second system, the RC of *Rb. sphaeroides* wildtype (WT) has shown ^{13}C photo-CIDNP of similar intensity as R26 (Chapter 2) (Matysik et al., 2001a). The third system, in which photo-CIDNP has been observed, is the D1D2 complex of the RC of photosystem II of plants, resulting in a hypothesis of the remarkable strength of the redox potential of the primary electron donor P680 (Matysik et al., 2000a; Diller et al., 2005). The fourth system in which photo-CIDNP has been observed is photosystem I of spinach leading to a complete set of assignments of the aromatic ring carbons to the P2 cofactor of the primary electron donor P700 (Alia et al., 2004b). Spatial selectivity and sensitivity of photo-CIDNP experiments can

be further improved by application of selectively isotope labelled samples. From selectively ^{13}C-isotope labelled RCs of *Rb. sphaeroides* WT, two-dimensional photo-CIDNP MAS NMR spectra have been obtained, which clearly demonstrate that the electron density of the two BChl molecules of the special pair is already different in the electronic ground state (for details, see Chapter 4).

In addition to the information on the electronic ground state provided by the NMR chemical shifts, photo-CIDNP solid-state NMR intensities are linked to the local electron spin densities occurring in the radical-pair state. The exact link between the local electron-spin densities and the photo-CIDNP intensities, however, remains the object of further studies since the mechanism producing photo-CIDNP in solids is currently under discussion. Originally, the net polarization in frozen RC under continuous illumination was assumed to be due to significant relaxation of the nuclear spins in the special pair triplet ^{3}P, while nuclear spins in the singlet ground state P with a much longer longitudinal relaxation time would retain their polarization (McDermott et al., 1998). However, this differential relaxation mechanism cannot explain photo-CIDNP effects for nuclear spins in the BPhe acceptor, which also have been observed (Zysmilich and McDermott, 1996b; Jeschke, 1998; Polenova and McDermott, 1999; Schulten et al., 2002). Two further mechanisms generating photo-CIDNP have been proposed. In the three-spin mixing mechanism, the presence of both an anisotropic hyperfine interaction and a coupling between the two electron spins, creates net nuclear polarization in the spin-correlated radical pair (Jeschke, 1997, 1998). In the differential decay mechanism, net nuclear polarization is accumulated due to the preferential decay of triplet radical pairs $^3(P^{+\bullet}\Phi^{-\bullet})$ to special pair triplets ^{3}P, which is faster than that of singlet radical pairs to the ground state (Polenova and McDermott, 1999). The singlet pairs exist long enough for a fraction of the electron spin polarisation to be transferred to nuclear polarization by evolution of the spin system under the anisotropic hyperfine interaction. Very recently, both mechanisms have been reassessed and the effects have been simulated (Chapter 2). According to both mechanisms, the photo-CIDNP effect is predicted to be highly anisotropic. The effect due to both mechanisms vanishes at the canonical orientations of the hyperfine tensor where the pseudosecular component B to the hyperfine coupling, which causes the electron-nuclear spin mixing, approaches zero. The contribution by the three-spin mixing mechanism vanishes for zero coupling between the electron spins, which would be expected if the dipole-dipole coupling compensates the J coupling at some orientations. Judging from the known distance between the radical ions and values for the J coupling found in the literature, this is unlikely to occur, however, some orientation dependence of the photo-CIDNP effect is still induced by the orientation dependence of the dipole-dipole coupling (Tang et al., 1996; Hulsebosch et al., 1999, 2001). Perhaps more significantly, the magnitude of the effect for both mechanisms depends strongly on the secular hyperfine coupling A; for the differential decay mechanism even the sign of the effect depends on the sign of A. This

may cause a strong orientation dependence of the magnitude of the effect and even sign changes, as for many ^{13}C nuclei, *A* is close to zero for orientations within the plane of the macrocycle. While these qualitative predictions are well founded in the theory of the mechanisms, quantitative predictions are difficult to make because of uncertainties in too many parameters. In this situation a better understanding of the relation between photo-CIDNP effects and the electronic structure of the radical ion pair is hampered by a lack of data on oriented systems. The tendency of PSUs to self-orient may provide such an oriented system (Jeschke, 1997; Jeschke and Matysik, 2003).

Photo-CIDNP data from RC bound in PSUs may be interesting in two aspects. Comparison with data collected from detergent-solubilised RCs may provide (i) information on the mode of interaction between LH I and the RCs as well as (ii) a clue on the mechanism of photo-CIDNP in solids, especially on its anisotropy. In this paper, we report for the first time photo-CIDNP in PSUs observed by ^{13}C MAS NMR, and discuss spectral differences with isolated RCs.

5.3 Materials and methods

5.3.1 Preparation of ^{13}C-labeled PSUs

δ-Aminolevulinic acid (ALA) is a precursor of naturally occurring tetrapyrroles, including BChl and BPhe (Jordan, 1991). In biosynthesis, two molecules of ALA are asymmetrically condensed to form the pyrrole porphobilinogen (Figure 1). Four molecules of porphobilinogen tetramerize and prior to macrocycle ring closure, the pyrrole ring IV is inverted via a spiro-intermediate. This sequence causes the asymmetry of the macrocycle backbones of BChl and BPhe. On the biosynthetic pathway, mono-^{13}C enriched ALA forms doubly ^{13}C-enriched porphobilinogen and eightfold ^{13}C-enriched BChl and BPhe macrocycles. Incorporation of (4-^{13}C)-ALA, as reported in this paper, produces BChl and BPhe macrocycles, labeled at the C-1, C-3, C-6, C-8, C-11, C-13, C-17 and C-19 (see Figure 5.1 for nomenclature). Cultures of *Rb. sphaeroides* WT (480 mL) were grown anaerobically in the presence of 1.0 mM (4-^{13}C)-δ-aminolevulinic acid·HCl (COOH CH_2CH_2 $^{13}COCH_2NH_2$·HCl, 99% ^{13}C-enriched), which was purchased from Cambridge Isotope Laboratories (Andover, USA). The cultures were allowed to grow for 7 days in light. Prior to harvesting the cells for the preparation of chromatophore and RCs, a 4 mL aliquot was taken from the culture and the extent of ^{13}C incorporation of (4-^{13}C)-ALA into BChl has been determined as described in detail earlier (Schulten et al., 2002). The total ^{13}C-label incorporation in BChl/BPhe ($^{13}C_{0\text{-}8}$) was about 60±5%. The chromatophore-membrane containing entire PSU (membrane-bound PSU) were prepared essentially as described in (Kondo et al., 2002).

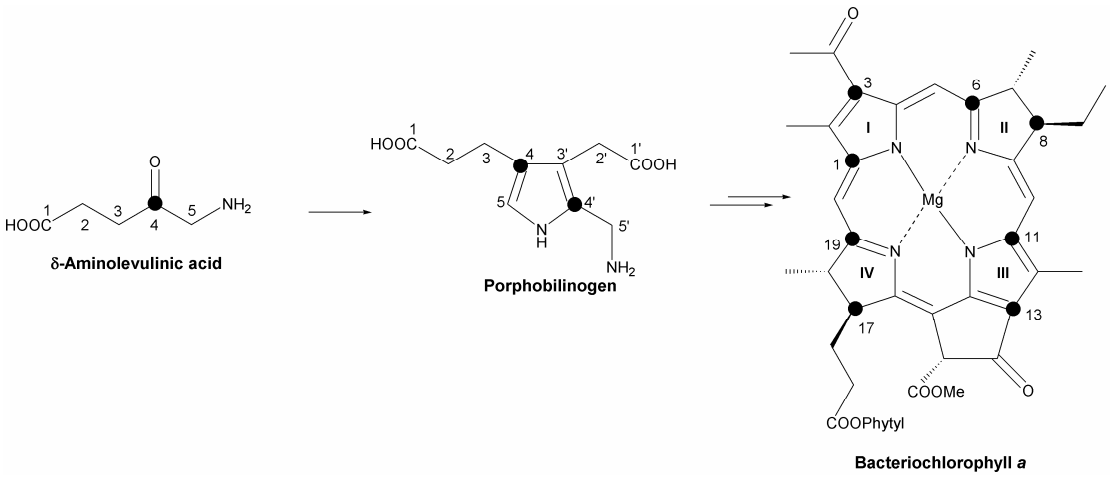

Figure 5.1. Schematic representation of the biosynthesis of ($^{13}C_{0\text{-}8}$)-labelled BChl *a* starting from (4-^{13}C)-δ-aminolevulinic acid (ALA). The positions of the ^{13}C-labels are indicated with filled circles (●). BPhe *a* is a derivative of BChl *a*, in which the magnesium is replaced by two hydrogen atoms. The numbering of BChl *a* is according to the IUPAC nomenclature.

For the preparation of a detergent-solubilized PSU sample, chromatophore-membrane containing entire PSUs (A_{865} of 200) were treated with 0.5% detergent (LDAO, Fluka Chemie GmbH, Buchs, Switzerland) for 1.5 h at 4°C. As a result, membranes were partially solubilised and the intact PSU was released from the membrane. This has been confirmed by linear sucrose gradient ultracentrifugation which resulted in the clear separation of the band of detergent-solubilized PSU (at ~30% sucrose) from membrane-bound PSU (at ~40% sucrose). The RCs were purified as described by (Shochat et al., 1994).

5.3.2 MAS NMR Measurements

MAS NMR experiments were performed with a DMX-400 NMR spectrometer (Bruker, Karlsruhe, Germany) that was equipped with a double-resonance MAS probe operating at 396.5 MHz for ^{1}H and 99.7 MHz for ^{13}C. The illumination setup has been described in detail in Chapter 1. A sample containing 30 mg wet weight of the PSU, which contains about 0.1 mg RC, was loaded into an optically transparent 7-mm sapphire rotor and ^{13}C MAS NMR spectra were recorded at a temperature of 223 K with $\omega_r/2\pi$ = 3.6 kHz. Several minutes before the start of the experiment, 10 mM sodium ascorbate and 0.5 mM terbutyn were added to photo-reduce the acceptor site Q_A in situ. The sample was frozen in the dark under slow spinning ($\omega_r/2\pi$ = 400 Hz). During the course of the experiment, the sample was continuously illuminated with white light. Dark and photo-CIDNP spectra were measured by simple Bloch decay followed by a Hahn echo in order to delay the response. The FID was collected with TPPM proton decoupling (Bennett et al., 1995). A recycle delay of 12 s was used. Spectra of PSU were measured in 48 hours. The spectrum of solubilised RCs has been obtained in 30 min at a spinning frequency $\omega_r/2\pi$ = 5 kHz. For details about the experiment on solubilised RC, see (Schulten et al., 2002). In order to distinguish absorptive and emissive signals, a

spectrum of solid (u-^{13}C)-tyrosine•HCl was recorded prior to the experiments on PSU. The phase correction for this reference was essentially conserved in the spectra of the PSU. The spectra were recorded in 2k data points with a sweep width of 50 kHz and an exponential line broadening of 70 Hz was used. All MAS NMR spectra were referenced to the ^{13}COOH response of solid tyrosine•HCl at 172.1 ppm.

5.4 Results

5.4.1 Apoprotein and lipids

The ^{13}C-MAS NMR spectrum of the membrane-bound PSU in the dark (Fig. 5.2A) show the features of the apoprotein, which also occur in solubilised RC samples, as well as two signals from the lipid molecules at 57.5 and 17.7 ppm (Zysmilich and McDermott, 1996a; Matysik et al., 2000b; Matysik et al., 2001a). Detected after a Hahn echo, these signals appear to be out of phase, indicating the mobility of the lipid phase at 223 K. This assignment is backed by ^{1}H→^{13}C cross-polarisation experiments, in which the lipid signals appear with low relative intensity. The signals of the ^{13}C-labelled cofactors are not observable under these experimental conditions.

5.4.2 The signs of the spectra

Upon illumination (Figure 5.2B), several weak absorptive (positive) features occur. Most prominent among the light-induced signals are the absorptive signals at 165 and 131 ppm. Their chemical shift anisotropy, which can be estimated from the side-band pattern at the low-frequency site, is in the range for aromatic carbons. Weaker signals occur at 155 and 150 ppm. No light-induced emissive (negative) signals are observed. Also in the aliphatic region, a light-induced absorptive signal occurs at about 50 ppm. Addition of detergent to the PSU sample changes the intensity pattern dramatically (Figure 5.2C). All signals appear to be emissive. In addition, several signals gain intensity and can be identified. Center bands appear at 168, 165, 160, 155, 150, 145, 139, 131 and 128 ppm in the aromatic region, and 56 and 50 ppm in the aliphatic region. These signals are in sign, intensity ratio, chemical shift and chemical shift anisotropy similar as those from detergent solubilised RCs (Figure 5.2D).

This spectrum has been reported recently by us, however, a careful re-investigation of the sign of this spectrum revealed that all signals appear to be emissive and not absorptive. This means that all signals in the photo-CIDNP spectrum of membrane-bound PSUs are absorptive (Figure 5.2B) whereas all signals from the detergent solubilised PSUs (Figure 5.2C) and isolated and detergent solubilised RCs are emissive (Figure 5.2D) (Schulten et al., 2002).

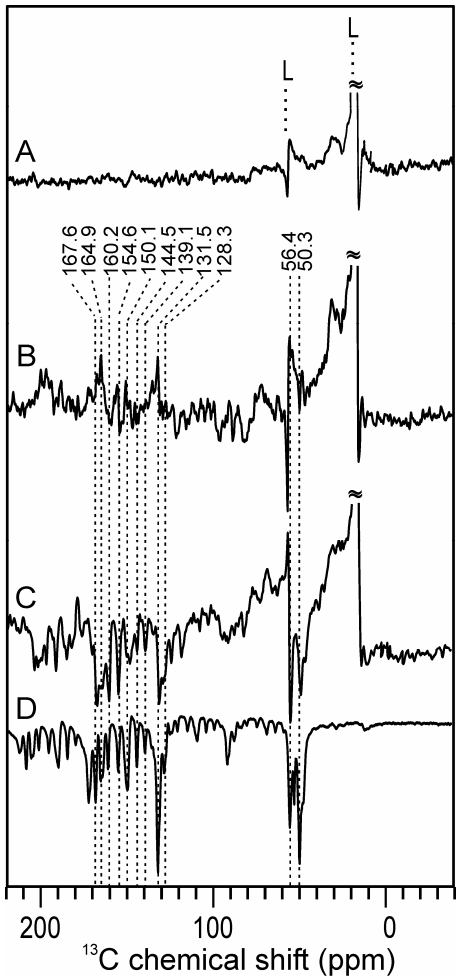

Figure 5.2. ^{13}C Photo-CIDNP MAS NMR spectra of entire ($^{13}C_{0\text{-}8}$-BChl/BPhe)-labelled PSU according to Figure 1: Spectra obtained in the dark (**A**) and under continuous illumination with white light in membrane-bound PSU (**B**) and in detergent-solubilised PSU (**C**). For comparison, the ^{13}C photo-CIDNP MAS NMR spectrum of purified ($^{13}C_{0\text{-}8}$-BChl/BPhe)-labelled RCs is shown in (**D**). Signals assigned to lipids are marked with "L". The center bands of the light-enhanced signal from purified RC have been marked with dotted lines. All spectra were recorded at 223 K with a spinning frequency of 3.6 kHz (spectra **A**-**C**) and 4 kHz (spectrum **D**).

5.5 Discussion

5.5.1 Effects of spin diffusion

Light-induced signals in the aliphatic region have not been observed in continuous illumination experiments on samples of unlabelled RCs, but have been observed for the RCs with selectively labelled BChl and BPheo cofactors (Figure 5.2D) (Zysmilich and McDermott, 1996a; Matysik et al., 2000b; Matysik et al., 2001a). Also in spectrum 5.2B, a small light-induced signal can be observed at 50 ppm. The aliphatic chlorophyll carbons do not gain the photo-CIDNP from the primary mechanism (Matysik et al., 2001b).

Since the weak NMR signals of the apoprotein at about 15 and 30 ppm in Figure 5.2D appear emissive, the polarisation of these carbons of the protein pocket is most likely induced by spin diffusion from the cofactors of the photochemical machinery. This observation

demonstrates the possibility to explore the protein pocket of the photochemically active cofactors by photo-CIDNP. Spin diffusion complicates the correlation of measured photo-CIDNP intensities to local electron spin densities. On the other hand, steady-state photo-CIDNP intensities may allow for a rough assignment of signals to different cofactors. In the isolated selectively labelled RCs (Figure 5.2D), as shown by Schulten et al., the signal of the special pair carbons is about three-times stronger than that for the BPheo response (Schulten et al., 2002). All signals observed in Figure 5.2B have been assigned to special pair carbons. The absence of BPheo carbon signals is probably due to the generally lower intensity in this spectrum rather than due to a change in the intensity ratio between signals from the special pair and from the BPheo.

5.5.2 Comparison of membrane-bound and detergent-solubilised PSUs

In membrane-bound PSUs, five absorptive lines at 165, 155, 150, 131 and 50 ppm can be identified (Figure 5.2B). Upon addition of detergent to the sample, emissive lines at 168, 165, 160, 155, 150, 145, 139, 131, 128, 56 and 50 ppm occur (Figure 5.2C). Differences in the chemical shifts induced by the detergent cannot be detected unequivocally. The striking difference is the change of sign and increase for most of the signals. These findings suggest that the changes of the electronic structure and sample state induced by the detergent involve the radical-pair state and not the electronic ground state of the photochemically active region of the RCs. Rather, the strong spectral effect of the detergent can either be due to changes of the electronic structure of the RC by its embedding in the LH I antenna, or can be caused by the destruction of the membrane structure and its orientation. If the latter were true, it would suggest that the sample measured in spectrum 5.2B has been self-oriented by the sample spinning.

5.5.3 Comparison of detergent-solubilised PSUs and RCs

The comparison of detergent-solubilised PSU and purified RC samples may provide a route to probe the effect of the LH I on the RC. As indicated by the similarity between the spectra of PSU after addition of detergent (Figure 5.2C) and isolated and detergent-solubilised RCs (Figure 5.2D), the electronic structures of the photochemically active regions as well as the sample states of the RCs are similar. Most of the differences between the spectra 5.2C and 5.2D can be explained by (i) different spinning frequency, (ii) occurrence of lipid signals in spectrum 5.2C, and (iii) different concentration of the RCs. The signal at 139.1 ppm has been assigned to BPheo (Schulten et al., 2002). Its intensity relative to signals assigned to the special pair is similar in both spectra. This observation suggests that the efficiencies of the different mechanisms producing photo-CIDNP are similar in both samples. Figure 5.3 allows for comparison of both systems in more detail. The spectrum of detergent-solubilised PSUs (Figure 5.3A) is identical to spectrum 5.2C.

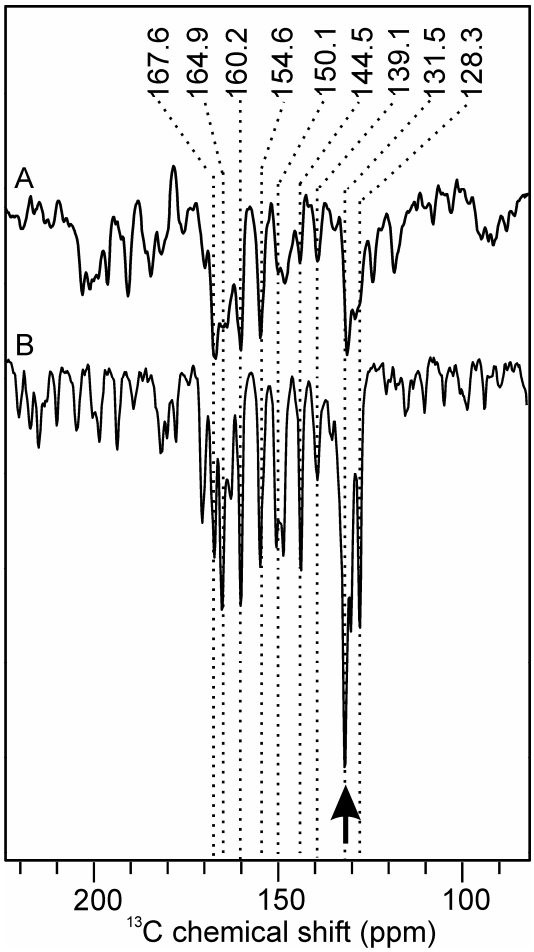

Figure 5.3. Expansion of the aromatic region of ^{13}C Photo-CIDNP MAS NMR spectra of detergent-solubilised (BChl/BPhe)-labelled PSU (**A**) and purified (BChl/BPhe)-labelled RCs (**B**). Both spectra were recorded at 223 K with a spinning frequency of 3.6 kHz (**A**) and 5 kHz (**B**). The arrow points to the difference in the relative intensity of signal at 131.5 ppm in detergent-solubilized PSU and RCs.

The spectrum of purified RCs (Figure 5.3B) has been obtained with a MAS rotational frequency of 5 kHz, allowing an unequivocal separation of center and spinning side bands. The dotted lines in Figure 5.3 refer to the center bands resolved by band fitting in spectrum 3B. No change of a chemical shift is observed. Hence, the electronic ground states of PSU-bound and purified RCs are essentially the same. This again demonstrates the insensitivity of the electronic ground state to sample solubilisation. The only difference between the center bands of spectra 3A and B is related to the intensity of the signal at 131.5 ppm (Arrow in Figure 5.3). In spectrum 5.3B, this signal has an intensity double of most other signals assigned to special-pair carbons and has been assigned to the two carbons 13 localised on rings III (Jeschke, 1998). Spectrum 5.3A shows this signal with less relative intensity. The loss in intensity may be explained to some degree by the overlap of absorptive signals, as observed in spectrum 5.2B at this position, indicating some amount of membrane-bound sample. On the other hand, the signal at 164.9 ppm, for which also a strong emissive signal appears in spectrum 5.2B, is not so dramatically reduced in spectrum 5.3A. Probably, this

difference in intensity is related to a variation of the electron-spin density distribution. Since the two carbon atoms 13 are localised at the ends of the special pair dimer, their involvement into the spin-diffusion driven polarization equilibration may be limited. The origin of the proposed difference in electron-spin density distribution in the radical-pair state may be related to the longer radical lifetime in membrane-bound RCs (Gibasiewicz et al., 1999).

5.5.4 Origin of the sign change

Photo-CIDNP ^{13}C MAS NMR spectra of membrane-bound PSUs show a completely different intensity pattern compared to data collected from detergent-solubilised PSUs and RCs, while the differences between solubilised PSUs and RCs are minor. In principle, two explanations are possible: Either the remarkable differences between membrane-bound and detergent-solubilised PSUs are caused by orientation of intact PSU membranes, and demonstrate the anisotropy of photo-CIDNP, or they are induced by the mode of interaction of the antenna with the RC.

Since ground state electronic structure changes have been shown to be limited, explanation of the sign change by interaction of LH I antenna to the electronic structure of RCs in the radical-pair state is difficult. On the other hand, due to the anisotropy of *g* and hyperfine tensors as well as the dipole-dipole coupling between the two electron spins, theory predicts a strong anisotropy of the photo-CIDNP enhancement and strong effects on the photo-CIDNP intensity pattern upon orientation as discussed above. Therefore, we assign tentatively the differences between membrane-bound and detergent-solubilised PSUs (Figure 5.2B and C) to self-orientation of PSU membranes upon sample spinning and to the detergent induced solubilisation of RCs. Photo-CIDNP MAS experiments on purified and oriented bacterial RC samples are on the way in our laboratory and can provide a definite explanation of this phenomenon.

5.5.5 The effect of light intensity

The PSU sample contains about 0.1 mg of RCs. In experiments on detergent solubilised RCs, sample preparations of ~5 mg were used. At such high concentration, the question arises whether the photo-CIDNP intensities are limited by the number of photons penetrating into the highly absorbing sample. The effective signal-to-noise ratio is comparable while the sample concentration is different for the spectra shown in Figure 5.2C and D. This suggests that the strength of the photo-CIDNP effect in RCs is not limited by the light intensity.

In previous work, we estimated that under continuous illumination with white light about 50 photons are absorbed per RC and per second on average (Matysik et al., 2001a). In optically dense samples, the number of photons available inside the sample depends strongly on the distance from the surface. The penetration depth of light into absorbing and scattering material has been treated in 1931 theoretically by Kubelka and Munk in order to investigate

the necessary thickness of coats of paint (Kubelka and Munk, 1931). Schrader and Bergmann extended in 1967 this concept in an attempt to optimise Raman scattering signals from crystal powders (Schrader and Bergmann, 1967). A quantitative theoretical treatment of photo-CIDNP in optically dense samples requires an analogous approach. One parameter, however, the build-up kinetics of photo-CIDNP, remains to be experimentally determined.

5.6 Conclusions

The occurrence of photo-CIDNP within membrane-bound PSUs opens up a new route to probe native photosynthetic proteins at atomic resolution and to compare their electronic structure to isolated and detergent-solubilised samples. For detergent-solubilised PSUs and RCs, the ground states are very similar, while there are clear indications for differences in the radical-pair states of both species. The pronounced variations of the photo-CIDNP intensity pattern between intact and partially solubilised PSUs can be explained by a loss of orientation of membrane-bound intact PSU in the rotating sample upon addition of detergent. This interpretation would imply that an anisotropy of the photo-CIDNP effect has been observed for the first time.

6 Current view and Outlook

6.1 Introduction

Previous Chapters in this thesis have shown that experimental results in combination with theoretical explanations have been important for the understanding of photo-CIDNP. This Chapter starts with presenting the current view on all the mechanisms involved in photo-CIDNP. It then reports the first time-resolved experiments on the build-up of photo-CIDNP. These experiments form the basis for more detailed studies in the future. As a technique, photo-CIDNP could have numerous applications. The ideas for advances in this direction are presented in the last section of this Chapter.

In Chapter 2, the photo-CIDNP effect in bacterial reaction centers of *Rb. sphaeroides* WT has been described by contributions from two parallel mechanisms. First, the electron-electron-nuclear three spin mixing (TSM) involves the polarization transfer from the electron-electron zero-quantum transition to the nuclear spins (Jeschke, 1997, 1998). The TSM depends on the electron-electron coupling in the spin-correlated radical pair and the anisotropic hyperfine coupling. Second, in the Differential Decay (DD) mechanism the anisotropic hyperfine coupling can cause a net photo-CIDNP effect between the two electron spins even in the absence of coupling provided the spin-correlated radical pairs have different lifetimes in their singlet and triplet states (Polenova and McDermott, 1999). The field dependence of photo-CIDNP has been studied at three different magnetic field strengths for RCs of *Rb. sphaeroides*. The simulations of photo-CIDNP intensities for the WT presented in Chapter 2 are based on the TSM and DD mechanisms. In the simulations all signals are emissive (negative), which is in line with the WT experiments and the field dependence. The distribution of spin density over the donor molecules is reproduced remarkably well, which is encouraging. On the other hand, it is shown that for R26 a description in terms of TSM and DD is essentially incomplete, since an absorptive (positive) response is detected, which is tentatively attributed to an additional mechanism, Differential Relaxation (DR), involving the donor (Chapter 3).

In the past, the interpretation of MAS photo-CIDNP intensities has been restricted by incomplete understanding of the underlying mechanisms. By resolving the differences between R26 and WT and by providing a detailed comparison between data and theory, this thesis (*i*) arrives at a new and improved self-consistent picture of the transfer mechanisms, (*ii*) paves the way for future biophysical studies and (*iii*) guides the theory development into new, unexplored directions.

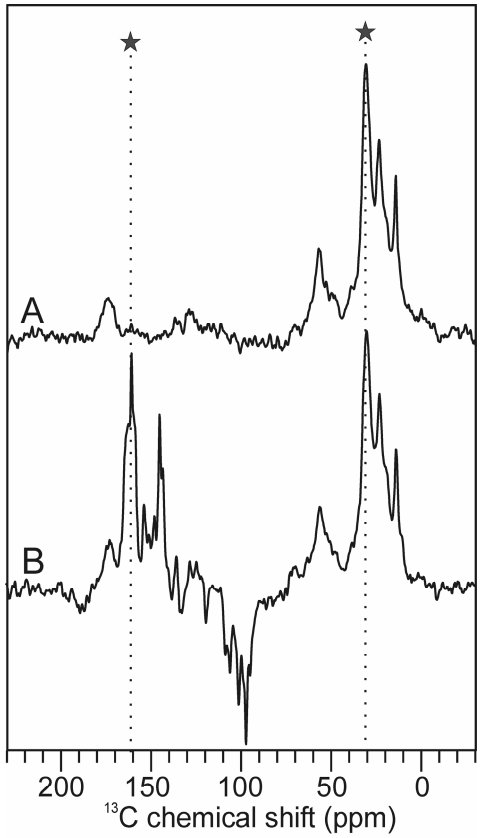

Figure 6.1. ^{13}C MAS NMR spectrum of *Rb. sphaeroides* R26 RC at 400 MHz, 223 K and a spinning frequency of 9 kHz in A) dark and B) under light. The peaks at 161 and 31 ppm used for determination of the build-up kinetics are marked with a star.

A sound experimental basis will ultimately lead to a consistent picture of the underlying mechanisms. In this respect, further theoretical developments will require extensive exploration of the anisotropy of the photo-CIDNP process as shown in Chapter 5 and time-resolved experiments to study the build-up of the polarization. The first steps in this direction are presented below.

6.2 The build-up of photo-CIDNP

The build-up to the steady state in photo-CIDNP takes ~500 photochemical cycles (see below). Studies of the build-up kinetics may help to quantify the contributions from the various mechanisms. The experimental kinetics of the photo-CIDNP build-up was thus studied by varying the light pulse length from 1 to 10 s.

Photo-CIDNP MAS NMR spectra were recorded from quinone-depleted RCs at 223 K and a field of 9.4 T using white light. The dark and photo-CIDNP spectra were recorded with a 90º-^{13}C pulse followed by a Hahn-echo and TPPM proton decoupling using a spinning frequency of 9 kHz. The build up was measured by placing a shutter in front of the fiber.

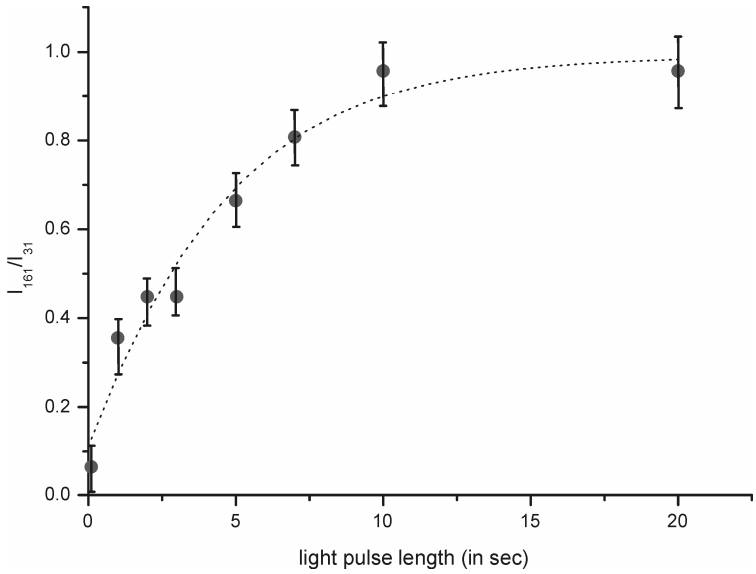

Figure 6.2. Build-up of light-induced nuclear polarization. The dashed line is the first order kinetics fit to the data.

The details of the light setup are described in Chapter 1. The light pulse was applied just before the 90º-^{13}C pulse. The delay between the light pulse and the 90º-^{13}C pulse was kept constant at 5 μs. The length of the light pulse plus 12 s was used always for relaxation as the recycle delay. 3k scans were collected for each experiment and a spinning frequency of 3.6 kHz was used.

6.2.1 Steady-state photo-CIDNP

Figure 6.1A shows the MAS NMR response from the protein matrix with strong signals in the aliphatic region and weak signals in the aromatic and carbonyl regions. The figure 6.1B has been obtained under continuous illumination with white light and represents photo-CIDNP in the steady state, i.e. a balance between light-induced production of nuclear polarisation on the one hand and relaxation on the other hand. Under these conditions, both enhanced absorptive (positive) and emissive (negative) signals are observed in the R26 RCs (Chapter 2 and 3). In natural abundance ^{13}C samples, spin diffusion can be neglected. All light-induced signals thus appear in the aromatic region and no enhancement is observed for signals in the aliphatic region. The emissive signals are detected in the region of methine carbon response. Thus, the signal in the aliphatic region (31 ppm), originating from the protein matrix, can be taken as an internal standard. In a similar way, the strongest light-induced signal at 161 ppm provides a standard for the photo-CIDNP intensity. Hence, both signals are good markers for studying the build-up of photo-CIDNP towards the steady state.

6.2.2 Build-up kinetics

Figure 6.2 shows the build-up of the light-induced nuclear polarization towards the steady state. Each point is the ratio of the intensities of the peak at 161 ppm to the peak at 31 ppm at

different light pulse lengths. A fit to first-order build-up kinetics I_{161}/I_{31} = 1- exp (-*kt*) +0.07 yields $k = 0.27\ s^{-1}$. The initial point (no light) is at 0.07 due to the background response from aromatic natural abundance ^{13}C in the dark spectrum. 50% of the steady-state photo-CIDNP is reached after ~ 4 s. After about ~ 10 s, the steady state is reached to ~ 90%. For comparable experimental conditions, an average value of 50 photons per second per RC has been estimated (Matysik et al., 2001a). Hence, the steady state is almost reached after ~500 photons per RC. The build-up kinetics of the absorptive and emissive signals is comparable. For the kinetics of the DD mechanism, the build-up of the steady state has been simulated by Polenova and McDermott (Polenova and McDermott, 1999), also assuming light excitation with 50 photons per second. Moreover, the time constant of $0.20\ s^{-1}$ for the simulated data is in line with $k = 0.27\ s^{-1}$ determined by the experimental data. The kinetic model proposed by Polenova and McDermott thus appears to be consistent with the data in figure 6.2. In fact, this is expected as the time scales of polarization build up from a single photon are less than 50 ns for the mechanisms are well separated from the build-up after more than 50 photons.

A mechanical shutter can not be extended to a nanosecond time resolution. This should be possible with a pulsed laser that produces nanosecond pulses. Such time-resolved studies with nanosecond time resolution would be ideal for probing the details of the single photon processes. In addition, time-resolved photo-CIDNP can be used to extract information on the electronic structure of the intermediate states of the photochemical cycle.

6.3 Ideas for application of photo-CIDNP

It has been shown that the photo-CIDNP MAS NMR intensities of the RCs of *Rb. sphaeroides* WT and R26 are enhanced by a factor of 10000 at a field strength of 4.7 T (Chapters 2 and 3). This strong enhancement in the photo-CIDNP MAS NMR intensities of the RCs can be used in many different ways for various applications. Some of these ideas are presented here.

6.3.1 Construction of artificial photosynthetic device

The first comprehensive map of the electronic ground state of the photochemically active cofactors in the RC has been presented in Chapter 4. In recent years, there has been a great deal of progress in mimicking the photosynthetic process by means of artificial molecular constructs based on porphyrins systems (Wasielewski, 1992). The knowledge about the electronic structure of the donor, P, the acceptor, Φ and the interaction with the histidine residue obtained from the bacterial RC provides sufficient impetus for strarting modelling studies with the aim of building artificial photosynthetic devices. Constructing models of such donor acceptor systems can be the first step in this direction. The model of the viable donor acceptor system can then be used to construct it through organic synthesis.

6.3.2 Use of photo-CIDNP as a 'spin torch'

Photo-CIDNP has been observed to diffuse away from the cofactors where it is generated (Matysik et al., 2001a; Matysik et al., 2001b). It can therefore be used as a 'spin torch'. This 'spin torch', based on a secondary polarization transfer mechanism such as spin diffusion, can explore the binding pocket in the reaction center and its influence on the cofactors. This may be done by labeling of particular amino acids in the binding pocket surrounding the cofactors in the active A-branch. The amino acids would gain polarization through spin diffusion from the cofactors and the polarization can then further diffuse to other parts of the protein backbone. 'Spin torches' may also be used to illuminate surfaces and to study the function of biological systems.

6.3.3 Study of intact cells with NMR

NMR is now routinely used to study structure, dynamics and functional mechanisms of biomacromolecules as well as for medical imaging. However, sensitivity and resolution are insufficient for routine investigations of molecules inside cells in the natural environment. On the other hand, the limited number of favorable cases where NMR of biomolecules in cells could be obtained have demonstrated the high potential of such studies. For instance, the metabolic composition in whole cells can be studied with High-Resolution Magic-Angle-Spinning (MAS) ^{1}H NMR provided a high concentration of cellular components is present (Chauton et al., 2003). Likewise, NMR images from single ova cells have been obtained but are limited to μm resolution (Aguayo et al., 1986). In this thesis it has been shown that the photo-CIDNP MAS NMR enabled the study of the special pair BChl molecules in the native cellular environment at nanomolar concentrations (Chapter 3). Photo-CIDNP MAS NMR can thus be extended to study cells from other photosynthetic bacteria.

6.3.4 Increasing sensitivity in Magnetic Resonance Imaging

Magnetic Resonance Imaging (MRI) as an experimental noninvasive technique can provide important information on physiological processes that is otherwise inaccessible. It can be used to study dynamic processes in biological systems. One such application is the investigation of the metabolic pathways in plants using ^{13}C labeled precursors (Köckenberger, 2001; Köckenberger et al., 2004). However, owing to the low sensitivity of ^{13}C NMR experiments, it is difficult to resolve ^{13}C tracers spatially in intact plants. In these experiments, if it is possible to transfer the primary polarization from the initially enhanced nuclei by photo-CIDNP to the secondary nuclei in plants, it might considerably increase the sensitivity. Contrast agents are added for better images of MRI, but these contrast agents are not always generally applicable. In this instance, 'spin torches' could provide a very good alternative.

6.3.5 Detection of a single nuclear spin with photo-CIDNP MRFM

Magnetic Resonance Force Microscopy (MRFM) in combination with photo-CIDNP may provide a method to overcome the inherent insensitivity of NMR allowing the detection of a single spin. Recently, a single electron spin has been detected by MRFM (Rugar et al., 2004). MRFM is based on mechanical detection using an AFM-type cantilever. The principle is based on the fact that when a sample carrying a magnetic dipole moment is put on a cantilever, a force $F_z = M_z \bullet \partial B/\partial z$ is exerted on this lever in the presence of a magnetic field gradient (Verhagen, 2002). The magnetization and, therefore, the force is made time dependent by inverting the magnetization adiabatically. This process then matches the cantilever frequency resulting in a oscillatory deflection observed in the MRFM experiment. MRFM has been used to observe quadropolar nuclei in ^{69}Ga, ^{71}Ga and ^{27}Al in device-type GaAs and AlGaAs layers (Verhagen et al., 2002). On the other hand, cofactors in intact cells have been observed at atomic resolution with photo-CIDNP (Chapter 3). MRFM in combination with photo-CIDNP may be used for looking at single nuclear spins in the cofactor molecules inside a cell.

To conclude, the great improvement in NMR signal sensitivity and selectivity reached with this thesis provides a number of applications in the world of magnetic resonance techniques. Hence, the author expects that photo-CIDNP will play an important role in the current efforts to overcome the intrinsic limits of NMR.

7 Bibliography

Aguayo, J.B., S.J. Blackband, J. Schoeniger, M.A. Mattingly, and M. Hintermann. 1986. Nuclear Magnetic Resonance imaging of a single cell. *Nature* 322, 190.

Alegria, G., and P.L. Dutton. 1991. Langmuir-Blodgett monolayer films of the *Rhodopseudomonas viridis* reaction center - Determination of the order of the hemes in the cytochrome-c subunit.2. *Biochim. Biophys. Acta* 1057, 258.

Alia, J. Matysik, I. de Boer, P. Gast, H.J. van Gorkom, and H.J.M. de Groot. 2004a. Heteronuclear 2D (^{1}H-^{13}C) MAS NMR resolves the electronic structure of coordinated histidines in light-harvesting complex II: Assessment of charge transfer and electronic delocalization effect. *J. Biomol. NMR* 28, 157.

Alia, J. Matysik, C. Soede-Huijbregts, M. Baldus, J. Raap, J. Lugtenburg, P. Gast, H.J. van Gorkom, A.J. Hoff, and H.J.M. de Groot. 2001. Ultrahigh field MAS NMR dipolar correlation spectroscopy of the histidine residues in light-harvesting complex II from photosynthetic bacteria reveals partial internal charge transfer in the B850/His complex. *J. Am. Chem. Soc.* 123, 4803.

Alia, E. Roy, P. Gast, H.J. van Gorkum, H.J.M. de Groot, G. Jeschke, and J. Matysik. 2004b. Photochemically Induced Dynamic Nuclear Polarization in photosystem I of plants observed by ^{13}C Magic-Angle Spinning NMR. *J. Am. Chem. Soc.* 126, 12819.

Bahatyrova, S., R.N. Frese, C.A. Siebert, J.D. Olsen, K.O. van der Werf, R. van Grondelle, R.A. Niederman, P.A. Bullough, C. Otto, and C.N. Hunter. 2004. The native architecture of a photosynthetic membrane. *Nature* 430, 1058.

Bargon, J., H. Fischer, and U. Johnsen. 1967. Kernresonanz-Emissionslinien wahrend rascher Radikalreaktionen I. Aufnahmeverfahren und Beispiele. *Z. Naturforsch.* A 22, 1551.

Beekman, L.M.P., R.W. Visschers, R. Monshouwer, M. Heerdawson, T.A. Mattioli, P. McGlynn, C.N. Hunter, B. Robert, I.H.M. van Stokkum, R. van Grondelle, and M.R. Jones. 1995. Time-Resolved and steady-state spectroscopic analysis of membrane-bound reaction centers from *Rhodobacter sphaeroides* - comparisons with detergent-solubilized complexes. *Biochemistry* 34, 14712.

Bennett, A.E., C.M. Rienstra, M. Auger, K.V. Lakshmi, and R.G. Griffin. 1995. Heteronuclear decoupling in rotating solids. *J. Chem. Phys.* 103, 6951.

Bernhardt, K., and H.W. Trissl. 2000. Escape probability and trapping mechanism in purple bacteria: revisited. *Biochim. Biophys. Acta* 1457, 1.

Blankenship, R.E. 1992. Origin and Early Evolution of Photosynthesis. *Photosynth. Res.* 33, 91.

Blankenship, R.E. 2002. Molecular mechanisms of Photosynthesis. Blackwell Science Ltd., Oxford.

Blankenship, R.E., A. McGuire, and K. Sauer. 1975. Chemically Induced Dynamic Electron Polarization in chloroplasts at room temperature: evidence for triplet state participation in photosynthesis. *Proc. Natl. Acad. Sci. U. S. A.* 72, 4943.

Blankenship, R.E., T.J. Schaafsma, and W.W. Parson. 1977. Magnetic-Field effects on radical pair intermediates in bacterial photosynthesis. *Biochim. Biophys. Acta* 461, 297.

Brune, D.C. 1995. Sulfur compounds as photosynthetic electron donors. *In* Anoxygenic Photosynthetic Bacteria. Blankenship RE, Madigan, M.T., Bauer, C.E., editor. Kluwer Academic Publisher, Dordrecht. 847.

Camara-Artigas, A., D. Brune, and J.P. Allen. 2002. Interactions between lipids and bacterial reaction centers determined by protein crystallography. *Proc. Natl. Acad. Sci. U. S. A.* 99, 11055.

Castellani, F., B. van Rossum, A. Diehl, M. Schubert, K. Rehbein, and H. Oschkinat. 2002. Structure of a protein determined by solid-state magic-angle-spinning NMR spectroscopy. *Nature* 420, 98.

Chan, C.K., T.J. Dimagno, L.X.Q. Chen, J.R. Norris, and G.R. Fleming. 1991. Mechanism of the initial charge separation in bacterial photosynthetic reaction centers. *Proc. Natl. Acad. Sci. U. S. A.* 88, 11202.

Chauton, M.S., T.R. Storseth, and G. Johnsen. 2003. High-resolution magic angle spinning H^1 NMR analysis of whole cells of *Thalassiosira pseudonana* (Bacillariophyceae): Broad range analysis of metabolic composition and nutritional value. *J. Appl. Phycol.* 15, 533.

Cherubini, A., and A. Bifone. 2003. Hyperpolarised xenon in biology. *Prog. Nucl. Magn. Reson. Spectrosc.* 42, 1.

Closs, G.L., and L.E. Closs. 1969. Induced Dynamic Nuclear Spin Polarization in reactions of photochemically and thermally generated triplet diphenylmethylene. *J. Am. Chem. Soc.* 91, 4549.

de Groot, H.J.M. 2000. Solid-state NMR spectroscopy applied to membrane proteins. *Curr. Opin. Struct. Biol.* 10, 593.

Diller, A., Alia, E. Roy, P. Gast, H.J. van Gorkum, H.J.M. de Groot, J. Zaanen, C. Glaubitz, and J. Matysik. 2005. Photo-CIDNP solid-state NMR on photosystems I and II: What makes P680 special? *Photosynth. Res.* 84, 303-304.

Dorlet, P., A.W. Rutherford, and S. Un. 2000. Orientation of the tyrosyl D, pheophytin anion, and semiquinone Q_A^- radicals in photosystem II determined by high-field electron paramagnetic resonance. *Biochemistry* 39, 7826.

Ermler, U., G. Fritzsch, S.K. Buchanan, and H. Michel. 1994. Structure of the photosynthetic reaction center from *Rhodobacter sphaeroides* at 2.65-angstrom resolution - cofactors and protein-cofactor interactions. *Structure* 2, 925.

Facelli, J.C. 1998. Density functional theory calculations of the structure and the ^{15}N and ^{13}C chemical shifts of methyl bacteriopheophorbide *a* and bacteriochlorophyll *a*. *J. Phys. Chem. B* 102, 2111.

Feher, D., and M.Y. Okamura. 1978. The Photosynthetic Bacteria. Plenum Press, New York.

Fischer, M.R., H.J.M. de Groot, J. Raap, C. Winkel, A.J. Hoff, and J. Lugtenburg. 1992. ^{13}C Magic-Angle Spinning NMR-study of the light-induced and temperature-dependent changes in

Rhodobacter sphaeroides R26 reaction centers enriched in 4'-^{13}C tyrosine. *Biochemistry* 31, 11038.

Gibasiewicz, K., K. Brettel, A. Dobek, and W. Leibl. 1999. Re-examination of primary radical pair recombination in *Rp. viridis* with Q_A reduced. *Chem. Phys. Lett.* 315, 95.

Goez, M. 1997. Photochemically Induced Dynamic Nuclear Polarization. *Adv. Photochem.* 23, 63.

Goldstein, R.A., and S.G. Boxer. 1987. Effects of nuclear-spin polarization on reaction dynamics in photosynthetic bacterial reaction centers. *Biophys. J.* 51, 937.

Goldstein, R.A., and S.G. Boxer. 1989. The effect of very high magnetic-fields on the reaction dynamics in bacterial reaction centers - Implications for the reaction-mechanism. *Biochim. Biophys. Acta* 977, 78-86.

Griffin, R.G. 1998. Dipolar recoupling in MAS spectra of biological solids. *Nature Struct. Biol.* 5, 508.

Hall, D.A., D.C. Maus, G.J. Gerfen, S.J. Inati, L.R. Becerra, F.W. Dahlquist, and R.G. Griffin. 1997. Polarization-enhanced NMR spectroscopy of biomolecules in frozen solution. *Science* 276, 930.

Hara, M., Y. Asada, and J. Miyake. 1993. Photoreaction unit sheet of *Rhodopseudomonas viridis*. *Biosci. Biotech. Biochem.* 57, 871.

Hartmann, S.R., and E.L. Hahn. 1962. Nuclear double resonance in rotating frame. *Phys. Rev.* 128, 2042.

Hoff, A.J. 1981. Magnetic-Field effects on photosynthetic reactions. *Q. Rev. Biophys.* 14, 599.

Hoff, A.J., and J. Deisenhofer. 1997. Photophysics of photosynthesis. *Phys. Rep.* 287, 2.

Hoff, A.J., P. Gast, and J.C. Romijn. 1977a. Time-resolved ESR and Chemically Induced Dynamic Electron Polarisation of the primary reaction in a reaction center particle of *Rhodopseudomonas sphaeroides* wild type at low temperature. *FEBS Lett.* 73, 185.

Hoff, A.J., H. Rademaker, R. van Grondelle, and L.N.M. Duysens. 1977b. Magnetic-Field dependence of yield of triplet-state in reaction centers of photosynthetic bacteria. *Biochim. Biophys. Acta* 460, 547.

Holzapfel, W., U. Finkele, W. Kaiser, D. Oesterhelt, H. Scheer, H.U. Stilz, and W. Zinth. 1989. Observation of a bacteriochlorophyll anion radical during the primary charge separation in a reaction center. *Chem. Phys. Lett.* 160, 1.

Holzapfel, W., U. Finkele, W. Kaiser, D. Oesterhelt, H. Scheer, H.U. Stilz, and W. Zinth. 1990. Initial electron-transfer in the reaction center from *Rhodobacter sphaeroides*. *Proc. Natl. Acad. Sci. U. S. A.* 87, 5168.

Holzwarth, A.R., and M.G. Muller. 1996. Energetics and kinetics of radical pairs in reaction centers from *Rhodobacter sphaeroides*. A femtosecond transient absorption study. *Biochemistry* 35, 11820.

Hore, P.J., and R.W. Broadhurst. 1993. Photo-CIDNP of biopolymers. *Prog. Nucl. Magn. Reson. Spectrosc.* 25, 345.

Hore, P.J., and R. Kaptein. 1982. Photochemically Induced Dynamic Nuclear Polarization of biological molecules using continuous wave and time-resolved methods. *In* ACS Symposium. Levy GC, editor, Washington.

Hu, K.N., H.H. Yu, T.M. Swager, and R.G. Griffin. 2004. Dynamic Nuclear Polarization with biradicals. *J. Am. Chem. Soc.* 126, 10844.

Hu, X.C., T. Ritz, A. Damjanovic, F. Autenrieth, and K. Schulten. 2002. Photosynthetic apparatus of purple bacteria. *Q. Rev. Biophys.* 35, 1.

Huber, M. 1997. On the electronic structure of the primary electron donor in bacterial photosynthesis - The bacteriochlorophyll dimer as viewed by EPR/ENDOR methods. *Photosynth. Res.* 52, 1.

Hulsebosch, R.J., I.V. Borovykh, S.V. Paschenko, P. Gast, and A.J. Hoff. 1999. Radical pair dynamics and interactions in quinone-reconstituted photosynthetic reaction centers of *Rb. sphaeroides* R26: A multifrequency magnetic resonance study. *J. Phys. Chem. B* 103, 6815.

Hulsebosch, R.J., I.V. Borovykh, S.V. Paschenko, P. Gast, and A.J. Hoff. 2001. Radical pair dynamics and interactions in quinone-reconstituted photosynthetic reaction centers of *Rb. sphaeroides* R26: A multifrequency magnetic resonance study. *J. Phys. Chem. B* 105, 10146.

Imhoff, J.F. 1995. Taxonomy and physiology of phototropic purple bacteria. *In* Anoxygenic Photosynthetic Bacteria. Blankenship RE, Madigan, M.T., Bauer, C.E., editor. Kluwer Academic Publishers, Dordrecht. 1.

Jeschke, G. 1997. Electron-electron-nuclear three-spin mixing in spin-correlated radical pairs. *J. Chem. Phys.* 106, 10072.

Jeschke, G. 1998. A new mechanism for Chemically Induced Dynamic Nuclear Polarization in the solid state. *J. Am. Chem. Soc.* 120, 4425.

Jeschke, G., and J. Matysik. 2003. A reassessment of the origin of Photochemically Induced Dynamic Nuclear Polarization effects in solids. *Chem. Phys.* 294, 239.

Jia, Y.W., T.J. Dimagno, C.K. Chan, Z.Y. Wang, M. Du, D.K. Hanson, M. Schiffer, J.R. Norris, G.R. Fleming, and M.S. Popov. 1993. Primary charge separation in mutant reaction centers of *Rhodobacter capsulatus*. *J. Phys. Chem.* 97, 13180.

Jordan, P.M. 1991. *In* Biosynthesis of tetrapyrroles. Jordan PM, editor. Elsevier, Amsterdam. 1.

Kaptein, R., and J.L. Oosterhoff. 1969. Chemically Induced Dynamic Nuclear polarization II (relation with anomalous ESR spectra). *Chem. Phys. Lett.* 4, 195.

Klette, R., J.T. Torring, M. Plato, K. Möbius, B. Bonigk, and W. Lubitz. 1993. Determination of the G Tensor of the primary donor cation Radical in single-crystals of *Rhodobacter sphaeroides* R26 reaction centers by 3-mm high-field EPR. *J. Phys. Chem.* 97, 2015.

Köckenberger, W. 2001. Functional imaging of plants by magnetic resonance experiments. *Trends Plant Sci.* 6, 286.

Köckenberger, W., C. De Panfilis, D. Santoro, P. Dahiya, and S. Rawsthorne. 2004. High resolution NMR microscopy of plants and fungi. *J. Microsc.* 214, 182.

Kondo, T., M. Arakawa, T. Hirai, T. Wakayama, M. Hara, and J. Miyake. 2002. Enhancement of hydrogen production by a photosynthetic bacterium mutant with reduced pigment. *J. Biosci. Bioengineering* 93, 145.

Kubelka, P., and F. Munk. 1931. Ein Beitrag zur Optik der Farbanstriche. *Z. Techn. Techn. Physik* 12, 593.

Laws, D.D., H.M.L. Bitter, and A. Jerschow. 2002. Solid-state NMR spectroscopic methods in Chemistry. *Angew. Chem. Int. Ed.* 41, 3096.

Lendzian, F., M. Huber, R.A. Isaacson, B. Endeward, M. Plato, B. Bonigk, K. Möbius, W. Lubitz, and G. Feher. 1993. The electronic-structure of the primary donor cation-radical in *Rhodobacter sphaeroides* R26 - ENDOR and Triple-Resonance studies in single-crystals of reaction centers. *Biochim. Biophys. Acta* 1183, 139.

Lin, X., H.A. Murchison, V. Nagarajan, W.W. Parson, J.P. Allen, and J.C. Williams. 1994. Specific alteration of the oxidation potential of the electron-donor in reaction centers from *Rhodobacter sphaeroides*. *Proc. Natl. Acad. Sci. U. S. A.* 91, 10265.

Lubitz, W., F. Lendzian, and R. Bittl. 2002. Radicals, radical pairs and triplet states in photosynthesis. *Acc. Chem. Res.* 35, 313.

Madigan, M.T., and J.G. Ormerod. 1995. Taxonomy, physiology and ecology of Heliobacteria. *In* Anoxygenic Photosynthetic Bacteria. Blankenship RE, Madigan, M.T., Bauer, C.E., editor. Kluwer Academic Publishers, Dordrecht. 17.

Martin, J.L., J. Breton, A.J. Hoff, A. Migus, and A. Antonetti. 1986. Femtosecond spectroscopy of electron-transfer in the reaction center of the photosynthetic bacterium *Rhodopseudomonas sphaeroides* R26 -direct electron-transfer from the dimeric bacteriochlorophyll primary donor to the bacteriopheophytin acceptor with a time constant 2.8 +/- 0.2 psec. *Proc. Natl. Acad. Sci. U. S. A.* 83, 957.

Mattioli, T.A., A. Hoffmann, B. Robert, B. Schrader, and M. Lutz. 1991. Primary donor structure interactions in bacterial reaction centers from near-infrared fourier-transform Resonance Raman-Spectroscopy. *Biochemistry* 30, 4648.

Matysik, J., Alia, P. Gast, J. Lugtenburg, A.J. Hoff, and H.J.M. de Groot. 2001a. Photochemically induced dynamic nuclear polarization observed in bacterial photosynthetic reaction centers observed by ^{13}C solid state NMR. *Perspect. Sol. State NMR Biol.* 1, 215.

Matysik, J., Alia, P. Gast, H.J. van Gorkom, A.J. Hoff, and H.J.M. de Groot. 2000a. Photochemically induced nuclear spin polarization in reaction centers of photosystem II observed by ^{13}C solid-state NMR reveals a strongly asymmetric electronic structure of the P^{+680} primary donor chlorophyll. *Proc. Natl. Acad. Sci. U. S. A.* 97, 9865.

Matysik, J., Alia, J.G. Hollander, T. Egorova-Zachernyuk, P. Gast, and H.J.M. de Groot. 2000b. A set-up to study Photochemically Induced Dynamic Nuclear Polarization in photosynthetic reaction centres by solid-state NMR. *Indian J. Biochem. Biophys.* 37, 418.

Matysik, J., E. Schulten, Alia, P. Gast, J. Raap, J. Lugtenburg, A.J. Hoff, and H.J.M. de Groot. 2001b. Photo-CIDNP ^{13}C magic angle spinning NMR on bacterial reaction centres: Exploring the electronic structure of the special pair and its surroundings. *Biol. Chem.* 382, 1271.

McDermott, A., T. Polenova, A. Bockmann, K.W. Zilm, E.K. Paulsen, R.W. Martin, and G.T. Montelione. 2000. Partial NMR assignments for uniformly (^{13}C, ^{15}N)-enriched BPTI in the solid state. *J. Biomol. NMR* 16, 209.

McDermott, A., M.G. Zysmilich, and T. Polenova. 1998. Solid state NMR studies of photoinduced polarization in photosynthetic reaction centers: mechanism and simulations. *Sol. State NMR* 11, 21.

Minard, K.R., and R.A. Wind. 2001. Solenoidal microcoil design - Part II: Optimizing winding parameters for maximum signal-to-noise performance. *Concept Magn. Res.* 13, 190.

Moore, L.J., H.L. Zhou, and S.G. Boxer. 1999. Excited-state electronic asymmetry of the special pair in photosynthetic reaction center mutants: Absorption and Stark spectroscopy. *Biochemistry* 38, 11949.

Okamura, M.Y., R.A. Isaacson, and G. Feher. 1975. Primary acceptor in bacterial photosynthesis - obligatory role of ubiquinone in photoactive reaction centers of *Rhodopseudomonas sphaeroides*. *Proc. Natl. Acad. Sci. U. S. A.* 72, 3491.

Owen, G.M., A.J. Hoff, and M.R. Jones. 1997. Excitonic interactions between the reaction center and antennae in purple photosynthetic bacteria. *J. Phys. Chem. B* 101, 7197.

Palaniappan, V., P.C. Martin, V. Chynwat, H.A. Frank, and D.F. Bocian. 1993. Comprehensive Resonance Raman study of photosynthetic reaction centers from *Rhodobacter sphaeroides* - Implications for pigment structure and pigment-protein interactions. *J. Am. Chem. Soc.* 115, 12035.

Papiz, M.Z., S.M. Prince, A.M. HawthornthwaiteLawless, G. McDermott, A.A. Freer, N.W. Isaacs, and R.J. Cogdell. 1996. A model for the photosynthetic apparatus of purple bacteria. *Trends Plant Sci.* 1, 198.

Pauli, J., M. Baldus, B. van Rossum, H. de Groot, and H. Oschkinat. 2001. Backbone and side-chain ^{13}C and ^{15}N signal assignments of the alpha-spectrin SH3 domain by magic angle spinning solid-state NMR at 17.6 tesla. *Chembiochem* 2, 272.

Pierson, B.K., and R.W. Castenholz. 1995. Taxonomy and physiology of filamentous anoxygenic phototrophs. *In* Anoxygenic Photosynthetic Bacteria. Blankenship RE, Madigan, M.T., Bauer, C.E., editor. Kluwer Academic Publishers, Dordrecht. 31.

Pines, A., M. G. Gibby, and J.S. Waugh. 1973. Proton-enhanced NMR of dilute spins in solids. *J. Chem. Phys.* 59, 569.

Polenova, T., and A.E. McDermott. 1999. A coherent mixing mechanism explains the photoinduced nuclear polarization in photosynthetic reaction centers. *J. Phys. Chem. B* 103, 535.

Prakash, S., Alia, P. Gast, G. Jeschke, H.J.M. de Groot, and J. Matysik. 2003. Photochemically Induced Dynamic Nuclear polarisation in entire bacterial photosynthetic units observed by ^{13}C magic-angle spinning NMR. *J. Mol. Struct.* 661, 625.

Raftery, D., and B.F. Chmelka. 1994. *Nuc. Magn. Reson.* 30, 112.

Rautter, J., F. Lendzian, W. Lubitz, S. Wang, and J.P. Allen. 1994. Comparative study of reaction centers from photosynthetic purple bacteria - Electron Paramagnetic Resonance and Electron Nuclear Double Resonance Spectroscopy. *Biochemistry* 33, 12077.

Rugar, D., R. Budakian, H.J. Mamin, and B.W. Chui. 2004. Single spin detection by Magnetic Resonance Force Microscopy. *Nature* 430, 329.

Schmidt, S., T. Arlt, P. Hamm, C. Lauterwasser, U. Finkele, G. Drews, and W. Zinth. 1993. Time-Resolved spectroscopy of the primary photosynthetic processes of membrane-bound reaction centers from an antenna-deficient mutant of *Rhodobacter capsulatus*. *Biochim. Biophys. Acta* 1144, 385.

Schrader, B., and G. Bergmann. 1967. Die Intensitat des Ramanspektrums polykristalliner substanzen I. Strahlungsbilanz von Substanz und Probenanordnung. *Z. Anal. Chem. Fresenius* 225, 230.

Schulten, E.A.M., J. Matysik, Alia, S. Kiihne, J. Raap, J. Lugtenburg, P. Gast, A.J. Hoff, and H.J.M. de Groot. 2002. ^{13}C MAS NMR and photo-CIDNP reveal a pronounced asymmetry in the electronic ground state of the special pair of *Rhodobacter sphaeroides* reaction centers. *Biochemistry* 41, 8708.

Shochat, S., T. Arlt, C. Francke, P. Gast, P.I. Vannoort, S.C.M. Otte, H.P.M. Schelvis, S. Schmidt, E. Vijgenboom, J. Vrieze, W. Zinth, and A.J. Hoff. 1994. Spectroscopic characterization of reaction centers of the (M)Y210W mutant of the photosynthetic bacterium *Rhodobacter sphaeroides*. *Photosynth. Res.* 40, 55.

Solomon, I. 1955. Relaxation processes in a system of two Spins. *Phys. Rev.* 99, 559-565.

Stoll, S. 2003. Spectral simulations in solid-state EPR. *PhD Thesis* ETH, Zürich.

Stowell, M.H.B., T.M. McPhillips, D.C. Rees, S.M. Soltis, E. Abresch, and G. Feher. 1997. Light-induced structural changes in photosynthetic reaction center: Implications for mechanism of electron-proton transfer. *Science* 276, 812.

Sündstrom, V., and R. van Grondelle. 1995. Kinetics of excitaiton transfer and trapping in purple bacteria. *In* Anoxygenic Photosynthetic Bacteria. Blankenship RE, Madigan, R.T., Bauer, C.E., editor. Kluwer Academic Publisher, Dordrecht. 349.

Suter, D., and J. Mlynek. 1991. Laser excitation and detection of magnetic resonance. *Adv. Magn. Opt. Reson.* 16, 1.

Tang, X.S., M. Zheng, D.A. Chisholm, G.C. Dismukes, and B.A. Diner. 1996. Investigation of the differences in the local protein environments surrounding tyrosine radicals Y-Z$^{\cdot}$and Y-D$^{\cdot}$ in photosystem II using wild-type and the D2-Tyr160Phe mutant of *Synechocystis* 6803. *Biochemistry* 35, 1475.

Till, U., I.B. Klenina, Proskuryakov, II, A.J. Hoff, and P.J. Hore. 1997. Recombination dynamics and EPR spectra of the primary radical pair in bacterial photosynthetic reaction centers with blocked electron transfer to the primary acceptor. *J. Phys. Chem. B* 101, 10939.

Tycko, R. 1998. Optical pumping in indium phosphide: ^{31}P NMR measurements and potential for signal enhancement in biological solid state NMR. *Sol. State NMR* 11, 1.

Tycko, R., and J.A. Reimer. 1996. Optical pumping in solid state nuclear magnetic resonance. *J. Phys. Chem.* 100, 13240.

van Brederode, M.E., F. van Mourik, I.H.M. van Stokkum, M.R. Jones, and R. van Grondelle. 1999. Multiple pathways for ultrafast transduction of light energy in the photosynthetic reaction center of *Rhodobacter sphaeroides*. *Proc. Natl. Acad. Sci. U. S. A.* 96, 2054.

van Gemerden, H., and J. Mas. 1995. Ecology of phototrophic bacteria. *In* Anoxygenic Photosynthetic Bacteria. Blankenship RE, Madigan, M.T., Bauer, C.E., editor. Kluwer Academic Publisher, Dordrecht. 49.

van Lenthe, E., P.E.S. Wormer, and A. van der Avoird. 1997. Density functional calculations of molecular g-tensors in the zero-order regular approximation for relativistic effects. *J. Chem. Phys.* 107, 2488.

Velde, G.T., F.M. Bickelhaupt, E.J. Baerends, C.F. Guerra, S.J.A. van Gisbergen, J.G. Snijders, and T. Ziegler. 2001. Chemistry with ADF. *J. Comput. Chem.* 22, 931.

Verhagen, R. 2002. Novel radio-frequency and force-detected approaches in Nuclear Magnetic Resonance. *PhD Thesis* Katholieke Universiteit, Nijmegen.

Verhagen, R., A. Wittlin, C.W. Hilbers, H. van Kempen, and A.P.M. Kentgens. 2002. Spatially resolved spectroscopy and structurally encoded imaging by Magnetic Resonance Force Microscopy of quadrupolar spin systems. *J. Am. Chem. Soc.* 124, 1588.

Visschers, R.W., S.I.E. Vulto, M.R. Jones, R. van Grondelle, and R. Kraayenhof. 1999. Functional LH1 antenna complexes influence electron transfer in bacterial photosynthetic reaction centers. *Photosynth. Res.* 59, 95.

Ward, H.R., and R.G. Lawler. 1967. Nuclear Magnetic Resonance emission and enhanced absorption in rapid organometallic reactions. *J. Am. Chem. Soc.* 89, 5518.

Wasielewski, M.R. 1992. Photoinduced electron-transfer in supramolecular systems for artificial photosynthesis. *Chem. Rev.* 92, 435.

Weiss, E.A., M.J. Ahrens, L.E. Sinks, A.V. Gusev, M.A. Ratner, and M.R. Wasielewski. 2004. Making a molecular wire: Charge and spin transport through para-phenylene oligomers. *J. Am. Chem. Soc.* 126, 5577-5584.

Yeates, T.O., H. Komiya, A. Chirino, D.C. Rees, J.P. Allen, and G. Feher. 1988. Structure of the reaction center from *Rhodobacter sphaeroides* R26 and 2.4.1-protein-cofactor (bacteriochlorophyll, bacteriopheophytin, and carotenoid) interactions.4. *Proc. Natl. Acad. Sci. U. S. A.* 85, 7993.

Zech, S.G., A.J. Wand, and A.E. McDermott. 2005. Protein structure determination by high-resolution solid-state NMR spectroscopy: Application to microcrystalline ubiquitin. *J. Am. Chem. Soc.* 127, 8618.

Zysmilich, M.G., and A. McDermott. 1994. Photochemically Induced Dynamic Nuclear-Polarization in the solid-state ^{15}N spectra of reaction centers from photosynthetic bacteria *Rhodobacter sphaeroides* R26. *J. Am. Chem. Soc.* 116, 8362.

Zysmilich, M.G., and A. McDermott. 1996a. Natural abundance solid-state carbon NMR studies of photosynthetic reaction centers with photoinduced polarization. *Proc. Natl. Acad. Sci. U. S. A.* 93, 6857.

Zysmilich, M.G., and A. McDermott. 1996b. Photochemically induced nuclear spin polarization in bacterial photosynthetic reaction centers: Assignments of the ^{15}N SSNMR spectra. *J. Am. Chem. Soc.* 118, 5867.

List of Abbreviations

1D	One dimensional
2D	Two dimensional
ALA	δ-Aminolevulenic acid
B	Accessory bacteriochlorophyll
BChl	Bacteriochlorophyll
BPhe, Φ	Bacteriopheophytin
C	Carotenoid
CIDNC	Chemically induced dynamic nuclear coherence
C-L	Carbon atom on cofactor P_L
C-M	Carbon atom on cofactor P_M
CP	Cross polarization
CSA	Chemical shift anisotropy
DD	Differential decay
DFT	Density functional theory
DR	Differential relaxation
DZP	Double zeta polarization
EDTA	Ethylene diamino tetra acetate
EPR	Electron paramagnetic resonance
H	Protein subunit H of the reaction center
His	Histidine
IUPAC	International union of pure and applied chemistry
L	Protein subunit L of the reaction center
LDAO	*N,N*-dimethyldodecylamine-*N*-oxide
LH I	Light harvesting complex I
LH II	Light harvesting complex II
M	Protein subunit M of the reaction center
MAS	Magic-angle spinning
MRI	Magnetic resonance imaging
MRFM	Magnetic resonace force microscopy
NMR	Nuclear magnetic resonance
OD	Optical density
ODV	Optical density per volume
P	Special pair, primary electron donor

Photo-CIDNP	Photochemically induced dynamic nuclear polarization
PS I	Photosystem I
PS II	Photosystem II
PSU	Photosynthetic unit
Q	Ubiquinone
Rb.	*Rhodobacter*
RC	Reaction center
RFDR	Radio frequency driven recoupling sequence
TPPM	Two pulse-phase modulation
TSM	Electron-electron-nuclear three spin mixing
TZP	Triple zeta polarization
WT	Wild type
ZORA	Zero order regular approximation

Summary

Solid state magic angle spinning (MAS) NMR is fast developing as an important technique for the study of large membrane protein systems. However, it suffers from an inherent problem of low sensitivity and selectivity (**Chapter 1**). Photochemically induced dynamic nuclear polarization (photo-CIDNP) MAS NMR increases NMR intensities by induction of photochemical reactions, which shuffle the nuclear spin system out of its Boltzmann equilibrium. The understanding and development of photo-CIDNP MAS NMR can therefore provide a method to overcome the intrinsic insensitivity and non-selectivity of MAS NMR. Until now, photo-CIDNP in the solid state has been observed only in the natural photosynthetic reaction centers. In the photosynthetic bacterium, *Rhodobacter sphaeroides,* the primary photosynthetic process takes place in the pigment protein complex known as reaction center (RC). Four molecules of bacteriochlorophyll *a* (BChl *a*), two molecules of bacteriopheophytin a (BPhe *a*), two ubiquinone-10 molecules (Q), a non-haem iron (Fe^{2+}) and a carotenoid molecule (C) form the cofactors of the RC. The light induced electron transfer process starts at the primary donor, formed of two BChl molecules P_L and P_M. The special pair, P donates an electron to the BPhe molecule, Φ_A.

Three different mechanisms have been proposed to describe photo-CIDNP in solids.

- The electron-electron-nuclear three spin mixing (TSM) mechanism: According to this mechanism a net nuclear polarization is created due to the presence of both anisotropic hyperfine interaction and coupling between the two electron spins in the spin-correlated radical pair.
- The differential decay (DD) mechanism: In this mechanism a net photo-CIDNP effect is caused due to the anisotropic hyperfine coupling if spin-correlated radical pairs have different lifetimes in their singlet and triplet states.
- The differential relaxation (DR) mechanism: This takes place due to the significant differential relaxation between the nuclear spins in the special pair triplet ^3P and the nuclear spins in the singlet ground state of P.

The reconstruction of local electronic spin densities from photo-CIDNP intensities requires a thorough understanding of the mechanisms involved. Understanding the photo-CIDNP process is thus equivalent to gaining information on the primary step of photosynthesis.

In **Chapter 2**, ^{13}C photo-CIDNP MAS NMR studies from RCs of *Rhodobacter sphaeroides* WT are presented. Photo-CIDNP has been observed at three different magnetic field strengths. At a magnetic filed strength of 4.7 Tesla (200 MHz proton frequency), the

strongest enhancement of more than 10000 above the Boltzmann polarisation is observed. At higher fields, the enhancement factor decreases. The light induced NMR signals at all fields are emissive (negative) and could be assigned to P_L and P_M of the donor and the acceptor Φ_A. The photo-CIDNP MAS NMR spectra at the three different magnetic field strengths have been simulated assuming two competing mechanisms of polarisation transfer from electrons to nuclei, three-spin mixing (TSM) and differential decay (DD) mechanisms. The assignment of the light induced signals has been done with the help of simulations. The simulated spectra agree well with the photo-CIDNP MAS NMR spectra demonstrating that photo-CIDNP effect in the RCs from *Rb. sphaeroides* WT can be interpreted by TSM and DD mechanism.

The photo-CIDNP studies from the mutant strain *Rhodobacter sphaeroides* R26 are shown and discussed in **Chapter 3**. In the R26 RCs as compared to WT, the donor triplet lifetime is longer since no carotenoid molecule is present. The magnetic field effect of photo-CIDNP is similar for both RCs. However, the light induced signals assigned to the donor, P in the RCs of the R26 strain, are absorptive which could not be explained by the TSM and DD mechanism. This led us to consider the DR mechanism to be operative in R26, in addition to the two other mechanisms. Simulations done with inclusion of the DR mechanism have been able to reproduce the sign change in the light induced signals for the donor, P. The polarization pattern of WT RCs has thus been interpreted in terms of the spin density distribution in the radical pair state and the polarization change between the WT and R26 spectra in terms of the spin density distribution in the triplet state of the donor.

The strong photo-CIDNP enhancement at a field strength of 4.7 T has enabled the observation of cofactor molecules at a concentration of ~100 nM inside intact R26 cells without isotope enrichment (**Chapter 3**). The overall photo-CIDNP intensity pattern is in some details distinct from the isolated reaction centres at 4.7 T. The overall similarity between the photo-CIDNP spectrum from the isolated RCs and intact cells suggests that the ground-state electronic structure of the special pair is not strongly influenced by the surrounding protein complexes in the natural environment of an intact cell. Photo-CIDNP MAS NMR is thus established as a method to study the electronic structure of photosynthetic cofactors at the molecular and atomic resolution as well as at cellular concentrations.

^{13}C-^{13}C dipolar correlation photo-CIDNP MAS NMR studies have been performed in **Chapter 4** on RCs of *Rhodobacter sphaeroides* WT, selectively isotope labelled in all the BChl and BPhe cofactors at positions C-4, 5, 9, 10, 14, 15, 16 and 20, to provide a comprehensive map of the ground-state electronic structure of the cofactors involved in the electron transfer process. Three strong components are observed in the ^{13}C-^{13}C dipolar correlation photo-CIDNP MAS NMR spectra. These have been assigned to two BChls, P1 and P2, and one BPhe, Φ_A. In addition a weak component is observed which is assigned to another BChl, denoted as P3. Pronounced upfield shifts are present for P2 in the pyrrole ring I as compared to P1 and P3. The large upfield shifts could be explained by a hydrogen bond to

His L168, located in the proximity of the 3-acetyl group of P_L. Thus P_L is assigned to P2 making it a special BChl in the special pair. Then P_M is assigned to P1 and the weak component P3 is assigned to B_A. The electronic structure of the special pair is thus asymmetric in the ground state.

Photo-CIDNP studies have been further extended to entire photosynthetic unit (PSU) bound to membrane selectively ^{13}C-isotope labelled in all the BChl and BPheo cofactors at positions C-1, 3, 6, 8, 11, 13, 17 and 19 (**Chapter 5**). All the light induced signals for the membrane bound PSU are absorptive. Addition of detergent released intact PSU from the chromatophore membrane and caused significant changes in the sign and intensity pattern of the light-induced MAS NMR spectrum. In contrast, detergent solubilised PSU and detergent solubilised RCs with the same isotope label pattern exhibit essentially the same chemical shifts with only minor differences in the intensity pattern. The pronounced differences between intact membrane bound and detergent solubilized photosynthetic units has been explained by the loss of self-orientation of the membrane-bound samples by solubilization.

Chapter 6 provides a future outlook for photo-CIDNP studies on the RCs of *Rhodobacter sphaeroides*. The first part of the Chapter is devoted to the build up of the photo-CIDNP response. This paves the way for time-resolved photo-CIDNP experiments. The second part describes future developments in four different directions from biophysical studies to magnetic resonance force microscopy. The biophysical studies have provided information towards building artificial photosynthetic devices. Photo-CIDNP can be used as a ‘spin torch’ to explore the binding pocket and its influence on the cofactors. ‘Spin torches’ could also be used as contrast agents in Magnetic Resonance Imaging (MRI). Photo-CIDNP in combination with Magnetic Resonance Force Microscopy (MRFM) may allow for detection of single nuclear spin in the near future.

Samenvatting

Vaste-stof "magische hoek roterend", oftewel *magic angle spinning* (MAS), NMR ontwikkelt zich snel als een belangrijke techniek voor het bestuderen van grote membraaneiwitsystemen. Het inherente probleem van deze techniek is de lage gevoeligheid en selectiviteit (**Hoofdstuk 1**). Photo-chemically induced dynamic nuclear polarization (photo-CIDNP) MAS NMR verhoogt NMR intensiteiten door middel van de inductie van fotochemische reacties die het nucleaire spinsysteem uit zijn Boltzmann evenwicht brengen. Kennis en ontwikkeling van photo-CIDNP MAS NMR kunnen hierdoor een methode opleveren om de intrinsieke ongevoeligheid en non-selectiviteit van MAS NMR te ondervangen. Tot nu toe werd photo-CIDNP in de vaste toestand alleen waargenomen in natuurlijke fotosynthetische reactiecentra. In de fotosynthetische bacterie *Rhodobacter sphaeroides* vindt het primaire fotosynthetische proces plaats in het pigment-eiwitcomplex, ook wel reactiecentrum (RC) genaamd. Vier bacteriochlorofyl *a* moleculen (BChl *a*), twee bacteriofeofytine *a* moleculen (BPhe *a*), twee ubiquinon-10 moleculen (Q), een niet-haem ijzer (Fe^{2+}), en een carotenoïde molecuul (C) vormen de cofactoren van het RC. Het lichtgeïnduceerde electronenoverdrachtsproces begint bij de primaire donor, die wordt gevormd door de twee BChl moleculen P_L en P_M. Het special pair P geeft een electron aan het BPhe molecuul Φ_A.

Er zijn drie verschillende mechanismen voorgesteld om photo-CIDNP in vaste stoffen te beschrijven.

- Het *electron-electron-nucleaire three-spin mixing* (TSM) mechanisme: Volgens dit mechanisme ontstaat er een netto nucleaire polarisatie als gevolg van de aanwezigheid van anisotrope hyperfijn-interactie en -koppeling tussen de twee electronen *spins* in het *spin*-gecorreleerde radicaalpaar.
- Het *differential decay* (DD) mechanisme: In dit mechanisme wordt een netto photo-CIDNP effect veroorzaakt als gevolg van de anisotrope hyperfijn-koppeling wanneer de singulet- en triplet-toestanden van de spin-gecorreleerde radicaalparen verschillende levensduren hebben.
- Het *differential relaxation* (DR) mechanisme: Dit vindt plaats als gevolg van het significante verschil in relaxatie tussen de nucleaire spins in het ^3P triplet van het *special pair* en de nucleaire spins in het singulet van de grondtoestand van P.

De reconstructie van de lokale electronen-spin-dichtheden uit photo-CIDNP intensiteiten vergt een diepgaand begrip van de betrokken mechanismen. Kennis van het photo-CIDNP

proces is dus equivalent aan het verkrijgen van informatie over de eerste stap in de fotosynthese.

In **Hoofdstuk 2** wordt ^{13}C photo-CIDNP MAS NMR onderzoek aan RC's van *Rhodobacter sphaeroides* WT beschreven. Photo-CIDNP is bij drie verschillende magnetische veldsterktes waargenomen. Bij een magnetische veldsterkte van 4,7 Tesla (200 MHz protonfrequentie) is de sterkste verhoging van meer dan 10.000 maal de Boltzmann polarisatie waargenomen. Bij hogere velden neemt de verhoging af. De lichtgeïnduceerde NMR geeft emissie signalen (negatief) bij alle velden en konden worden toegekend aan P_L en P_M van de donor en de acceptor Φ_A. De photo-CIDNP MAS NMR spectra bij de drie verschillende magnetische veldsterktes zijn gesimuleerd onder de aanname dat er twee concurrerende mechanismen zijn waarbij de polarisatie wordt overgedragen van electronen naar kernen, *three-spin mixing* (TSM) en *differential decay* (DD). De lichtgeïnduceerde signalen zijn toegekend met behulp van simulaties. De gesimuleerde spectra komen goed overeen met de photo-CIDNP MAS NMR spectra, wat aantoont dat het photo-CIDNP effect in de RC's van *Rb. sphaeroides* WT kan worden geïnterpreteerd door middel van de TSM en DD mechanismen.

De photo-CIDNP studies aan de mutant stam *Rhodobacter sphaeroides* R26 worden besproken in **Hoofdstuk 3**. Vergeleken met het WT is de levensduur van de donor triplet in de R26 RC's langer omdat er geen carotenoïde molecuul aanwezig is. Het effect van de magnetische veldsterkte op photo-CIDNP is vergelijkbaar voor beide RC's. Toch zijn de lichtgeïnduceerde signalen die zijn toegekend aan de donor P in de RC's van de R26 stam *absorptie signale*, wat niet kon worden verklaard door de TSM en DD mechanismen. Hierdoor hebben we overwogen of het DR mechanisme actief kon zijn in R26, naast de twee andere mechanismen. Simulaties waarbij het DR mechanisme is inbegrepen, konden de verandering in het teken van de lichtgeïnduceerde signalen van donor P reproduceren. Om die reden is het polarisatiepatroon van de WT RC's geïnterpreteerd door de spin-dichtheidsverdeling van de radicaal paar toestand te beschouwen, en is de verandering in polarisatie tussen de WT en R26 spectra geïnterpreteerd via de spin-dichtheidsverdeling in de triplettoestand van de donor.

De sterke photo-CIDNP verhoging bij een veldsterkte van 4,7 T maakt het mogelijk om zonder isotoopverrijking cofactor moleculen met een concentratie van ~100 nM in intacte R26 cellen te bestuderen (**Hoofdstuk 3**). Het globale photo-CIDNP intensiteitpatroon wijkt op sommige details af van de geïsoleerde reactiecentra bij 4,7 T. De overeenkomst tussen het photo-CIDNP spectrum van de geïsoleerde RC's en de intacte cellen duidt erop dat de electronenstructuur van de grondtoestand van het special pair niet sterk wordt beïnvloed door de omringende eiwitcomplexen in de natuurlijke omgeving van een intacte cel. Kortom, photo-CIDNP MAS NMR heeft zich bewezen als methode om de electronenstructuur van

fotosynthetische cofactoren te bestuderen, zowel met moleculaire en atomaire resolutie als bij cellulaire concentraties.

In **Hoofdstuk 4** zijn ^{13}C-^{13}C dipolaire correlatie photo-CIDNP MAS NMR studies uitgevoerd aan RC's van *Rhodobacter sphaeroides* WT, selectief isotoop gelabeld in alle BChl en BPhe cofactoren op de posities C-4, 5, 9, 10, 14, 15, 16 en 20, om zodoende een uitgebreid beeld te krijgen van de electronenstructuur van de grondtoestand van de cofactoren die betrokken zijn bij het electronenoverdrachtsproces. Er zijn drie sterke componenten waargenomen in de ^{13}C-^{13}C dipolaire correlatie photo-CIDNP MAS NMR spectra. Deze zijn toegekend aan twee BChls, P1 en P2, en een BPhe, Φ_A. Daarnaast is er een zwakke component waargenomen die is toegekend aan een andere BCh1, aangeduid met P3. Er zijn duidelijke verschuivingen naar hoog veld aanwezig voor P2 in de pyrrool ring I vergeleken met P1 en P3. De grote verschuivingen kunnen worden verklaard door een waterstofbrug met His L168, die zich in de buurt van de 3-acetyl groep van P_L bevindt. Zodoende kan P_L worden toegekend aan P2, waardoor het een *special* BChl wordt in het special pair. Vervolgens kan P_M worden toegekend aan P1 en de zwakke component P3 aan B_A. De electronenstructuur van het *special pair* is dus asymmetrisch in de grondtoestand.

Photo-CIDNP studies zijn verder uitgebreid naar de membraangebonden complete fotosynthetische unit (PSU) die selectief ^{13}C-isotoop gelabeld is in alle BChl en BPheo cofactoren op posities C-1, 3, 6, 8, 11, 13, 17 en 19 (**Hoofdstuk 5**). Alle lichtgeïnduceerde NMR pieken van het membraangebonden PSU zijn absorptie signalen. Toevoeging van detergens leidde tot dissociatie van PSU uit het chromatofoormembraan en dat gaf significante veranderingen in het teken en het intensiteitpatroon van het lichtgeïnduceerde MAS NMR spectrum. Daarentegen vertonen de in detergens opgeloste PSU en RC's met hetzelfde patroon van isotopenlabels nagenoeg dezelfde chemische verschuivingen, met slechts geringe verschillen in het intensiteitpatroon. De duidelijke verschillen tussen de intacte membraangebonden en de met detergens opgeloste fotosynthetische units kan worden verklaard door het verlies van zelforiëntatie van de membraangebonden samples ten gevolge van het oplossen.

Hoofdstuk 6 geeft een toekomstperspectief voor photo-CIDNP studies aan de RC's van *Rhodobacter sphaeroides*. Het eerste deel van het hoofdstuk is gewijd aan het toenemen van de photo-CIDNP respons. Dit baant een weg voor tijdopgeloste photo-CIDNP experimenten. Het tweede deel beschrijft toekomstige ontwikkelingen in vier verschillende richtingen, van biofysische studies naar Magnetic Resonance Force Microscopy. De biofysische studies hebben informatie opgeleverd over het bouwen van kunstmatige fotosynthetische machines. Photo-CIDNP kan als een 'spin torch' worden gebruikt om de bindingsplaats en diens invloed op de cofactoren te onderzoeken. 'Spin torches' zouden ook gebruikt kunnen worden als contrastmiddel in Magnetic Resonance Imaging (MRI). Photo-CIDNP in combinatie met

Magnetic Resonance Force Microscopy (MRFM) zou de detectie van geïsoleerde kernspins in de nabije toekomst mogelijk kunnen maken.

List of Publications

Photochemically induced dynamic nuclear polarization in entire bacterial photosynthetic units observed by ^{13}C- magic-angle spinning NMR.
S. Prakash, Alia, P. Gast, G. Jeschke, H. J. M. de Groot, J. Matysik.
J. Mol. Struc. (2003) 661, 625-633.

Build-up kinetics of light induced nuclear polarization observed in reaction centers of *Rhodobacter sphaeroides.*
S. Prakash, Alia, P. Gast, H. J. M. de Groot, G. Jeschke, J. Matysik.
Photosynthesis: Fundamental Aspects to Global Perspectives (A. van der Est and D. Bruce Eds.), (2004) Allen Press Montreal, pp. 301-303.

^{15}N photo-CIDNP MAS NMR on reaction centers of *Rhodobacter sphaeroides.*
S. Prakash, S. H. Tong, Alia, P. Gast, H. J. M. de Groot, G. Jeschke, J. Matysik.
Photosynthesis: Fundamental Aspects to Global Perspectives (A. van der Est and D. Bruce Eds.), (2004) Allen Press Montreal, pp. 236-238.

Magnetic field dependence of photo-CIDNP MAS NMR on photosynthetic reaction centres of *Rhodobacter sphaeroides* WT
S. Prakash, Alia, P. Gast, H. J. M. de Groot, G. Jeschke, J. Matysik.
J. Am. Chem. Soc. (2005) 127, 14290-14298.

Long-living triplet state of electron donor allows signal separation of cofactors in photo-CIDNP MAS NMR in *Rhodobacter sphaeroides* R26
S. Prakash, Alia, P. Gast, H. J. M. de Groot, J. Matysik, G. Jeschke.
Submitted (2006).

Ground-state electronic structure of special pair in *Rhodobacter sphaeroides* reaction centers revealed by ^{13}C photo-CIDNP MAS NMR.
S. Prakash, Alia, P. Gast, H. J. M. de Groot, G. Jeschke, J. Matysik.
In preparation (2006).

Curriculum Vitae

In May 1996 after finishing my schooling from Kendriya Vidyalaya, Mumbai, I joined St. Xavier's College affiliated to the University of Mumbai. There I followed the bachelor's programme in Mathematics, Physics and Chemistry, and graduated with a specialization in Chemistry in December 1999. The same year I joined the Department of Chemistry at the University of Mumbai to follow the master's programme in Chemistry. During this period I also worked on a short research project, under the guidance of Prof. S.R. Kasturi, at Tata Institute of Fundamental Research, Mumbai to study a peptide in the tubulin protein. In December 2001, I received the master's degree in Physical Chemistry. In April 2002, I started my PhD under the supervision of Dr. J. Matysik in the Solid State NMR group at Leiden University led by Prof. dr. H.J.M. de Groot. During my PhD time, I attended the EMBO course "Multidimensional NMR in Structural Biology" (2002) held at Il Ciocco, Italy. I had the opportunity to present my work through poster presentations at various international conferences. These include the *3rd Alpine conference on solid-state NMR* (2003) in Chamonix, France, the *13th International conference on Photosynthesis* (2004) in Montreal, Canada, *EUROMAR* (2005) in Veldhoven, The Netherlands and the *Spin Chemistry Meeting* (2005) in Oxford, United Kingdom. Also, through talks I presented my work at the *27th Annual Discussion Meeting* of the Gesellschaft Deutscher Chemiker (GDCh) Magnetic Resonance Spectroscopy Division (2005) in Mainz, Germany and at the annual meeting of the *Study group Theory and Spectroscopy* of the Chemical society section of the NWO (2006) in Lunteren, The Netherlands.

Nawoord

Many people have been involved in the work that I have presented in this thesis. I had the opportunity to continue the study of selectively labeled *Rhodobacter sphaeroides* WT reaction centers started by Els Schulten. The knowledge for isolation of reaction centers came from the Biophysics group. In this I was helped by Peter Gast who gave me some of his precious time. I worked with Dre de Wit for growing the bacterial cells. Wouter van der Meer provided a nice atmosphere to work in the lab at the Biophysics group. Since my first year, Alia shared with me her valuable experience through many discussions and suggestions. She helped me with sample preparation and provided me with the selectively labeled reaction center sample used for the study reported in Chapter 4. The patient explanations on the photo-CIDNP theory given by Gunnar Jeschke in Aachen and Bingen not only helped me in understanding the mechanism better but also were extremely useful for designing the experiments. The discussions with Piotr Wawrzyniak and Francesco Buda were useful in formulating an overall picture of the reaction center. Prativa Dawadi was kind enough to provide me with u-^{13}C- *δ-aminolevulinic acid* for reaction center preparations. The discussions on photosynthesis with Prasanna Mohanty were very helpful to me.

On the NMR side, Johan Hollander, Fons Lefeber and Kees Erkelens always gave me their time and help with the solid state NMR setup, initially at the 400 MHz magnet and later at 200 MHz magnet.

In the last four years I have formed many pleasant memories of social interactions with my colleagues: Ania, Arjan, Arjan, Eugenio, Geerten, Karthick, Muhammed, Niels, Piotr, Prashant, Reinier, Richard, Rob, Samira, Swapna, Sylvia, Tatyana, Thierry and Yan. Sitting in the same room as Ido, I learnt a lot about the Dutch politics and history from him. Liesbeth's efficient help in the administrative matters always solved many problems for me. The closest personal and work association has been with my *paranymphs* Anna and Esha. They helped me settle in my apartment and provided me with their company during work.

A very special place belongs to Gerty and Fritz who not only welcomed me to Zirndorf but have always been interested in the progress that I am making.

My coming to Netherlands and taking the first step towards building a scientific career has only been possible due to the constant support from my family. Both my sisters, Ira and Ruchira, have contributed in giving me the best of advice, scientific and otherwise. Through Ruchira, her husband and his parents, I had the pleasure of participating in the unique Dutch 'Sinterklaas' celebration. Finally, it is to my parents that I owe my development as a scientist. They helped cultivate a scientific attitude in me that has formed the foundation of my scientific endeavors.